

8-2011

Enforced expression of Tbx1 in fetal thymic epithelial cells antagonizes thymus organogenesis

Kim T. Cardenas

Follow this and additional works at: https://digitalcommons.library.tmc.edu/utgsbs_dissertations



Part of the [Cancer Biology Commons](#), [Cell Biology Commons](#), [Developmental Biology Commons](#),
[Genetic Processes Commons](#), and the [Immunity Commons](#)

Recommended Citation

Cardenas, Kim T., "Enforced expression of Tbx1 in fetal thymic epithelial cells antagonizes thymus organogenesis" (2011). *The University of Texas MD Anderson Cancer Center UTHealth Graduate School of Biomedical Sciences Dissertations and Theses (Open Access)*. 157.
https://digitalcommons.library.tmc.edu/utgsbs_dissertations/157

This Dissertation (PhD) is brought to you for free and open access by the The University of Texas MD Anderson Cancer Center UTHealth Graduate School of Biomedical Sciences at DigitalCommons@TMC. It has been accepted for inclusion in The University of Texas MD Anderson Cancer Center UTHealth Graduate School of Biomedical Sciences Dissertations and Theses (Open Access) by an authorized administrator of DigitalCommons@TMC. For more information, please contact digitalcommons@library.tmc.edu.

ENFORCED EXPRESSION OF TBX1 IN FETAL THYMIC
EPITHELIAL CELLS ANTAGONIZES
THYMIC ORGANOGENESIS

by

Cardenas, Kim B.S.

APPROVED:

Ellen Richie, Ph.D.

Bradley McIntyre, Ph.D.

Pierre McCrea, Ph.D.

Mark Bedford Ph.D.

David Johnson, Ph.D.

APPROVED

Dean, The University of Texas

Graduate School of Biomedical Sciences at Houston

***Enforced expression of Tbx1 in fetal thymic epithelial cells
antagonizes thymus organogenesis***

A

DISSERTATION

Presented to the Faculty of

The University of Texas

Health Science Center at Houston and

The University of Texas

MD Anderson Cancer Center

Graduate School of Biomedical Sciences

in Partial Fulfillment

of the Requirements

for the Degree of

DOCTOR OF PHILOSOPHY

by

Kim T. Cardenas, B.S.

Houston, Texas

August 2011

Copyright © 2011 Kim Cardenas
All rights reserved

Acknowledgements

I would like to thank my mentor Dr. Ellen Richie, who has been the most wonderful mentor a graduate student could have. Without you, this work would have not been possible and I could never have come this far. Thank you for always pushing me to go farther and always having faith in me. Thank you to my committee members, Dr. Brad McIntyre, Dr. Mark Bedford, Dr. Pierre McCrea, Dr. David Johnson and Dr. Sue Fischer. You have been an inspiring group and have made learning exciting and fun. Thank you to Becky Brooks for all of your help. I don't know what I would have done without you. Thank you to all the support staff in the animal facility. I could not have asked for a better group of caregivers for my mice. It has been a pleasure working with everyone. Thank you to the Histology Core. Special thanks to Dr. Irma Conti, Jimi Lynn Brandon and Nancy Otto, for being dedicated, patient and always willing to help. To, Pam Whitney, thank you for always sorting and analyzing my cells at all hours of the day, night and weekend. I'm sorry I couldn't give you more cells. Thank you to all lab members of the Richie lab, past and present, Dr. Anne Griffith, Dr. Micheline Laurent, Dr. Dakshayni Lomada, Dr. Manju Jain, Dr. Nandani Singarapu, Carla Carter, Michelle Bolner, Katie Gutierrez, Jia Li and Rhea Kang. I have had a great time working with you. Special thanks to Carla for sharing her infinite knowledge and experience. Thanks to Michelle and Katie for being the most awesome lab mates one could have. I am going to miss seeing you everyday but know I won't be too far away. Jia thanks for always listening to me and being a great friend. Wherever you go, you are only a plane ride away. Thank you to my

mom and dad, Charles and Alicia Cardenas, for always being supportive and loving. To Casey, Misty, Chrystal and my brother, Timothy and sister, Alta, thanks for listening to all my mouse stories at the “dancehall” over a beer. I can’t express my gratitude enough.

**Enforced expression of *Tbx1* in fetal thymic epithelial cells
antagonizes thymus organogenesis**

Kim T. Cardenas

The thymus and parathyroid glands originate from organ-specific domains of 3rd pharyngeal pouch (PP) endoderm. At embryonic day 11.5 (E11.5), the ventral thymus and dorsal parathyroid domains can be identified by *Foxn1* and *Gcm2* expression respectively. Neural crest cells, (NCCs) play a role in regulating patterning of 3rd PP endoderm. In addition, pharyngeal endoderm influences fate determination via secretion of Sonic hedgehog (Shh), a morphogen required for *Gcm2* expression and generation of the parathyroid domain. *Gcm2* is a downstream target of the transcription factor *Tbx1*, which in turn is positively regulated by Shh. Although initially expressed throughout pharyngeal pouch endoderm, *Tbx1* expression is excluded from the thymus-specific domain of the 3rd PP by E10.5, but persists in the parathyroid domain. Based on these observations, we hypothesized that *Tbx1* expression is non-permissive for thymus fate specification and that enforced expression of *Tbx1* in the fetal thymus would impair thymus development.

To test this hypothesis, we generated knock-in mice containing a Cre-inducible allele that allows for tissue-specific *Tbx1* expression. Expression of the *R26^{iTbx1}* allele in fetal and adult thymus using *Foxn1^{Cre}* resulted in severe thymus hypoplasia throughout ontogeny that persisted in the adult. Thymic epithelial cell

(TEC) development was impaired as determined by immunohistochemical and FACS analysis of various differentiation markers. The relative level of *Foxn1* expression in fetal TECs was significantly reduced. TECs in *R26^{iTbx1/+}* thymi assumed an almost universal expression of Plet-1, a marker associated with a TEC stem/progenitor cell fate. In addition, embryonic *R26^{iTbx1/+}* mice develop a perithymic mesenchymal capsule that appears expanded compared to control littermates. Interestingly, thymi from neonatal and adult *R26^{iTbx1/+}* but not *R26^{+/+}* mice were encased in adipose tissue. This thymic phenotype also correlated with a decrease in thymocyte cellularity and aberrant thymocyte differentiation. The results to date support the conclusion that enforced expression of *Tbx1* in TECs antagonizes their differentiation and prevents normal organogenesis via both direct and indirect effects.

Table of Contents

Introduction	1
Overview of thymus composition, organization and involution	1
Lymphoid Cells within the thymus.....	3
Thymocyte Development	4
Thymic Epithelial Cells.....	7
Contribution of neural crest cells to the embryonic and postnatal thymus.....	11
Thymus organogenesis.....	17
Molecular mediators of 3 rd PP development and thymus organogenesis.....	21
The role of Tbx1 in 3 rd PP formation and fate determination	26
Materials and Methods	32
Results	44
 Chapter 1- Development of <i>R26^{iTbx1}</i> mice and studies in	
Embryogenesis.....	44
Generation of the <i>R26^{iTbx1}</i> mouse model	44
Expression of <i>Tbx1</i> in <i>R26^{iTbx1/+}</i> , <i>Foxn1^{Cre/+}</i> mice.....	47
Patterning in the <i>R26^{iTbx1/+}</i> 3 rd PP is conserved at E11.5	50
Fetal thymic lobes are hypoplastic with abnormal morphology	53
<i>R26^{iTbx1/+}</i> fetal TECs are impaired in differentiation.....	56
<i>R26^{iTbx1/+}</i> are characterized by an accumulation of Plet-1 progenitor TECs	62

<i>R26^{iTbx1/+}</i> E17.5 TECs proliferate at a frequency comparable to controls	65
Fetal <i>R26^{iTbx1/+}</i> thymi have an altered pattern of gene expression but not an increase in cell death	69
Postnatal <i>R26^{iTbx1/+}</i> thymi are hypoplastic with aberrant thymic architecture	77
<i>R26^{iTbx1/+}</i> TECS are impaired in differentiation and organization.....	80
Plet-1 progenitor cells are retained in adult <i>R26^{iTbx1/+}</i> thymi.....	85
Thymocyte maturation is impaired in <i>R26^{iTbx1/+}</i> mice	91
Autoimmune manifestations arise in some <i>R26^{iTbx1/+}</i> individuals	94

Chapter 2- Perithymic adipose tissue forms in the *R26^{iTbx1/+}*

postnatal thymus.....	103
-----------------------	-----

Discussion.....115

Tbx1 plays many dynamic roles during development.....	116
Blocks in TEC differentiation in <i>R26^{iTbx1/+}</i> thymi coincide with a decrease in <i>Foxn1</i> expression.....	121
Sustained expression in <i>R26^{iTbx1/+}</i> TECs results in progenitor arrest.....	124
Forced expression of <i>Tbx1</i> in TECs negatively regulates <i>Hes1</i>	126
CCL25 and IL-7 chemokines are reduced in <i>R26^{iTbx1/+}</i> TECs.....	128
Potential sources of postnatal adipose tissue.....	131

Conclusions.....	136
Bibliography.....	140
Curriculum Vitae.....	156

Figure Legend

Figure I. Neural crest cells arise from the dorsal neural tube and pattern the pharyngeal arches	13
Figure 1. Development of $R26^{iTbx1}$ mice and studies in in embryogenesis.....	46
Figure 2. $Foxn1^{Cre}$ induces $R26^{iTbx1}$ expression in thymic epithelial cells	49
Figure 3. In situ hybridization of $Foxn1$ and $Gcm2$ expression in the 3 rd PP	52
Figure 4. Embryonic $R26^{iTbx1/+}$ have a progressive hypoplastic thymus phenotype	55
Figure 5. TEC organization and architecture are impaired in fetal thymi	58
Figure 6. TEC differentiation and maturation is impaired in E17.5 $R26^{iTbx1/+}$ thymi	61
Figure 7. $R26^{iTbx1/+}$ thymi have an increased frequency of Plet-1 cells at E17.5.....	64
Figure 8. Proliferation is not impaired in E17.5 $R26^{iTbx1/+}$ thymi	67
Figure 9. $R26^{iTbx1/+}$ fetal thymic phenotypes do not result from an increase in apoptosis.....	71
Figure 10. Expression of selected genes in $R26^{iTbx1/+}$ fetal TECs.....	74
Figure 11. Impaired architecture and organization of post-natal $R26^{iTbx1/+}$ thymi are progressive with age.....	79

Figure 12. $R26^{iTbx1/+}$ postnatal thymi at newborn and 1 week of age have a block in TEC differentiation.....	82
Figure 13. 4 wk $R26^{iTbx1/+}$ TECs sustain a block in differentiation.....	84
Figure 14. Postnatal TECs are impaired in differentiation in $R26^{iTbx1/+}$ thymi.....	87
Figure 15. Accumulation of Plet-1 progenitors in postnatal thymi.....	90
Figure 16. Thymocyte maturation is impaired in postnatal $R26^{iTbx1/+}$ thymi.....	93
Figure 17. $R26^{iTbx1/+}$ 8 wk mice have hypoplastic thymi and lymphocytic infiltration.....	96
Figure 18. $R26^{iTbx1/+}$ eyes have inflammatory infiltrates not observed in controls.....	98
Figure 19. Ciliated epithelial cysts are found in 1 yr. $R26^{iTbx1/+}$ thymi.....	102
Figure 20. Gross examination of $R26^{iTbx1/+}$ thymi <i>In situ</i> reveal perithymic adipose	105
Figure 21. Adipocytes are not observed in fetal $R26^{iTbx1/+}$ thymi but accumulate progressively with postnatal age.....	107
Figure 22. $Ppar-\gamma$ is up-regulated in fetal stroma and prominent in $R26^{iTbx1/+}$ postnatal thymi	109
Figure 23. Fetal $R26^{iTbx1/+}$ thymi are surrounded by a prominent NCC-derived capsule.....	112

Figure 24. Figure 24. NCC-derived mesenchyme is aberrantly localized	
through-out postnatal $R26^{i\text{Tbx1/+}}$ thymi.....	114
Figure 25. Model for TEC development in $R26^{i\text{Tbx1/+}}$ thymi	139

Introduction

Overview of thymus composition, organization and involution

The thymus plays a critical role in the development of a competent immune response. It is required for the generation of T-cells with a vast T-cell receptor (TCR) repertoire and thus the generation of a functional immune system. The cellular composition of the thymus is made up largely of developing thymocytes; however, thymic stromal cells, of which thymic epithelial cells, (TECs), are an essential component, play an indispensable role in thymocyte development. The thymus is organized into two main regions that can be identified based on their histological appearance in tissue sections stained with hematoxylin and eosin (H&E). The outer dark staining region is the thymic cortex and contains the most immature thymocytes. Inner lighter staining areas are referred to collectively as the thymic medulla and contain fewer but more mature thymocytes. Each region not only contains different thymocyte subsets, but also different TEC subsets that are specialized in supporting specific stages of thymocyte maturation. Differentiation, proliferation and survival of both cell types in an interdependent process, referred to as crosstalk, that relies upon reciprocal signaling events between different cell types.

TECs form a three-dimensional meshwork that facilitates thymocyte migration into different microenvironmental zones of the cortex and medulla. In addition, they also provide essential signals to developing thymocytes required for their survival, proliferation and maturation. Each region within the thymus contains phenotypically

and functionally distinct TECs. Cortical TECS (cTECs) express cytokines and chemokines that support the earliest stages of thymocyte development and medullary TECs (mTECs) play a role in later stages of T-cell development. The details of these dynamic processes will be elaborated upon in a later section.

The thymus is largest in preadolescent individuals and undergoes progressive age-related thymic atrophy referred to as thymic involution that is initiated around the onset of puberty and is associated with a decline in naïve T-cell output. While the molecular mechanisms responsible for thymus involution are not known, it is correlated with a failure in TEC homeostasis and the ability to support thymopoiesis. The consequences of thymus involution are critical to human health and disease. Decreased T-cell output results in a deficiency of naïve T-cells and homeostatic expansion of memory T-cells in peripheral lymphoid organs. Therefore, there are fewer naïve T-cells available to respond to new antigenic challenges. Older individuals are more susceptible to infectious disease, autoimmunity and cancer. This is likely due in part to the diminished ability to mount an effective T-cell response to newly encountered antigens. Reversing thymic involution and/or sustaining thymic function would allow for a lasting competent immune response and the ability to efficiently combat a wide array of pathogens and disease. My work is aimed at understanding the molecular events required to generate a functional thymus in order to devise future therapeutic strategies targeted at its regeneration or maintenance.

Lymphoid Cells Within the Thymus

B-cells develop and mature in the bone marrow while T-cell progenitors migrate to the thymus where they continue maturation. There are two classes of T cells distinguished by the nature of their TCRs. The majority of T-cells in the adult are of the $\alpha\beta$ lineage (reviewed in(1)). These T cells express $\alpha\beta$ TCRs consisting of a TCR- α chain and a TCR- β chain linked by a disulfide bond to form an $\alpha:\beta$ heterodimer. Mature $\alpha\beta$ T-cells circulate through the peripheral lymph nodes and spleen. A small subset of $\gamma\delta$ T cells found mainly in skin and at mucosal surfaces expresses $\gamma\delta$ TCRs consisting of a TCR γ :TCR δ heterodimer. Rearrangement of TCR- γ , - δ and - β loci occurs in a simultaneous fashion. However if a successful $\gamma\delta$ TCR is generated prior to the rearrangement of the β chain gene, signaling through the newly generated $\gamma\delta$ TCR will result in cessation of further gene rearrangements and commitment to the $\gamma\delta$ lineage. If instead complete β -chain rearrangement occurs first, pairing of this β -chain with a pre-T-cell α chain will result in formation of a pre-TCR through which signaling will occur and result in commitment to the $\alpha\beta$ lineage (reviewed in (1), (2)). Since the majority of T-cells generated in the adult are $\alpha\beta$ T-cells, for the remainder of this dissertation T-cells will refer only to those of this lineage.

Both α - and β - chains of the TCR, consist of a variable (V) region and a constant (C) region. Two short stalk segments interconnect the chains and also anchor them to the membrane. Both chains span the lipid-bilayer and end in short cytoplasmic tails. There are two main types of mature T-cells that arise from the $\alpha\beta$ -lineage, namely, CD4⁺ and CD8⁺. Mature CD4⁺ T-cells are negative for CD8 and

recognize antigenic peptides presented by self- MHC class II molecules, while CD8⁺ T-cells are negative for CD4 and recognize peptides presented by self-MHC class I. These T cell subsets also differ in effector and regulatory functions. CD4⁺ T-cells differentiate into specialized T helper (T_H) cells that secrete various cytokines that activate B-cells or cells of the innate immune system, (reviewed in (3)) For example, T_H1 cells produce cytokines such as IL-2 and IFN γ that activate inflammatory cells to destroy intracellular pathogens (reviewed in (3)). T_H2 cells produce IL-4 and other cytokines that promote antibody production by B-cells. T_H17 cells produce IL-17, a potent pro-inflammatory cytokine. T_H cells also promote the differentiation of CD8⁺ T-cells into cytotoxic effector cells. T regulatory (T_{reg}) cells are another class of T-cells that develop in the thymus and play an essential role in suppressing T-cell responses.

Thymocyte Development

Common lymphoid progenitors in the bone marrow are the source of thymus seeding lymphoid cells (4). After entry into the adult thymus through the vasculature, at the corticomedullary junction (CMJ), thymocyte progenitors undergo a progressive differentiation process that depends on continual interactions with TECs in the thymic microenvironment (reviewed in (5), (6)). Different thymocyte maturation stages can be recognized by the expression pattern of key cell surface markers and distinct thymocyte phenotypes that correlate with passage through developmental checkpoints required for the eventual production of self-tolerant and self-restricted T-cells.

The earliest thymocyte progenitors are double negative (DN) for CD4 and CD8 (2). DN thymocytes gradually become committed to a T-cell lineage as they proceed through distinct differentiation stages (DN1-DN4) defined by the expression patterns of CD44 or c-kit and CD25 (2). DN1 thymocytes (CD44⁺ CD25⁻) retain the capability to develop into natural killer cells, dendritic cells and retain some myeloid differentiation potential (7). Activation of Notch receptors on DN2 (CD44⁺ CD25⁺) and DN3 (CD44⁻ CD25⁺) thymocytes by Delta like 4 (Dll4) ligand expressed on TECs is necessary but not sufficient for T lineage commitment (reviewed in (8)). Rearrangement of the TCR β locus begins at the DN2 stage (2). DN3 thymocytes with productive TCR β gene rearrangements express a TCR β polypeptide that pairs with the monomorphic pre-T α polypeptide to generate a pre-TCR (reviewed in (9)). Signaling through the pre-TCR allows DN3 cells to survive and differentiate to the DN4 (CD44⁻ CD25⁻) stage. The DN3 to DN4 transition is referred to as the β -selection checkpoint and is required for continued thymocyte maturation (reviewed in (9)). The DN4 stage coincides with a proliferative burst, as the CD4 and CD8 co-receptors are up-regulated yielding CD4⁺ CD8⁺ double positive (DP) thymocytes (reviewed in (10)). *Tcr α* gene rearrangement then proceeds resulting in one of two possible fates: positive selection or cell death by neglect (reviewed in (9)). DP thymocytes expressing $\alpha\beta$ TCRs with moderate affinity for self-peptide-MHC complexes presented on cortical TECs, are rescued from programmed cell death (reviewed in (9)). Positively selected DP thymocytes down-regulate either CD4 or CD8 to produce single positive (SP) semi-mature thymocytes that migrate into the medulla.

The exact mechanisms that determine CD4 versus CD8 lineage commitment are not clear. Classical models predict lineage commitment to be either a stochastic or directed consequence of TCR-signaled DP thymocytes resulting in transcriptional silencing of either the CD4 or CD8 co-receptor (1). However work by Al Singer's group proposes a different model in which lineage commitment is dependent on persistence or cessation of a TCR-signal during positive selection (1). The kinetic signaling model postulates that positively selected DP thymocytes proceed through a CD4⁺CD8⁻ intermediate that retains the capability to differentiate into either a CD4 or CD8 SP thymocyte (1). The determining factor is the persistence of the TCR signal itself. If a CD4⁺CD8⁻ intermediate thymocyte receives a sustained TCR signal then the developing thymocyte will proceed to develop into a CD4 SP thymocyte (1). However if this intermediate does not receive this persistent signal then a process called "co-receptor reversal" will be initiated and the thymocyte will adopt a CD8 SP fate (1).

The cytokine IL-7 is secreted by the thymic epithelium to developing thymocytes and is required for their survival and proliferation (reviewed in (11), (12)). Early studies by Ursula von Freeden-Jeffry, demonstrate DN2 thymocytes lacking *IL-7* are impaired in cell-cycle regulation and expression of the pro-survival molecule Bcl-2 (13). *IL-7* is expressed early in ontogeny throughout the developing epithelium its expression is dependent on thymocyte derived signals (12, 14).

Auto-reactive SP thymocytes are eliminated in the medulla by a process referred to as negative selection (reviewed in (15)). Medullary TECs have the unique ability to express a vast array of tissue-restricted antigens (TRAs) (reviewed

in (15)). In addition to directly presenting TRAs to SP thymocytes, mTECs can transfer TRAs for cross-presentation by dendritic cells. SP thymocytes that express $\alpha\beta$ TCRs with high affinity for self-antigens presented by mTECs and/or dendritic cells undergo apoptosis. Only those T-cells that are self-tolerant and able to recognize antigen in the context of the self-MHC molecules will gain entry into the periphery.

While millions of thymocytes proliferate and differentiate within the thymus, the vast majority, (~98%), undergo apoptosis at some point along their developmental journey. Only 2-4% of incoming thymocytes will fulfill all of the maturational requirements to become naïve T cells and gain access to the periphery where they undergo further maturation to become fully competent and exert an effector function. This intense, selective screening allows for the formation of a diverse T-cell repertoire capable of responding to a vast array of pathogens while maintaining self-tolerance. The entire thymocyte maturational process is guided and shaped by the thymic epithelium, which plays an indispensable role in the formation of a functional T-cell repertoire.

Thymic Epithelial Cells

TECs are the major constituent of the thymic stromal microenvironment and play an indispensable role at all stages of thymocyte development (16). They provide essential growth, survival and differentiation signals for the generation of naïve T-cells (reviewed in (17)) . Evidence for the importance of TECs in thymocyte maturation is provided by examination of athymic *nude* mice, which harbor an

inactivating point mutation in the coding region of Foxn1, a transcription factor required for TEC differentiation and survival ((18), reviewed in (19)). Thymic development in this model is severely impaired beyond embryonic day E11.5 in mouse gestation (E11.5) resulting in an essentially athymic phenotype. Despite competent thymus seeding progenitors in the bone marrow, the early block in TEC differentiation not only prevents expression of chemokines that attract thymocyte progenitors, but also prevents expression of cytokines required to support thymocyte survival (reviewed in (20)). Therefore, *nude* mice are devoid of essentially all T-cells because thymocyte maturation cannot occur in the absence of functional TECs. The roles of Foxn1 in thymus organogenesis, maintenance and homeostasis will be discussed in greater detail during the organogenesis portion of this dissertation.

In the adult, TEC subsets can be defined on the basis of morphology, function and phenotype. Each subset varies in the types of intermediate keratin filaments expressed. cTECs express high levels of keratin 8 (K8) and are negative for keratin 5 expression (K5) (reviewed in (17)). Several non-overlapping mTEC subsets exist. One subset of mTECs expresses low levels of K8 and high levels of K5 and K14 while another distinct subset expresses high levels of K8 and binds the lectin UEA-1 but is negative for K5 and K14. TECs that reside at the CMJ co-express both K8 and K5, (K8⁺K5⁺) (reviewed in (17)). During thymus organogenesis, the expression of keratins and other differentiation markers is dynamic and the phenotype of cTECs and mTECs corresponds to their differentiation stage (reviewed in (17)) . Studies by Klug et. al., have demonstrated the E11.5 thymic primordia consists largely of K5⁻

K8⁺ TECs, which begin to up-regulate K5 expression at E12.5 (21). The majority of cells within the thymus at E12.5 are epithelial and express the marker EpCAM1 (22). At this time in development a central core of K5⁺K8⁺ TECs is present surrounded by K8⁺K5⁻ TECs (21). TEC progenitors also express MTS24. Isolated MTS24⁺ cells have shown to retain the capability to reconstitute the TEC microenvironmental compartment when grafted under the kidney capsule of a *nude* host, suggesting that a common MTS24 progenitor may give rise to differentiated cTEC and mTEC populations (23). MHC class II (MHC II) molecules are expressed on TECs after E12.5 (24). While the exact time at which commitment to a cTEC or mTEC lineages is not known, work by the Jenkinson lab suggests that the expression of CD205 is associated with adoption of a cortical fate (22). Later stages of cTEC maturation include expression of the proteasome-specific subunit *β5t* and *Cathepsin-L* (5). Expression of both CD205 and *β5t* are evident as early as E12 with the overall percentage of CD205⁺, *β5t*⁺ TECs increasing with age (22, 25)

Emergence of defined K5⁺K14⁺K8^{lo} medullary islets occurs at approximately E17.5 (21). During embryogenesis activation of the NFκB signaling pathway by lymphoid tissue inducer (Lti) cells is required for initial mTEC development (reviewed in (26)). At postnatal stages the requirement of the NFκB pathway for mTEC development persists. The mTEC subset expresses several receptors of the TNFα family including RANK, CD40 and LTβR (reviewed in (26)). The ligands RANKL, CD40L and LTβR are expressed by CD4⁺ SP thymocytes and activate NFκB target genes needed for mTEC maturation. As mTECs undergo maturation, they up-regulate expression of MHCII, CD80 and other surface molecules (27). In

addition, mTEC differentiation is associated with the expression of the *Aire* transcription factor. *Aire* is responsible for the expression of many, but not all, of the TRAs expressed by mTECs (15).

In addition to their direct roles in negative and positive selection, TECs also provide migrational cues to developing T-cells that aid their navigation through the thymic microenvironment. Chemokine ligands such as CCL21 and CCL25 are expressed by fetal TECs and support thymus colonization by thymus seeding cells (5). Migration of DN thymocytes to the outer subcapsular region, where they continue to mature, is a chemokine-guided process whereby TECs signal thru the receptor CCR9, expressed on immature T-cells (28). Furthermore, CCL19 and CCL21 expressed by mTECs attract positively selected thymocytes into the medulla where they are subject to negative selection (28). These chemokines also guide self-tolerant mature T-cells out of the thymus and into the periphery (reviewed in (26)).

Thymocyte-derived signals are also essential for organization and maintenance of TECs after initial patterning of the fetal thymus. This is evidenced by the hCD3 ϵ transgenic mouse model in which thymocyte development is arrested at the DN1 stage that results in a block in TEC development at the immature K5⁺K8⁺ stage (21, 29). *RAG-1*^{-/-} and *RAG-2*^{-/-} have a block in thymocyte development at the DN3 stage; whereas *TCR α* ^{-/-} mice generate DP thymocytes that cannot undergo positive selection due to the absence of $\alpha\beta$ TCR expression (21). Both of these experimental models have thymi that contain predominantly cTECs, whereas mTECs are sparse and medullary regions are underdeveloped (21, 29). These

results further demonstrate that signals derived from positively selected thymocytes are required for normal medullary formation. In summary, the intra-thymic crosstalk between TECs and thymocytes is mutually required for proper establishment, organization and maturation of both cell types.

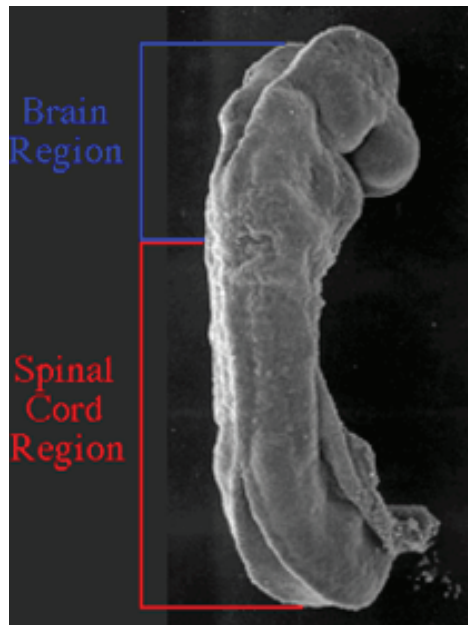
Contribution of neural crest cells to the embryonic and postnatal thymus

Epithelial-mesenchymal interactions are a common theme in developmental biology and in thymic development contribute to inductive signaling required for proper organogenesis. Mesenchyme is a supportive-type of loosely packed, tissue that is migratory in nature and contains a fibrous matrix. Mesenchyme is derived from two main sources in the embryo, namely the mesoderm or NCCs (30). The majority of perithymic mesenchyme is NCC derived and thus termed ectomesenchyme.

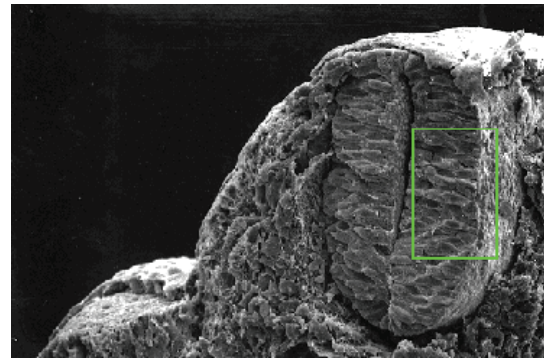
NCCs are derived from ectoderm and originate as neurulation proceeds in the embryo. During this process signaling between neural and non-neural ectoderm occurs which induces NCC precursors to form between the neural folds, dorsal to the neural tube (Figure IA and Figure I-B). Delamination from the neural tube occurs followed by an epithelial-to-mesenchymal transition yielding a migratory population of cells that is developmentally plastic. Ventrolateral migration occurs throughout the embryo as NCCs travel to their target destination where they differentiate giving rise to various structures such as the peripheral nervous system, facial cartilage, pericytes and melanocytes (reviewed in (31)).

Figure I. Neural crest cells arise from the dorsal neural tube and pattern the pharyngeal arches. (I-A) Dorsolateral view of embryological day 8 (E8) embryo depicting the neural folds and tube. (I-B) Transverse sections of E9 embryo showing the neural tube, (depicted by green box). (I-C) E9 embryo showing lateral view. Pouches are pointed out with pink arrows. All images are scanning electron micrographs used with the permission of the author Dr. Kathy Sulik from the University of North Carolina Medical School website: (www.med.unc.edu/embryo_images).

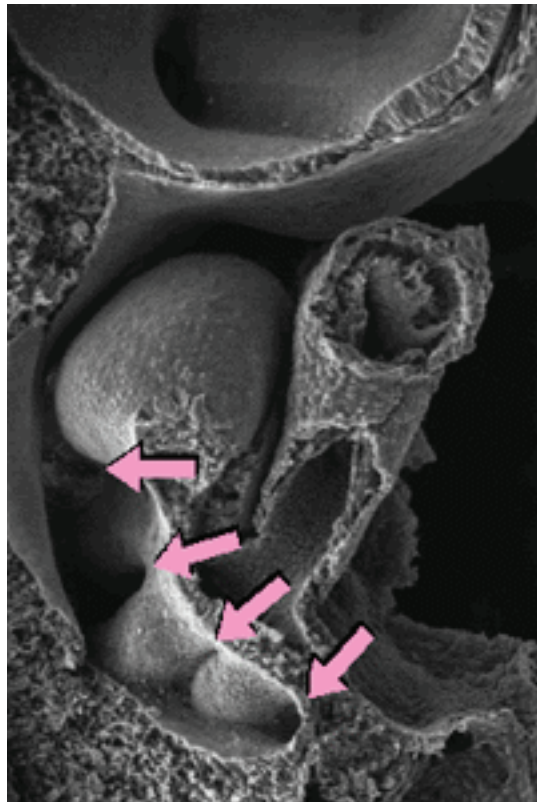
I-A



I-B



I-C



Perithymic mesenchyme is also NCC-derived as shown by quail-chick chimera experiments that used quail NCCs to generate a mesenchymal thymic capsule in the recipient chicks (reviewed in(32)). More recent work by Foster et. al. used lineage-tracing experiments to analyze the contribution of NCCs to the embryonic and adult thymus (33). NCC-specific *Wnt-1^{Cre}* and *Sox-10^{Cre}* mice were utilized to indelibly label NCCs and their progeny in a reporter assay (33). Reporter mice containing yellow fluorescent protein (YFP) under the control of a ubiquitous *Rosa26* promoter and downstream of a floxed stop cassette, were crossed to either Cre driver and YFP positive cells were analyzed in a fate mapping experiment (33). Consistent with previous reports, this study showed that developing thymic lobes became encapsulated with NCC-derived mesenchyme by E12.5, further emphasizing their role in early thymus development (33, 34). This study also demonstrated a novel role for these cells in postnatal development as NC-derived cells were found to migrate into the thymic lobes as early as E13.5 and persist throughout gestation differentiating into supportive structures of the vasculature such as pericytes and cells that express smooth muscle actin protein (33).

Robert Auerbach first described initial studies demonstrating the importance of epitheliomesenchymal interactions in thymus organogenesis in 1960 (35). Although the ability to conduct allogeneic or syngenic transplantation experiments was limited by the lack of an immunodeficient model, as they preceded discovery of the *nude* mouse, Auerbach performed a series of epithelial-mesenchymal recombination experiments which utilized the anterior eye chamber of a mouse host to decipher the morphogenic relationship between these two tissues (35). Fetal thymic epithelial

lobes stripped of mesenchyme remained hypoplastic and round in shape while those supplemented with various sources of mesenchyme grew and achieved lobulation in vitro to varying degrees depending on the source of supplemented mesenchyme (35). Subsequent experiments revealed mesenchymal cells could affect thymus growth when physically separated from the thymic epithelium by a thin Millipore filter suggesting that the interacting factors were morphogenic and soluble in nature (35).

Later studies performed by Bockman and Kirby in chick, reiterated the requirement for neural crest mesenchyme in thymic development (36). Ablation of cephalic regions of NCC prior to migration from the dorsal neural tube resulted in hypoplastic thymi that were less developed compared to control thymi (36). This study further concluded that NCC-derived mesenchyme differed from somatic mesoderm in its ability to support and sustain thymopoiesis. NCC-derived mesenchyme could induce thymic epithelial development and proliferation, which supported thymocyte maturation, whereas other sources of mesenchyme were less effective.

Studies performed by Jenkinson et. al., analyzed the effects of thymic mesenchyme on both thymic epithelial cell differentiation and proliferation (37). Thymi from E12 thymic lobes stripped of mesenchyme or epithelial isolates from E14 mice were cultured and pulsed with BrdU (37). Compared to intact lobes, proliferation of TECs in the stripped lobes decreased three-fold (37). Addition of the fibroblast growth factors (FGF) -7 and -10, rescued this proliferative defect. Both mitogenic factors were expressed almost exclusively in thymic mesenchyme by quantitative RT-PCR (qRT) analysis (37). The common Fgf-7 and Fgf-10 receptor

FgfR2-IIIb is expressed on thymic epithelial cells and mediates proliferative signals required for expansion and outgrowth of the thymic epithelium (30). This is consistent with the hypoplastic thymic phenotype observed in *FgfR2-IIIb* and *Fgf-10* deficient mice and implicates NCC-derived perithymic mesenchyme as an essential source of growth factors required for fetal TEC expansion (38). In addition, some investigators reported that NC-derived mesenchyme is required to signal TECs to express MHC class II (39). However, another study refuted this claim (37).

There is some data suggesting that NCC-derived mesenchyme is required for thymocyte maturation (40). E12 day thymic lobes cultured in the absence of mesenchyme produced significantly less thymocytes (40). Those recovered were mostly blocked at the CD4⁺CD8⁻ stage of development and only very few progressed to the SP stage, suggesting mesenchymal-dependent signals are a requirement for DN to DP progression (40). Taken together, the current data supports the notion that crosstalk between thymocytes, TECS and mesenchyme is required mutually, by each cell type, for proper maturation and function. Molecular interactions between each cell type occur dynamically throughout organogenesis to support normal thymic development.

Recent studies undertaken in our lab have demonstrated a novel role for NCC prior to E12.5 in patterning the common primordia, which will eventually give rise to both the parathyroid and thymus (41). These mesenchymal-epithelial interactions are critical in early thymus organogenesis but have yet to be fully elucidated. These early patterning events are the foundation of this dissertation project. As such they will be discussed in greater detail below.

Thymus Organogenesis

Thymus organogenesis can be divided into two distinct phases: 1. Remodeling of the pharyngeal endoderm and consequent formation of the pharyngeal pouches and 2. Patterning of the shared primordia into their prospective organ domains as evidenced by complementary expression patterns of the transcription factors Foxn1 and Gcm2 (reviewed in (42), (43)).

The thymus is derived from pharyngeal endoderm (44). During embryogenesis five pairs of segmental bulges known as the pharyngeal arches form (45), (Figure I-C). These arches develop in a cranial to caudal manner during embryogenesis and contain components, which will differentiate into specialized structures within the body, reviewed in (45). The inner lining of the arch is comprised of endoderm while the outer arch is lined by ectoderm. The core of each arch consists of mesoderm surrounded by NCC-derived mesenchyme (reviewed in (45)). During development the pharyngeal region between each arch, evaginates toward the midline forming an epithelial pouch (Figure I-C, depicted by arrows). The external ectoderm proceeds to depress in an opposing fashion forming outer pharyngeal clefts. The results of these movements facilitate interactions between endoderm, ectoderm and mesenchyme necessary for development.

Previously the thymus was thought to originate from contributions of both surface ectoderm and pharyngeal endoderm. This model was coined the “dual-origin model” and previously widely accepted (44). Studies undertaken by investigators have disproved this theory, demonstrating that only third pouch

pharyngeal (3rd PP) endoderm gives rise to the thymic epithelium interactions and contributions from the surface ectoderm are not required for the generation of a functional thymic epithelium (44). For example, studies performed by Gordon et. al. utilized ectoderm labeling experiments along with whole-embryo culture techniques to trace the contribution of cells derived from an ectodermal lineage (44). They found no labeled cells present in the thymic primordium suggesting lack of an ectodermal contribution. Furthermore, pharyngeal endoderm isolated from second and third pharyngeal pouch at E8.5-E9.0 was able to form both cTEC and mTEC subsets when transplanted under the kidney capsules of *nude* mice (44). The grafts contained an organized epithelial architecture and a TEC profile similar to normal thymi (44). TEC functionality was also assessed by the ability to support thymopoiesis (44). All thymocyte subsets were recovered in percentages comparable to wild-type (WT) thymi indicating formation of a functional thymic epithelium (44).

In mouse development the thymus and parathyroid originate from a common endodermal primordium arising from the 3rd PP (reviewed in (42)). At E11.5 the cells within the pouch are morphologically indistinguishable, however they are already fated to become either thymus or parathyroid (PT), (reviewed in (46)). We can distinguish these distinct, non-overlapping domains by the expression of the transcription factors *Foxn1*, expressed by the thymus domain and *Gcm2*, expressed by the PT domain, respectively (43). *Gcm2* is expressed by 3rd PP endoderm by E9.5 and is restricted to the dorsal anterior domain during pouch outgrowth. The adjacent posterior ventral domain expresses *Foxn1* by E11.25 (43). *Foxn1* and

Gcm2 are not required for specification of the 3rd PP but are required for thymus or parathyroid development, respectively (47, 48). *Foxn1* is expressed in thymic endodermal derivatives, and thus all TECs where it is required for their survival and differentiation (47, 49). *Gcm2* is required for expression of parathyroid-specific genes such as *CasR*, *CCL21* and *Pth* and also for survival of parathyroid progenitor cells (48).

While the exact molecular mechanisms required to establish fate-specification are not known, Griffith et. al. demonstrated that NCCs play a role in this process (43). Given that NCCs secrete growth factors required for expansion and outgrowth of the epithelium, it is not surprising that NCC-deficient models have long been reported as having a hypoplastic thymic phenotype. However, studies in our lab challenged this central dogma as NCC-deficient *Spotch* (*Pax3^{Sp/Sp}*) E12.5 fetal thymic lobes were larger than their wild-type counterparts (43). Furthermore, overall PT volume was decreased in *Pax3^{Sp/Sp}* mutants compared to control littermates (43). I confirmed this in other NCC-deficient models, specifically *Pax3^{Cre/Cre}* and *Tcof^{+/-}* mice (unpublished results). No significant changes in pouch volume, TEC proliferation or apoptosis were observed. Instead, there was a shift in the parathyroid-thymus fate-boundary such that the *Foxn1* thymus-fated domain was expanded and the *Gcm2* PT-fated domain was reduced. This result is consistent with a previous report linking thymus size to the number of progenitor cells (50). Furthermore, it suggests a novel role for NCCs prior to E12 in patterning the 3rd PP into their respective organ domains and emphasizes a requirement for migrating NCCs to mediate inductive interactions required to sustain parathyroid fate (50).

One hypothesis generated from this data predicts that NCCs may directly or indirectly influence fate by regulating the expression pattern of key transcription factors such as *Tbx1*, which is thought to act upstream of *Gcm2* (48, 51). Whether *Tbx1* truly serves as a molecular fate switch is a question that still remains to be addressed. However, the effects of *Tbx1* on thymic development will be discussed in greater detail in a subsequent chapter, as the regulatory role of *Tbx1* in thymus versus PT development is the central question addressed in this dissertation.

The thymus has not yet undergone vascularization at E11.5; however, early hematopoietic progenitors are attracted to the thymus by chemokines secreted from the developing pouch (28, 52). The *Gcm2*-dependent chemokine ligand (CCL) 21 is expressed by endoderm in the dorsal parathyroid-fated domain and binds to the chemokine receptor (CCR) 7 expressed on lymphoid progenitors (28). In addition, *CCL25*, which is in part regulated by *Foxn1*, is expressed by both PT and thymus domains in E11.5 common primordia and binds the receptor *CCR9* (28). These ligand-receptor interactions mediate thymic colonization by hematopoietic progenitors prior to thymus vascularization.

At E12.5, NCCs begin to condense around the developing primordia and form a mesenchymal capsule around the fetal thymus, (reviewed in (19)). The early thymus-parathyroid primordia detaches from the pharyngeal endoderm and by E13.5 the thymic rudiments separate from the parathyroids and begin migrating medially and caudally until they reach their final destination anterior to the heart at approximately E14.5 (reviewed in (19)). Separation of the common primordia and migration of the thymic lobes is mediated, at least in part, by NCCs (53).

Establishment of an organized functional thymic vasculature is dependent upon signals from TECs such as VEGF (reviewed in (54, 55)). Endothelial cells enter the developing thymus around E14 and become organized into a vascular network that will later function as both an entry and exit site for thymocytes and mature T-cells, respectively, (reviewed in (19)).

Molecular mediators of 3rd PP development and thymus organogenesis

The initial stages of thymus organogenesis begin with formation and positioning of the pharyngeal arches and pouches. Previous analysis of mouse models deficient in transcription factors implicated in organ patterning, have revealed a role for these factors in early thymus organogenesis. However, how these signals are integrated into a transcriptional network that functions to support pouch formation and initial thymic development is unclear. Loss of the genes discussed below may result in thymus aplasia, hypoplasia or ectopia. However, their precise roles in thymic organogenesis is complicated by their pleiotropic effects on other aspects of embryonic development.

The transcription factor *Hoxa-3* is thought to play the earliest role in specifying the 3rd pouch PP and initiating thymus and PT formation (56-58). Mice harboring a mutation in *Hoxa3* are characterized by numerous pharyngeal defects, lack parathyroids and are athymic (57). *Hoxa-3* is expressed in both 3rd PP endoderm and in NCC mesenchyme at E10.5, however only its endodermal expression is thought to be required for 3rd PP specification and formation, as mice with a NCC-specific deletion of *Hoxa-3* initially develop normally patterned 3rd PPs but

separation of the common primordia does not occur and there is a failure of organ migration, (reviewed in (58)). *Hoxa-3* is expressed in the pharyngeal endoderm at E10.5 and persists in the TEC compartment during later stages of organogenesis (reviewed in (58)). TEC-specific deletion of *Hoxa-3* after pouch formation and specification caused no apparent defects in TEC development (reviewed in (58)), suggesting that *Hoxa-3* function in thymus may be limited to an early window in development.

While the direct downstream targets of *Hoxa-3* are not yet known, potential effectors of its function include the transcription factors *Pax-1* and *Pax-9*, which are both expressed throughout the pharyngeal pouches ((59, 60) also reviewed in (19)). Knockout mice for *Pax-1* or *Pax-9* develop hypoplastic thymi that range in severity, with *Pax-9* null mice having the most pronounced defects (reviewed in (58)). Given their overlapping pattern of expression and structural similarity, it has been suggested that these factors play functionally redundant roles in the pharyngeal endoderm, although analysis of thymic development in compound mutants has yet to be performed. A redundancy in gene function is a likely explanation for the failure of either null model to precisely phenocopy *Hoxa-3*^{-/-} thymic defects. Studies performed in the Manley lab analyzing development in *Hoxa-3*^{+/-}, *Pax-1*^{-/-} mice have shown impaired TEC differentiation, proliferation and survival resulting in significant thymus hypoplasia (59, 60). In addition, these mice fail to develop normal parathyroid glands as a consequence of their inability to sustain normal *Gcm2* expression (59). These data reveal that the phenotype found in *Pax-1* null mice is enhanced by the loss of a single copy of *Hoxa-3*, suggesting that these factors

interact to regulate development of the 3rd PP (59). Compound homozygous *Pax-1/Pax-9* null mice have a normal expression pattern of *Hoxa-3* in the endoderm and mesenchyme further implicating its upstream effector position in these tissues (61).

Additional downstream mediators of *Hoxa-3* signals include *Eya-1* and *Six1/4* (61). *Eya-1* is a transcriptional co-activator expressed in pharyngeal endoderm, ectoderm and mesenchyme (61). Expression of the drosophila homolog *Six-1* is similar to that of *Eya-1* except it is not expressed in derivatives of the fourth pouch. (61) Both factors have been found to physically interact during development and play an indispensable role in thymus and parathyroid organogenesis, as null mutations of either *Six-1* or *Eya-1* result in thymus and parathyroid aplasia (61).

Six-4 is also a member of the *Six* family of transcription factors and is closely related to *Six-1*. Both *Six-1* and *Six-4* have been found to have synergistic roles in regulating genes expressed in the 3rd PP (61).

Eya-1 null mice are blocked at early stages of thymus development and fail to express detectable levels of either *Foxn1* or *Gcm2*; however, *Hoxa-3* expression is preserved and expression of *Pax-1/9* from E9.5-E10.5 was not altered (62). Xu et. al., describe a reduction in *Six-1* expression in *Eya-1* homozygous null mice in regions where the two genes have overlapping patterns of expression suggesting a requirement for *Eya-1* in *Six-1*-dependent tissues (62). *Six-1*^{-/-} mice express reduced levels of *Foxn1* and initiate *Gcm2* within the 3rd PP but fail to sustain its expression. *Hoxa-3* expression however is not altered in either single (*Six-1*^{-/-}) or double (*Six-1*^{-/-}, *Six-4*^{-/-} and *Six-1*^{-/-}, *Eya-1*^{-/-}) mutants suggesting it lies genetically upstream of these factors (62). In addition normal *Eya-1* expression has been

observed in *Six-1*^{-/-} mice (61). Taken together these data suggest a model in which *Eya-1* initiates early stages of patterning, downstream of *Hox-3*, and subsequently promotes the expression of *Six-1/4* to maintain this developmental blueprint.

The direct molecular mechanisms by which *Eya-1* and *Six-1/4* act to regulate *Foxn1* and *Gcm2* expression and patterning in the 3rd PP are unclear. However several recent developmental clues have emerged. *Tbx1* and its downstream target *Fgf8* appear to be initially expressed independently of *Six-1/4* (63). Although *Tbx1* and *Fgf8* expression are reduced in the 3rd PPs of *Six-1/4* homozygous null mice, this may be due to secondary defects in pouch formation as investigators have observed an overall smaller 3rd PP(61). Studies analyzing *Eya-1* null mice showed reduced expression of *Tbx1* and *Fgf8* as well as a complete loss of the Wnt glycoprotein Wnt-5b, a potential upstream regulator of *Foxn1* in the 3rd PP (63). This suggests some of the morphogenesis defects observed are at least in part mediated through regulation of these factors. A clear understanding of this transcription factor network is complicated by the fact that *Eya-1 null* mice fail to form a shared thymus-parathyroid primordia preventing a detailed analysis of gene regulation during later times in development (62, 63). Absence of shared thymus-parathyroid primordia limits the conclusions that can be drawn considering the profound consequences that occur due to loss of this structure. Clearly, the initial molecular events involved in specifying the 3rd PP are necessary for formation of the shared organ primordia. However it is difficult to pinpoint the requirement for these genes in an exact cell type(s) for the purposes of correlating gene deficiencies with specific defects as almost all of these factors are found in multiple cell types each of which participate

in inductive interactions responsible for influencing cell fate decisions and organogenesis.

Another molecular player implicated in patterning of the pharyngeal endoderm and thymic development is the morphogen Sonic hedgehog, Shh. Shh is a secreted glycoprotein that can migrate distances from 80-300µm, exerting its effects in a concentration-dependent manner. The Shh pathway is activated when Shh ligand binds to the twelve-pass transmembrane protein Patched (Ptc). When Ptc is not bound to Shh ligand it represses the adjacent transmembrane receptor Smoothed (Smo), the Shh signal transducer. Binding of the Shh ligand to Ptc releases this repression and allows the *Gli* family of transcription factors Gli1-3 to translocate into the nucleus where they can exert their activity on downstream Shh-responsive target genes.

Shh and its receptor *Ptc* are expressed in a restricted manner within the pharyngeal endoderm and arch mesenchyme (51). *Ptc* is up-regulated during activation of the Shh pathway and is therefore used as readout of Shh activity. At E10.5-E11.5 *Shh* expression is found throughout the pharyngeal endoderm in 1st and 2nd PPs but is absent from the 3rd and 4th PPs (51). At the same time *Ptc* is expressed not only throughout the first and second arches and surrounding mesenchyme, similar to its ligand Shh, but also in the distal tips of the 3rd PP endoderm where *Shh* expression is absent (51). This suggests that while the dorsal anterior region of the 3rd PP does not produce Shh ligand it remains competent to respond to gradients of Shh that are produced by other cells types.

Interestingly, E11.5 *Shh* null mice lack expression of *Tbx1* and, similar to *Spotch* mice, have an expansion of the thymus-fated *Foxn1*-domain in the 3rd PP (51). This expansion however was more pronounced extending throughout the organ primordia and into the pharyngeal region (51). *Gcm2*-expression was completely lacking from E10.5 onwards eventually resulting in an aparathyroid phenotype (51). Studies by previous investigators have shown *Shh* regulates expression of *Tbx1* in the pharyngeal endoderm through transcriptional activation of the transcription factors *Foxa2* and *Foxc1/2* (64, 65).

The Role of Tbx1 in 3rd PP formation and fate determination

The transcription factor *Tbx1* is required for development of the pharyngeal apparatus and is most commonly investigated in the context of the several syndromes associated with deletions in human chromosome 22q11.2, (reviewed in (66)). DiGeorge's syndrome (DGS) and velocardiofacial syndrome (VCFS) result from such deletions and arise in 1:4000 live births (reviewed in (66)). The majority of affected individuals have a hemizygous deletion that ranges in size from 1.5-3kb and affects 23-35 genes, including *Tbx1* (reviewed in (66)). Individuals affected by either syndrome display common defects such as thymus aplasia or hypoplasia, craniofacial abnormalities, hypoparathyroidism and cardiac abnormalities (reviewed in (67)). These disease components vary in presentation and severity and a specific phenotype does not coincide with known deletions, as even individuals with the same deletion can vary drastically in the defects they present (reviewed in (66)). This variation is thought to be mediated, at least in part, by genetic modifiers, which

either restrict or enhance the phenotype (reviewed in (66)). A clear understanding and identification of these factors has yet to be obtained; however it is postulated that *Fgf8* and the retinoic-acid-signaling pathway may be involved (68-70).

Tbx1 belongs to the T-box family of transcription factors, which includes over twenty members each containing a common DNA binding sequence referred to as a T-box, (reviewed in (71)) . Expression of *Tbx1* in the developing embryo is found in the pharyngeal endoderm, and arch mesenchyme but not in NCCs, (reviewed in (58)). Initially at E9.5 *Tbx1* is expressed throughout the 3rd PP but by E10.5 it becomes restricted to the dorsal parathyroid-fated domain and is turned off in the ventral thymic-fated domain (reviewed in (19)). Mice harboring homozygous mutant alleles of *Tbx1* rendering it functionally null are characterized by athymia, lack parathyroids and exhibit severe cardiac abnormalities resulting in late embryonic lethality (72). Heterozygous mice are viable but display milder cardiac abnormalities associated with DiGeorge/VCF, owing to a reduction in gene dosage (72, 73). These defects widely overlap those observed in patients with the human syndromes leading to the widely held belief that *Tbx1* plays a direct role in promoting thymus organogenesis.

Early work by Jerome et. al., identifying *Tbx1* as a major candidate gene responsible for many of the DiGeorge/VCF phenotypes, showed that *Tbx1* is required for formation of pharyngeal pouches 2-4 and therefore also for formation of the organs and tissues they later give rise to (72). Temporal and tissue-specific deletion of *Tbx1* in the pharyngeal endoderm has been achieved by generating *Foxg1*^{Cre/+}, *Tbx1*^{flox/null} mice (74). The transcription factor *Foxg1* is expressed

throughout the pharyngeal endoderm early in mouse development (75). *Foxg1*^{Cre/+}, *Tbx1*^{flox/null} conditional mice show a lack of *Tbx1* expression by E9.5 in the pharyngeal pouches and endoderm (74). The resulting phenotype observed was indistinguishable from *Tbx1*^{-/-} mice suggesting *Tbx1* is required by the pharyngeal endoderm for pouch formation in a cell-autonomous fashion (74).

Interestingly, conditional null mice were also found to have muscular and skeletal defects attributable to defects in proper NCC-migration and consequently development of these plastic cells into their prospective structures (74). This implicates a non-cell autonomous role for *Tbx1* in NCCs. It is postulated that NCC-specific defects observed in the pharyngeal endoderm and its derivatives occur secondary to abnormalities that arise as a failure of pouch formation. Although NCCs do not express *Tbx1*, inductive interactions from the pharyngeal endoderm are required for their migration and distribution throughout the embryo (72, 76, 77). Studies using a genetic approach to specifically delete *Tbx1* in mesodermal mesenchyme (non-NCC derived) have also found a similar requirement for *Tbx1* in mediating reciprocal interactions for the mutual development of both cell types and remodeling the pharyngeal endoderm (77). Thus, *Tbx1* is genetically pleiotropic, and functions dynamically in different cell types that cooperate in proper formation and outgrowth of the pharyngeal apparatus.

In addition, *Tbx1* function also varies temporally and plays different roles depending on developmental stage and context. This has been demonstrated by *in vivo* experiments in which timed deletions of *Tbx1* were performed at various gestational ages (78). In short, *Tbx1* deletion was achieved by generation of the

drug-inducible conditional mouse model, *Tbx1*^{flox/+}, *TgCAGG-CreER*TM, in which site-specific activation of the Cre recombinase occurs upon injection of tamoxifen resulting in excision of a *Tbx1*-coding exon (78). Deletion of *Tbx1* at E7.5 resulted in a phenotype that was identical to that observed in homozygous *Tbx1* null mice, (abnormalities of the aortic arch, cardiac outflow tract, development and aplasia of the thymus and aberrant formation of the palate) (78). Injection of mice with tamoxifen one day later, E8.5, resulted in a milder phenotype (78). Pharyngeal arch arteries of the 4th PP, which later give rise to regions of the aorta, subclavian and carotid arteries in the adult heart, were only mildly hypoplastic or normal (78). These outflow tract abnormalities occurred to a lesser degree upon deletion at E9.0-E9.5 implying a time-sensitive developmental window through which *Tbx1* acts to pattern the 4th PP arteries (78).

Interestingly, normal thymus formation required *Tbx1* expression prior to E9.5, preceding development of the primordia (78). This suggests a model in which thymic development requires the establishment of segmented pharyngeal arches and pouches, which in turn require expression of *Tbx1*. Loss of *Tbx1* at E10.5, a time during which outgrowth of the 3rd PP normally occurs, was reported to impair formation of the 3rd PP and therefore, result in a hypoplastic thymus (78). In addition, *Tbx1* positive cells were found to contribute to a small percentage of cells within the late fetal thymus, however the authors did not elaborate on the identity or precise contribution of these cells (78).

This suggests a model for thymus organogenesis in which initial patterning of

the pharyngeal endoderm and subsequent formation of the 3rd PP is orchestrated through a *Hoxa3-Pax-1/9-Eya-1-Six-1/4* transcription factor network. Subsequent patterning of the 3rd PP into organ-specific domains is required and mediated by *Shh*-dependent activation of *Tbx1*, a candidate master regulator of patterning events in the 3rd PP. *Shh* regulates *Tbx1* expression in the pharyngeal endoderm and is required for expression of *Gcm2* and thus establishment of parathyroid identity (51, 64). *Gcm2* null mice lack parathyroids but have a normal expression pattern of *Tbx1* at E10.5 in the 3rd PP, suggesting an upstream role for *Tbx1* in maintaining *Gcm2* expression. Taken together, the following signaling cascade emerges for establishment of normal patterning events in the 3rd PP. *Shh* regulates *Gcm2* expression through *Foxa2/Foxc2*-dependent activation of *Tbx1* in the pharyngeal endoderm. While we propose that *Tbx1* is required for the establishment of parathyroid identity in the 3rd PP, we speculate that it is not permissive for normal thymic maturation.

It is possible that *Tbx1* expression in the 3rd PP could play a role in development that promotes thymic organogenesis. However, data obtained from the Manley and Richie labs as well as data presented in later chapters of this dissertation, contradict this documented prediction and support the notion that *Tbx1*, while initially required for the development of the pharyngeal pouches, promotes the establishment of parathyroid identity in the 3rd PP and must be down-regulated in the ventral-posterior thymus fated domain at E10.5 for normal thymus organogenesis to occur. In order to test the hypothesis that *Tbx1* expression must be down-regulated in the ventral-thymus fated domain for normal thymus

development to occur, we generated *Tbx1* inducible mice that activated and sustained *Tbx1* expression early in embryogenesis in all *Foxn1*-expressing cells, therefore in all TECs, and subsequently investigated thymic development.

Materials and Methods

Generation of mice and of embryonic tissues

Conditional *R26CAGGTbx1-GFP* mice were generated using a vector kindly provided by A. McMahon that was modified and targeted to the *R26 locus*. *Tbx1* cDNA as well as an *IRES-GFP* were inserted downstream of a *stop-floxed polA* site and under the control of a strong CAGG promoter. In the presence of Cre, recombination occurs resulting in excision of the stop cassette and conditional expression of our target gene. The modified construct was electroporated into 129 mouse embryonic stem cells and positive cells were selected for based on their ability to grow in neomycin containing media. Several clones were given to the UT Austin Mouse Genetic Engineering Facility for injection into C57Bl/6 blastocysts. Chimeric mice were generated and mated back to C57Bl/6 mice. The resulting litters were selected for based on coat color. Black mice were characterized by southern blot analysis and PCR analysis. Two founder lines positive for germ line transmission were bred and used for initial characterization. Both yielded identical thymic phenotypes when crossed with *Foxn1^{Cre}*, gifted from N. Manley (49). For the duration of the study only mice derived from a single founder were used to generate progeny harboring the conditional allele. The colony was breed back to C57Bl/6 for maintainence of the line. *R26^{iTbx1/+}* mice were set up for timed matings with *Foxn1^{Cre/Cre}* mice. The morning of a vaginal plug was considered as embryonic day 0.5 (E0.5)

Sothern Blot Analysis

This protocol was adapted from an established protocol in the lab of Dr. Mark Bedford. Mouse tails were inoculated and digested in 0.5ml of Proteinase K (10mg/ml) (Ambion) and Tail Lysis Buffer mixture (17 μ M Tris-HCl (Fischer) pH 7.5, 17 μ M EDTA (Fischer) 170 μ M NaCl, 0.85% SDS (Fischer) at 50°C until fully digested. After this, add 0.25 mLs of saturated NaCl (5-6M). Shake 200 times and chill for 10 minutes on ice. Spin in microcentrifuge at 6K for 5 minutes. Transfer 0.5mL of the upper layer to a new tube and add 1mL of 100% EtOH and mix. Spool DNA with a capillary tube. Rinse with 70% EtOH and air dry for a few minutes. Resuspend the DNA in 100 μ L of water. Cut 15 μ L of DNA (in 30 μ L volume) with EcoRV restriction enzyme (NEB labs, use 50 units of enzyme/30 μ L reaction) and digest for 3-5 hours at the appropriate temperature. Run the digest on a 0.8% agarose gel at constant voltage of 35V overnight or 50V for 8 hours. Take a picture of the gel with a ruler next to it, lining the wells to the ruler. Denature the DNA by soaking the gel in denaturing solution (1.5M NaCl/0.5M NaOH) for 30 minutes at room temperature with agitation. Neutralize the gel in neutralizing solution (0.5M Tris-HCl pH 7.5/1.5 M NaCl) for 30 minutes at room temperature while shaking. Next perform the gel transfer as follow. Wrap a piece of Whatmann 3MM paper around a piece of plexiglass and place the wrapped support inside a large baking dish. Fill the dish with 10X SSC and smooth out bubbles in the paper. Place the gel on the damp 3MM paper, making sure there are no air bubbles between the gel and the membrane. Cut the membrane to the size of the gel and float it on a solution of 2XSSC until it wets completely. Immerse the filter in 2XSSC for 2-3 minutes. Then

place the wet membrane on top of the gel and carefully remove any air bubbles between the gel and the membrane. Place a piece of dry 3MM paper that is the same size as the gel and again remove air bubbles from the wet and dry papers. Place a stack of paper towels onto of the 3MM paper. Place a glass plate on top of this stack and weight in down. Allow the transfer to proceed for about 6-24 hours. After this transfer, cross-link the DNA to the membrane by exposing the filter to UV irradiation. Generate the radioactive probe as follows using instructions from the Stratagene probe kit (Agilent Technologies). During probe labeling add 2X SSC to pre-wet the membrane. Drain and add 10mLs of hybridization buffer/ "SLURP" plus 500 μ L of 20% SDS. SLURP/Hybridization Solution: 200 mLs 50% dextran sulfate, (Amersham), 480mLs formamide deionized (Americ. Bioan), 240mLs 20XSSC, 20mLs 1M Tris-pH7.5, 10mls 100x Denhardt's, 1ml 20mg/mL herring sperm DNA (boiled 10 minutes). Incubate at 42°C for at least 15 minutes. After completion of probe labeling, add 50 μ L of salmon sperm DNA and run the probe + salmon sperm DNA over a G50 Sephadex column (Amersham). Collect the eluted sample and use 1 μ l to count over the scintillation counter. Boil the probe and the salmon sperm for 5 minutes and then place it on ice for 5 minutes. Then add the probe to the membrane + hybridization buffer and incubate overnight at 42°C. The next day wash the membranes in 50mLs of 0.5SSC/0.1% SDS at 65°C for 10 minutes each. Expose to auto-rad (BioRad) cassette.

In Situ Hybridization

Dissection tools and materials were wiped with RNase OFF (Ambion) prior to use according to the manufacturers instructions in order to avoid contamination with RNases. Slide mailers were soaked in 1M sodium hydroxide overnight, rinsed with dH₂O and autoclaved to sterilize prior to use. Embryos taken for *in situ* hybridization were collected in 1X DEPC (diethylpyrocarbonate)-treated (Sigma) 1X-phosphate-buffered saline (PBS) (Hyclone). Tissue was allowed to fix overnight in 4% paraformaldehyde (PFA)/1XDEPC PBS overnight and then dehydrated in a gradient of Ethanol/DEPC-H₂O dilutions as follows: 30, 50, 70, 80, 95, 100%. Incubations were performed at 4°C for 10 minutes. Dehydrated tissue was then paraffin-embedded and sectioned using 1X DEPC H₂O at 10µm for analysis. Sectioned slides were dried overnight in a 37°C incubator overnight. The following day slides were placed in pretreated slide mailers and de-paraffinized in Citrisolve (Fischer Scientific). Two 15-minute washes were performed using this solution. After dewaxing, slides were rehydrated using a series of EtOH/DEPC H₂O solutions as follows: 100, 95, 90, 70, 70 50 and 30%. With the exception of the first 100% wash, all washes were performed once for 2 minutes at room temperature. The first wash was performed twice, 5 minutes per wash. The last wash was then preceded by two 5-min washes in 1XPBS. Slides were re-fixed in 4% PFA/1XDEPC PBS for 20-minutes and washed twice, 5 minutes per wash in 1X PBS. This was followed by two 2-minute washes in 2XSSC and then a 30 minute incubation in Tris/Glycine buffer which is made as follows: Tris-base 12.1g/L / Glycine 7.5g/L. Sections were then placed flat on top of a humidity chamber containing 250µL with 2XDEPC SSC.

Each slide was covered with hybridization solution containing the appropriate dig-labeled riboprobe. Hybridization buffer was made as follows: 50% Formamide (Ambion), 5X SSC DEPC-treated, 50 mg/mL Heparin (Sigma), 0.1% Tween 20 (Sigma), 100 mg/ml tRNA (Sigma), 5% dextran-sulfate (Sigma), 8mM citric acid (Sigma). Probes were diluted 1/55 and an appropriate volume was applied to each slide depending on the number of tissue sections per slide (for 2 pieces of tissue a volume of 55 μ L was applied). The total volume was adjusted for slides that contained more pieces of tissue by doubling or tripling if necessary. Slides were then covered with pieces of parafilm (Fischer) that had previously been cut to size. Humidity chambers were wrapped in cellophane wrap and aluminum foil and placed in the 65°C overnight to incubate. The following day the parafilm was removed and slides were transferred to new slide mailers and washed at 65°C three times in 0.5X SSC/2% formamide for 20 minutes per wash. During the last incubation, NTE buffer (292g NaCl, 100mM Tris pH7.5, 50mM EDTA (all from Sigma)) was pre-warmed to 37°C. Slides were then washed for 15 minutes in NTE at 37°C. After this time the NTE solution was replaced with NTE containing 10mg/mL RNase A. The slides were incubated at 37°C for 30 minutes and then washed in NTE alone for 15 minutes again at the 37°C. After this, the slides were washed again in 0.5X SSC/2% formamide at 65°C. Four washes were performed for 1 hour each. Slides were then rinsed with 2XSSC DEPC-treated at room temperature for 30 minutes. Next, slides were blocked for one hour at room temperature in 1% blocking solution (Roche) diluted in MABT. MABT can be made as follows: 11.6g/L Maleic Acid (Sigma), 8.8g/L NaCl, pH to 7 and then add 0.1% Tween 20. Following this

blocking step, alkaline phosphatase-conjugated anti-Dig Fab fragments (Roche) were diluted in the 1% block/MABT at a 1:5000 concentration. Slides were placed on top of a humidity chamber as done before. 500 μ L was added to each slide and again a pre-cut parafilm cover slip was placed on top. Boxes were wrapped as previously described and left overnight to incubate at 4°C. The following day each parafilm strip was removed and the slides were washed with TBST at room temperature. TBST can be made as follows: 150mM NaCl and 10mM Tris-HCl pH 8.0, 0.1% Tween 20. One 5-minute wash was performed first, followed by one 10 minute wash, and then one 20 minute wash. This was followed by seven 1 hour washes performed at room temperature. After this time slides were incubated for 10 minutes in alkaline phosphatase buffer made as follows: 100mM Tris pH 9.5, 50 mM MgCl₂, 100mM NaCl, 0.1% Tween 20 and 0.5mg/ml levamisole (Sigma). After this incubation slides were placed on an incubation chamber and BM purple (Roche) was applied. The incubation chamber was covered in foil, placed in the dark and allowed to develop for 1-5 days. After the desired color reaction was obtained, slides were rinsed in PBST (1XPBS, .01% Tween 20) for 5 minutes 3 times and then counterstained with nuclear fast red. Slides were then mounted using Cytoseal (Thermo Scientific) for viewing.

Plasmids for generation of dig-labeled mRNA riboprobes

Both Foxn1 and Gcm2 plasmids were gifts from Dr. Nancy Manley.

Generation of riboprobes

Gcm2 plasmid was digested with the restriction enzyme NcoI (Promega) and Foxn1 AccIII (Promega) according to the manufacturers instructions. Purification of the digest was performed by phenol chloroform extraction as follows. Volume was brought to 400 μ l with 1XDEPC H₂O and 400 μ l of phenol chloroform was added. Mixing was performed by vortexing for 1 minute. Spin for 10 minutes at 14K rpm and remove top phase to a new tube. Add 400 μ l of phenol chloroform to this top layer and repeat vortex step. Spin for 8 minutes at 14K rpm. Remove the top phase and add 0.1% volume of 3M NaOH (made up with DEPC H₂O) plus 2.5 times the volume of 100% EtOH. Place this sample at -80°C for 30 minutes or more. Then spin sample at 14K rpm for 15 minutes and remove supernatant. Wash with 70% EtOH/DEPC H₂O for 5 minutes and then spin at 14K for 5 minutes. Air dry and then resuspend DNA in 15 μ l of DEPC H₂O. In vitro transcription was performed in a 20 μ l reaction with SP6 (Roche) for Gcm2 or T3 (Roche) for Foxn1 according to the manufacturers instructions. Precipitation of the product was performed by adding 1.8 μ L of 8M LiCl (made with DEPC H₂O) and 58.5 μ L of 100% EtOH. Samples were then placed at -80°C for at least 2 hours. Samples were then spun at 14k rpm for 15 minutes at 4°C. Supernatant was removed and the pellet washed in 70% EtOH/DEPC H₂O. Spinning was again performed at 14K for 10 minutes. The supernatant was removed and the pellet allowed to air dry. The probe was then resuspended in 80 μ L of DEPC H₂O, aliquoted and stored at -80°C for later use.

Preparation of adult and fetal tissue for epithelial FACS analysis

Adult thymi were dissected and prepared according to the standard protocol established in Gray et. al (79). Fetal thymi were harvested in RPMI (Fischer)/5% fetal calf serum (Hyclone). $R26^{iTbx1/+}$ thymi were pooled for digest and control thymi were digested in pairs. Both genotypes were digested in 1.5mL eppendorff tubes (BioExpress) using the collagenase/DnaseI solution referenced in Gray et. al (79). Unlike adult thymi, fetal thymi were digested for two to three 10 minute incubations only in a 37°C water bath without agitation and the collagenase/dispase digestion steps omitted. Both adult and fetal epithelial cells preparations were counted using trypan blue viability stain (Fischer) and a Countess® automated cell counter (Invitrogen). Cells were then distributed into FACS polystyrene tubes (BD Falcon) for staining.

Preparation of thymic tissue for thymocyte FACS analysis

Tissue from adult mice was dissected in 1XPBS/5% fetal calf serum and then pressed through a 70-micron cell strainer (Falcon) placed over a 50ml conical tube (Fischer) for collection. Using the plunger end of a 3ml syringe (BD Biosciences) thymi were pressed through a strainer. Strainers were rinsed with 1XPBS and the cell suspension was collected in the conical tube below. Tubes were spun down at 4°C at 1250 rpm. The supernatant was removed and the cell pellet resuspended in 1XPBS. Cells were distributed in polystyrene FACS tubes for addition of antibodies.

Antibodies used for FACS

Cells from fetal or adult thymi were stained with the following primary antibodies, anti-CD45-PerCPCy5.5 (eBioscience), anti-EpCAM-PeCy7 (Biolegend) or anti-EpCAM-APC (Biolegend), anti-CD4-eFluor-605 (Invitrogen), anti-CD8-PeCy7 (eBioscience), anti-CD80-PE (eBioscience), anti-Ly51-biotin (BD Pharmingen), anti-MHCII-Pacific Blue (Biolegend), antiCD44-APC (eBioscience), anti-CD25-Alexa488 (eBioscience), anti-CD3-biotin (eBioscience) or anti-CD3-PE-Cy5 (eBioscience), CD117-PE-Cy5 (eBioscience), CD127-PE-Cy5 (eBioscience) $\alpha\beta$ TCR-PE-Cy5 (Biolegend) $\gamma\delta$ TCR-PE-Cy5 (eBioscience), TER119-Pe-Cy5 (eBioscience), Gr1.1-PE-Cy5 (eBioscience), Nk1.1-PE-Cy5 (Biolegend). Primary antibodies were incubated for 15 minutes and cells rinsed with FACS wash buffer, (as prepared in (79)). Samples were spun at 1400 rpm for 4 minutes and the supernatant removed. Secondary antibodies were added if necessary. Secondary antibody used were: SA-qDot655 (Invitrogen). Incubation of this secondary antibody was performed in the dark for 15 minutes. Samples were then rinsed and spun as before. Cells were resuspended in 1XPBS for FACS analysis using the Arianal or Fortessa benchtop analyzer (BD). Analysis of data obtained from FACS was performed using the program FlowJo (version 9.3) by Treestar.

BrdU FACS

BrdU FACS analysis was performed in fetal thymi by injecting 300 μ l, intraperitoneally (IP), of a 10mg/mL (BD Pharmigen) stock solution into pregnant mice 7 hours prior to sacrifice. Fetal thymi were prepared using the above protocol and stained for surface antigens. After surfacing staining, samples were prepared according to the manufacturers instructions found in the Brdu-APC labeling kit (BD Pharmigen).

FACS staining of thymi

BrdU (BD Pharmigen) was injected, same concentration as above, into pregnant dams or individual mice (IP) 90 minutes prior to sacrifice. Thymic were frozen and sectioned at 10 μ M. Slides were stained according the to manufactures instructions (BD Pharmigen).

TUNEL Staining

Staining was performed on cryopreserved sections. Slides were warmed to room temperature and staining was performed according to the manufacturer's instructions in the kit (Roche) for cytopreserved tissue sections.

Immunohistochemistry

Hematoxylin and eosin staining was performed on paraffin slides sectioned at 5-10 μ M in thickness. Staining was performed as follows. Dewax sections in xylene for 2 incubations, 10 minutes each. Rehydrate tissue through decreasing ethanol

dilutions as follows: 100%, 96%, 90%, 70% for 5 minutes each. Then rinse 5 minutes in tap water. Apply Hematoxylin (Fischer) for 3-10 minutes. Rinse under running tap water until water runs clear. Apply Eosin (Sigma), dilute a 1% stock to 1:50 for use and add three drops glacial acetic acid, for 3-10 minutes. Rinse as before. Dehydrate through a rapid ethanol series as follows: 70%, 90%, 96% and 100%. Rinse in xylene (Fischer) twice for five minutes each. Coverslip with cytooseal. (ThermoScientific).

Immunohistochemistry was performed in frozen sections as follows. Warm slides to room temperature. Acetone fixation was performed for 20 minutes at 4°C, unless sections were fixed prior to sectioning. Rinse for three 5-minute incubations in TNT (Perkin Elmer) made according to the manufacturers instructions). Slides were blocked for 15 minutes using block provided in TSA kit (Perkin Elmer), prepared according to the manufacturers instructions. Primary antibodies ((1µg/µL)/tissue section in TNB) were incubated for 1-hour at 4°C and rinsed for three incubations of 5-minutes each. Secondary antibodies were diluted at ((1µg/µL)/tissue section in TNB) and applied for 30 minutes. Sections were rinsed three times for 5 minutes per wash and Dapi 1:1500 of a 1 mg/mL stock (Vector labs) was applied for 5 minutes. Slides were rinsed 3 times at 5 minutes per incubation and mounted with Vectashield (Vectashield) mounting medium. The following primary antibodies were used for immunohistochemistry without amplification by a TSA-system: K5 (Covance), K14 (Covance), UEA-Biotin (Vector), Pancytokeratin (Sigma), K8 (Troma-1), gift from Manley lab. The following primary antibodies were used with a TSA amplification kit (Perkin Elmer). MHCII

(Biolegend), Cleaved Caspase-3 (Cell Signaling), Ppar γ (Cell Signaling), PdgfR α (eBioscience), Plet-1 (Millipore). Staining of cleaved-caspase-3, Ppar γ and GFP required 4% PFA fixation of tissue prior to sectioning. Secondary antibodies applied were obtained from Jackson and include: SA-fitc, donkey-anti-rat-Texas-red, donkey-anti-rat-fitc, SA-Texas red, donkey-anti-rabbit-Texas-red, donkey-anti-rabbit-fitc, and donkey-anti-mouse-Texas-red.

Three-dimensional analysis of E11.5 pouches

Serial sections of control and $R26^{iTbx1/+}$ 3rd pouches were traced and aligned using the program Surf Driver. Three-dimensional rendering and volume analysis was also performed using this software.

Results

Chapter 1. Development of $R26^{iTbx1}$ mice and studies in embryogenesis

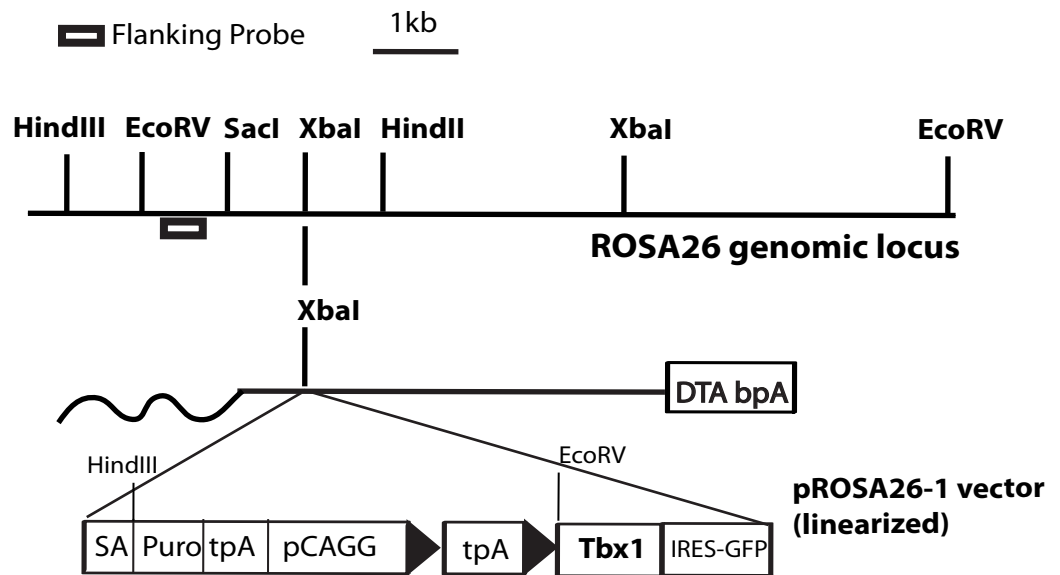
Generation of the $R26^{iTbx1}$ mouse model

We generated a conditional knock-in strain that expresses an inducible *Tbx1* allele after Cre-mediated recombination. A targeting vector for the *R26* locus was obtained from Dr. Andy McMahon and modified to permit temporal and spatial specific expression of *Tbx1* (Figure 1A). *Tbx1* cDNA was cloned downstream of a *loxP*-flanked poly-A stop cassette and under the control of a strong CAGG promoter. An *IRES-GFP* tag was inserted downstream of *Tbx1* to confirm expression.

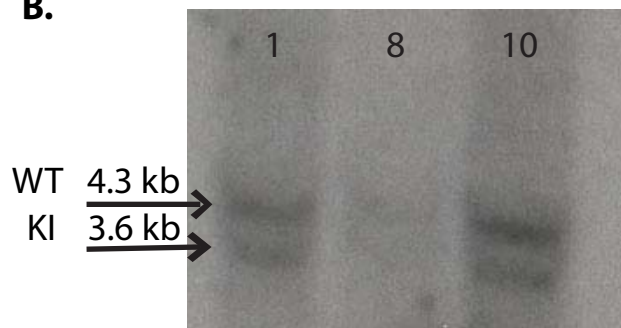
Mouse embryonic stem (ES) cells derived from a C57/Bl6 line were transformed with the modified vector and grown in the presence of neomycin containing media at the University of Texas at Austin Mouse Genetic Engineering Facility. Antibiotic resistant clones were selected for injection into Bl6.SF129 blastocysts. ES cells were analyzed post-blastocyst injection by Southern blots to assay for the presence of the conditional *Tbx1* allele (Figure 1B). Three clones were found to contain the modified vector and used for injection into blastocysts, which were then implanted into pseudo-pregnant dams for generation of chimeras. The resulting litters were analyzed and selected based on coat-color composition. We analyzed F1 founder lines to confirm germ-line transmission. Two founders contained the $R26^{iTbx1}$ allele as verified by a 5kb band obtained after enzyme EcoRV digestion and Southern blot analysis (Figure 1C). These mice were bred to C57Bl/6 mice for establishment of

Figure 1. Generation of $R26^{iTbx1}$ mouse strain. (A) The modified $R26$ targeting construct contains *Tbx1* cDNA under control of a strong CAGG promoter and a floxed-stop cassette. An IRES-GFP tag is located downstream of *Tbx1*. (B) Southern blot analysis of post-blastocyst injected ES cells containing 4.3 and 3.6 kb bands corresponding to $R26^{+}$ and $R26^{iTbx1}$ alleles, respectively. (C) Southern blot analysis of F1 mice confirms the presence of a 5kb wild-type (WT) band and /or a 14kb $R26^{iTbx1}$ band. (D) PCR analysis of genomic tail DNA from F1 progeny results in a 298bp WT band alone or in addition to a 456bp $R26^{iTbx1}$ corresponding to WT or heterozygous progeny, respectively.

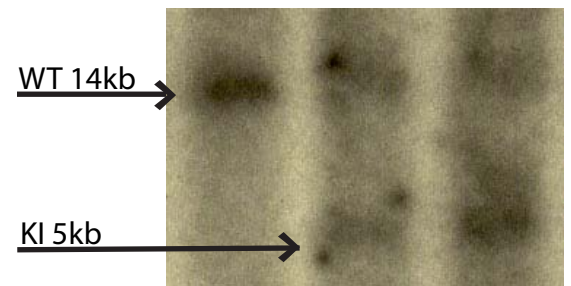
A.



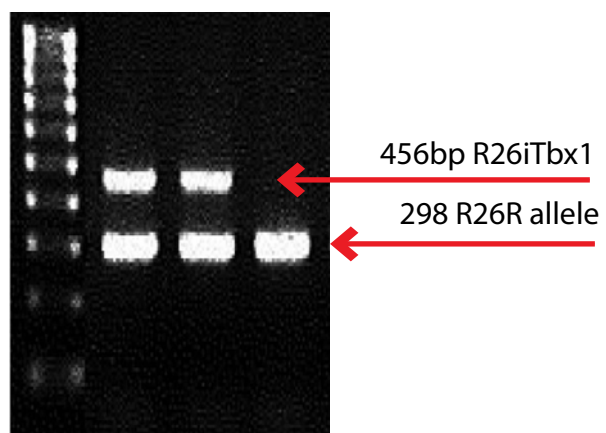
B.



C.



D.

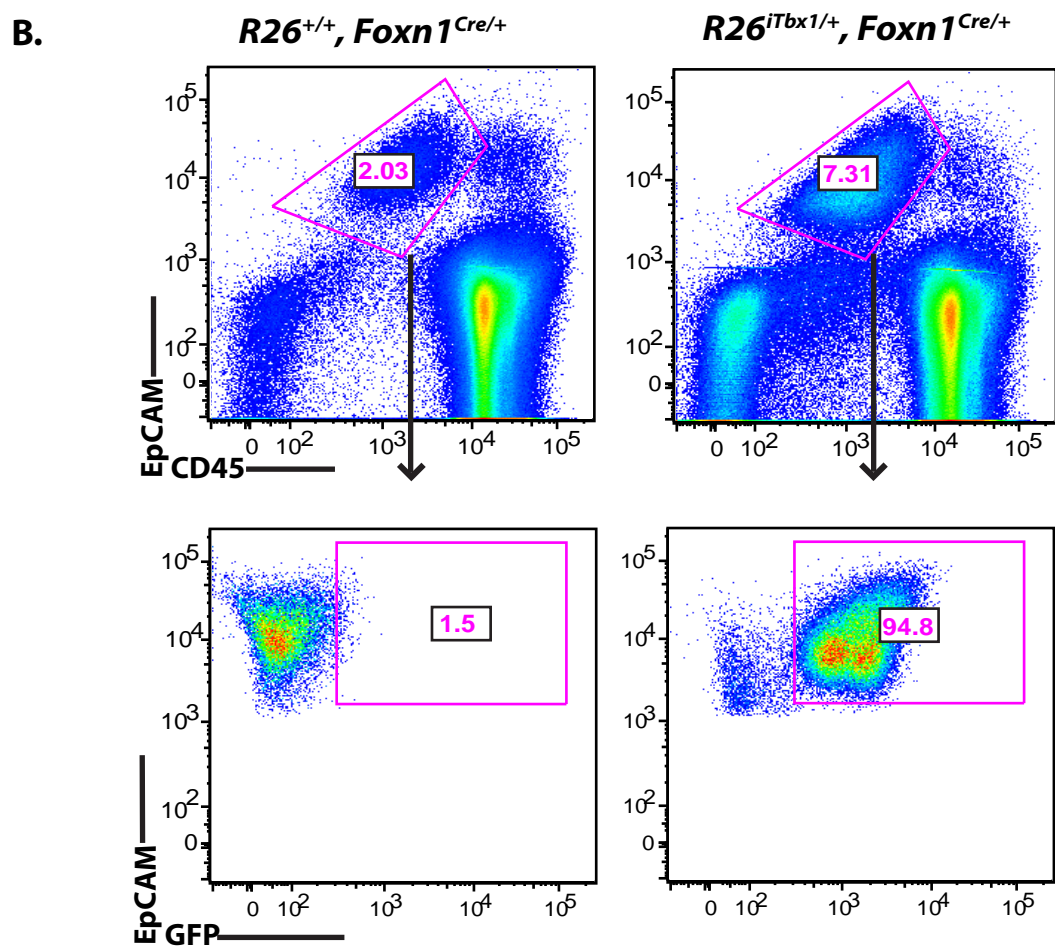
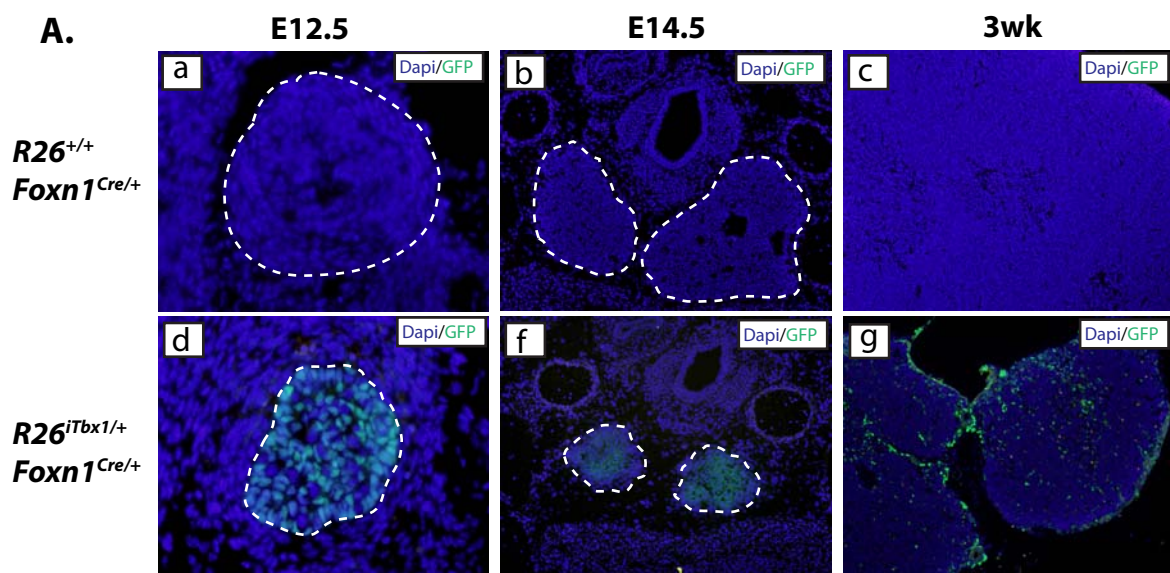


two separate lines, which later were confirmed to result in comparable thymic phenotypes when crossed with *Foxn1*^{Cre/Cre} mice (unpublished observation). After this initial observation, one line (Line 1) was chosen for the duration of this study and all experiments were performed using progeny derived from this founder. Mice were genotyped by PCR analysis of tail DNA. DNA from wild-type (WT) mice yielded a single 298 base pair (bp) band while heterozygous mice for the *R26*^{iTbx1} allele yielded one WT 298bp band and also a 456bp indicating the presence of our conditional allele (Figure 1D).

***Expression of Tbx1 in R26*^{iTbx1/+}, *Foxn1*^{Cre/+} mice**

Foxn1 is expressed in the thymic-fated ventral domain of the 3rd PP by E11.25 and, thus by all endodermal progenitors which give rise to the thymic epithelium (reviewed in (19)). *Foxn1*^{Cre/+} mice generated in the lab of Dr. Nancy Manley have been used to achieve spatial and temporal activation of *loxP*-flanked target genes (49). When crossed to *R26*^{LacZ/+} reporter lines staining of beta-galactosidase at E12.5 was found throughout the thymic epithelium. In order to activate *Tbx1* in the ventral-thymus fated domain and sustain expression in all TECs we crossed *R26*^{iTbx1/+} mice to *Foxn1*^{Cre/Cre} mice. Temporal and tissue specific expression was analyzed by anti-GFP staining performed at E12.5, E14.5, E17.5 and 3 wks of age (Figure 2). GFP expression was observed as early as E12.5 in embryogenesis. Furthermore, GFP expression was restricted to fetal thymic lobes and later persisted in the adult thymus but was absent in age matched littermate controls. For the remainder of this dissertation *R26*^{iTbx1/+}, *Foxn1*^{Cre/+} mice will be referred

Figure 2. *Foxn1^{Cre}* induces *R26^{iTbx1}* expression in thymus epithelial cells. (A) GFP expression in *R26^{+/+}*, (a-c) and *R26^{iTbx1/+}* (d-f) thymi at indicated ages. (B) FACS analysis of cells from E17.5 pooled thymic lobes. In the upper panel anti-EpCAM APC conjugate detects TECs and anti-CD45-PerCP Cy5.5 detects hematopoietic cells. Arrows show the gating strategy. The percentage of cells within each electronic gate is shown on the plot.



to in the text as $R26^{iTbx1/+}$ while $R26^{+/+}$, $Foxn1^{Cre/+}$ mice will be denoted as controls or $R26^{+/+}$.

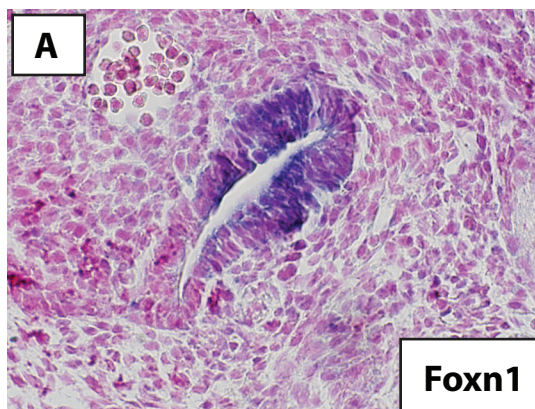
To further examine the specificity of $R26^{iTbx1/+}$ expression pooled thymi from $R26^{iTbx1/+}$ or $R26^{+/+}$ E17.5 embryos were analyzed by flow cytometry. Thymic lobes were digested with collagenase to produce single cell suspensions and stained for the epithelial-specific marker EpCAM, as well as the hematopoietic-specific marker CD45. Dead cells were gated out based on propidium iodide (PI) exclusion. GFP was expressed in $CD45^{-}$ EpCAM⁺ TECs from $R26^{iTbx1/+}$ but not control thymi. $CD45^{+}$ hematopoietic cells and $CD45^{-}$ EpCAM⁻ stromal cells were GFP negative (data not shown). The FACS data is consistent with the pattern of GFP staining detected by immunohistochemistry (Figure 2 A) and was further validated by qRT-PCR analysis (see Figure 10). Sorted cells from E14.5 and E17.5 thymi show *Tbx1* expression in $R26^{iTbx1/+}$ TECs but not in TECs from control thymi (Figure 10, later section). Furthermore, *Tbx1* expression was not present in $CD45^{+}$, EpCAM⁻ cells or $CD45^{-}$, EpCAM⁻ cells from either genotype (data not shown).

Patterning in the $R26^{iTbx1/+}$ 3rd PP is conserved at E11.5

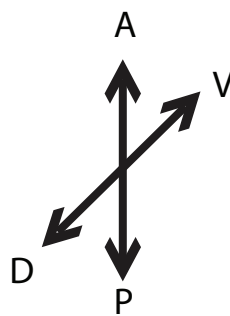
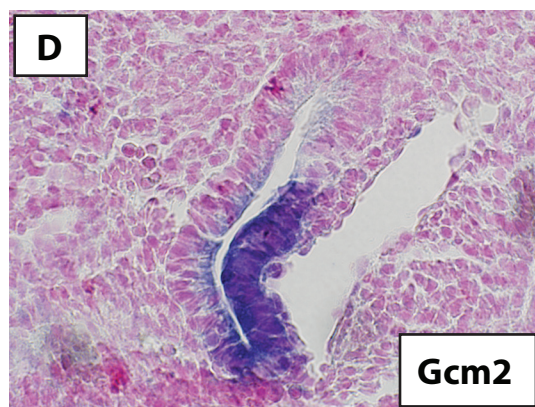
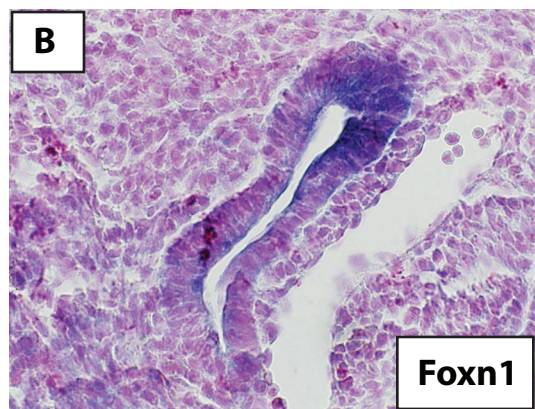
In situ hybridization (ISH) for *Foxn1* and *Gcm2* was performed to analyze patterning in the 3rd PP at E11.5. Consistent with patterning found in control littermates, the 3rd PP in $R26^{iTbx1/+}$ embryos showed normal ventral-anterior expression of *Foxn1* as well as normal dorsal-posterior expression *Gcm2* (Figure 3). Distinct non-overlapping boundaries between the thymus- and PT-fated domains were present in both genotypes with no obvious expansion or reduction in either

Figure 3. *In situ* hybridization of *Foxn1* and *Gcm2* expression in the 3rd PP. Sagittal sections of E11.5 *R26^{iTbx1/+}* and *R26^{+/+}* embryos were analyzed for *Foxn1* (A,B) and *Gcm2* (C,D) expression. All images were captured at 40x. Spatial orientation is depicted by the arrows below. n = 2

R26^{+/+}, Foxn1^{Cre/+}



R26^{iTbx1/+}, Foxn1^{Cre/+}



domain (Figure 3). To determine whether any defects in pouch formation were present, overall pouch volume was measured by tracing serial sections using Surf Driver 3-D reconstruction software. Generation of 3-dimensional models revealed no significant difference in pouch volume between $R26^{iTbx1/+}$ and control embryos (data not shown). These data suggest that establishment and patterning of the 3rd PP is intact in $R26^{iTbx1/+}$ embryos and that the initial stages of thymus and parathyroid organogenesis are not impaired.

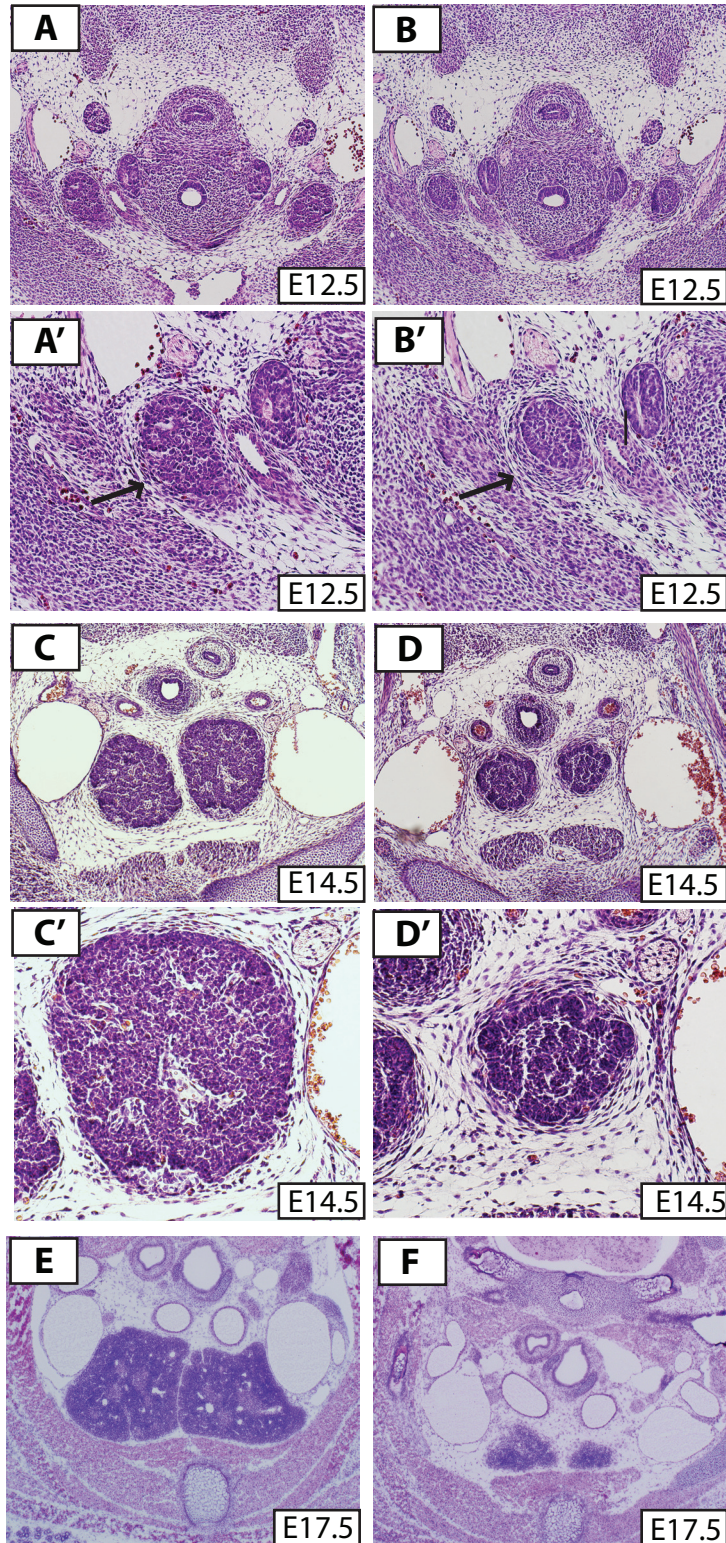
Fetal thymic lobes are hypoplastic with abnormal morphology

Timed matings between $R26^{iTbx1/+}$ and $Foxn1^{Cre/Cre}$ lines were performed and the resulting litters sacrificed at various developmental stages for histological analysis. Expected genotypes were present at normal Mendelian ratios indicating there was no embryonic lethality from inducing ectopic *Tbx1* expression. Hematoxylin and eosin (H&E) stained anterior sections were obtained from control and $R26^{iTbx1/+}$ embryos at an anatomical location where fetal lobes are normally found at this developmental stage. We observed a hypoplastic thymic phenotype as early as E12.5 in $R26^{iTbx1/+}$ embryos compared to control littermates (Figure 4 A-B). In addition, a prominent, expanded mesenchymal capsule was found to encase the $R26^{iTbx1/+}$ lobes. We subsequently confirmed that these mesenchymal cells are of NC origin. (Figure 4 B' and D', Figure 22). During normal thymus organogenesis, the thymus rudiments are surrounded by a NC-derived mesenchymal capsule as seen in A' (Figure 4). The NC-derived capsule thins during the later stages of

Figure 4. Embryonic $R26^{iTbx1/+}$ have a progressive hypoplastic thymic phenotype. (A-E) Transverse sections of paraffin embedded embryos stained with Hematoxylin and Eosin (H&E). (A-B) Control and $R26^{iTbx1/+}$ sections, respectively, at 100x lobes at E12.5. (A'-B') 200x images of the corresponding lobes, note the mesenchymal capsule is denoted with arrows. (C-D) Transverse sections of control (C) and $R26^{iTbx1/+}$ (D) E14.5 thymic lobes taken at 100x. (C'-D') 200x images of the above lobes. (E-F) E17.5 sections of control (E) and $R26^{iTbx1/+}$ (F) thymic lobes at 4x. In all images dorsal is up and ventral is down. (n = greater than 3 individuals per genotype analyzed)

R26^{+/+}, Foxn1^{Cre/+}

R26^{iTbx1/+}, Foxn1^{Cre/+}



organogenesis as NCCs invade the thymic lobes and become pericytes that support the thymic vasculature. In contrast, the expanded perithymic mesenchymal capsule remains prominent in $R26^{iTbx1/+}$ thymi even at E17.5 (Figure 22).

The hypoplastic phenotype observed at E12.5 appeared progressive, as severity of this thymic defect increased during ontogeny (Figure 4). A disruption of normal thymic morphology was increasingly aberrant with developmental stage as thymic lobes became more lobular in appearance and failed to retain normal thymic morphology (Figure 4 D', F).

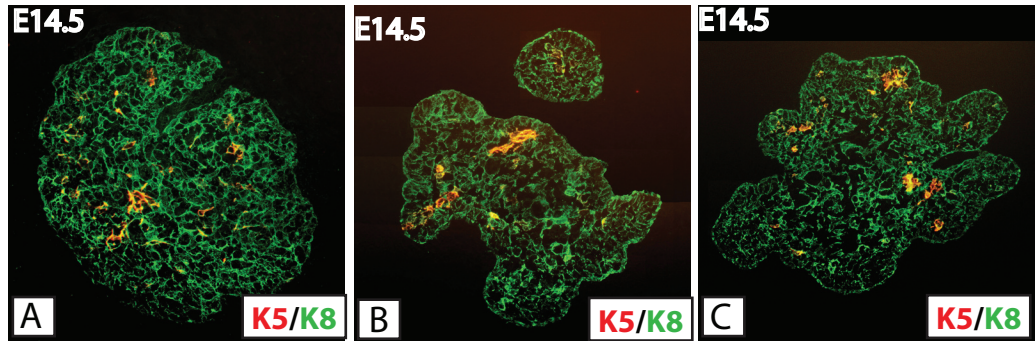
$R26^{iTbx1/+}$ fetal TECs are impaired in differentiation

H&E staining primarily shows the localization of developing thymocytes within the thymic lobes and does not readily detect epithelial cells in the microenvironment. To visualize TECs, we stained for markers of TEC differentiation, such as K5, K8, K14 and UEA1. At E14.5, control thymi consisted predominantly of $K8^+$ cortical TECs (cTECs) (Figure 5 A). Small pre-medullary islets that costained with K5 and K8 were dispersed throughout the thymic lobes (Figure 5 A). This is consistent with work previously published by our lab describing development of the epithelium (21). In contrast, $R26^{iTbx1/+}$ thymic lobes were highly lobulated with some thymi containing small adjacent epithelial regions that appeared to have detached from the main lobe (Figure 5 B). $K8$ positive cortical epithelial regions were present comprising the majority of the epithelium. $K5^+K8^+$ medullary islets formed aberrantly with clusters forming near the outer sub-capsular region (Figure 5 A, B). This epithelial phenotype appeared more severe at E17.5, suggesting it may be

Figure 5. TEC organization and architecture are impaired in fetal thymi. E14.5 control (A) and *R26^{iTbx1/+}* (B-C) thymic lobes stained with K5 and K8. E17.5 control (D,F,H) and *R26^{iTbx1/+}* (E,G,I) thymi stained as indicated. Magnification x100. (A-G) ; x200 (H,I). n=2 for each genotype.

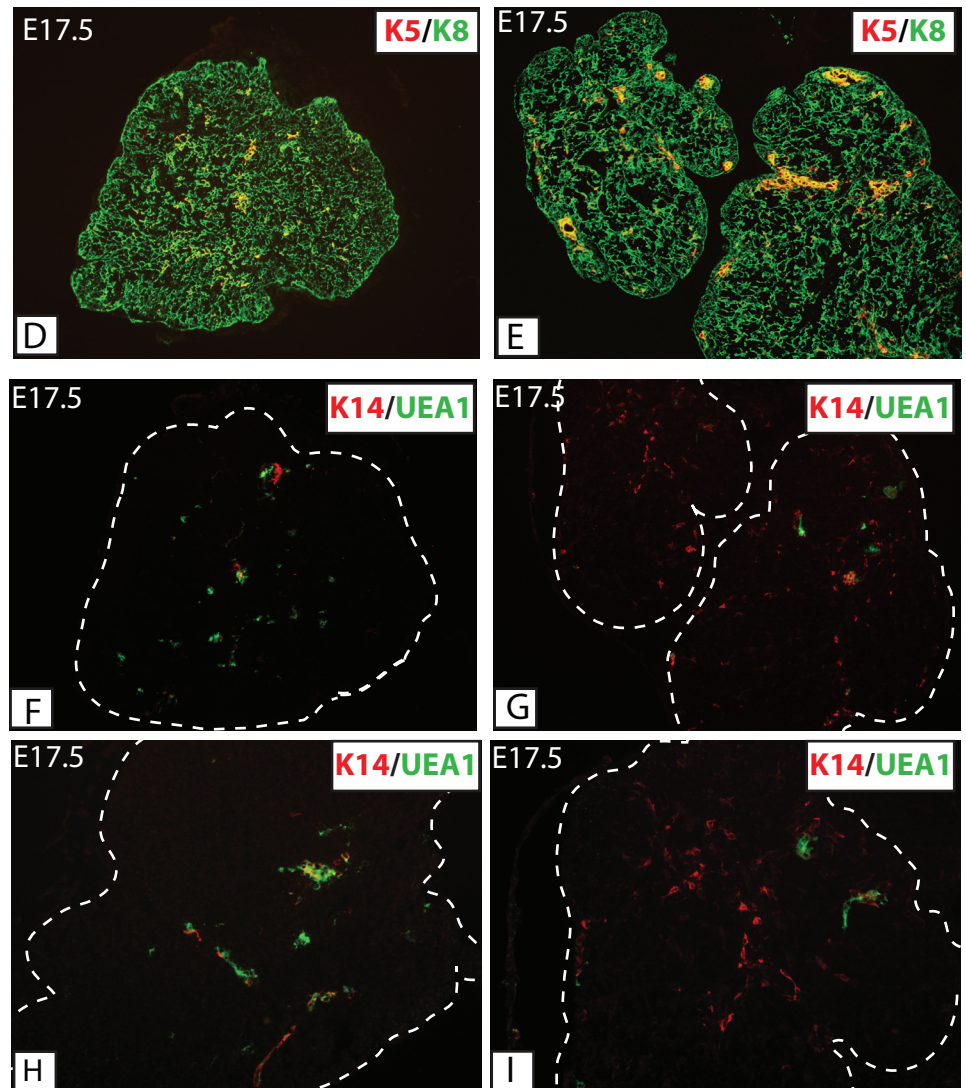
R26^{+/+}, Foxn1^{Cre/+}

R26^{iTbx1/+}, Foxn1^{Cre/+}



R26^{+/+}, Foxn1^{Cre/+}

R26^{iTbx1/+}, Foxn1^{Cre/+}



progressive with age. Control thymi retained normal thymic architecture with defined cortical and medullary subsets, expressing K5⁺ or K5⁺K8⁺ respectively (Figure 5 D). In addition the expression patterns of K14 and UEA1, (Figure 5 F and H) revealed two non-overlapping medullary populations as expected, one medullary TEC population that binds K14 and K5 but not UEA1 and another that binds K8 and UEA1 but not K5 or K14. In the *R26^{iTbx1/+}* thymic lobes, expression of both medullary markers was aberrant (Figure 5 B, C, E, G, I). An increase in K14 positive TECs appeared dispersed throughout the fetal lobes and did not appear to mark medullary populations as defined by K5 expression (Figure 5 G, I). UEA1⁺ cells appeared reduced compared to control thymi (Figure 5 G, I). Taken together, these data suggest TEC differentiation is aberrant in *R26^{iTbx1/+}* fetal thymi and thymic morphology is impaired.

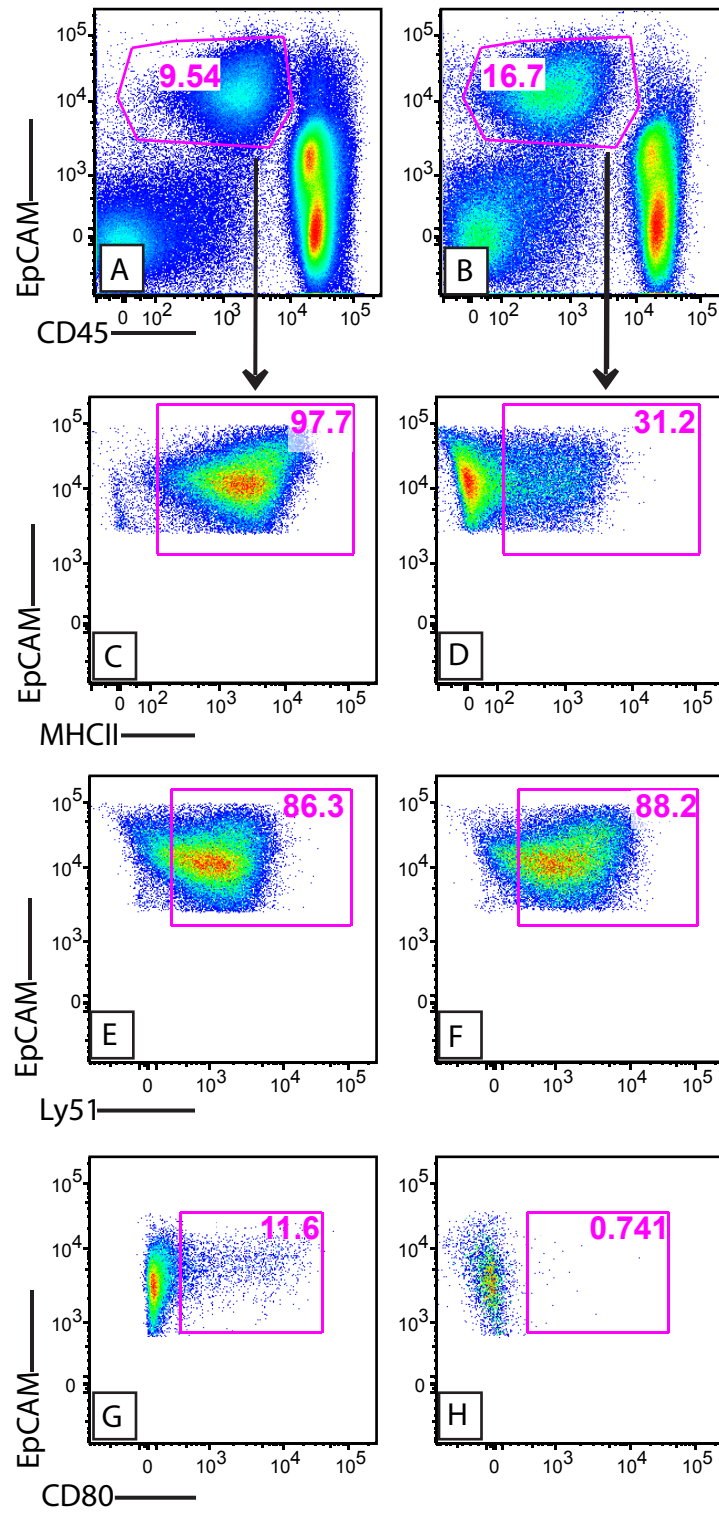
In order to further analyze TEC subsets, FACS analysis was performed on pooled cell suspensions from E17.5 thymi (Figure 6 A-D). The percentage of EpCAM⁺ TECs was increased in *R26^{iTbx1/+}* thymic lobes relative to control littermates. However, total cellularity at E17.5 was decreased by approximately 2-fold and therefore the increased percentage of TECs reflects a decrease in thymocyte numbers (mean control cellularity $1.4 \times 10^6 \pm .03$ (n=3) versus mean *R26^{iTbx1/+}* cellularity $.613 \times 10^6 \pm .04$ (n=5), p= .035, using standard t-test).

Nearly all TECs obtained from control littermates expressed MHC class II (MHCII) (97%), suggesting they are functionally competent to present antigen to developing T-cells for both positive and negative selection (Figure 6 C). In striking contrast, TECs in *R26^{iTbx1/+}* thymi were dramatically reduced in MHCII expression,

Figure 6. TEC differentiation and maturation is impaired in E17.5 $R26^{iTbx1/+}$ thymi. (A-H) FACS analysis of E17.5 pooled TECs from control and $R26^{iTbx1/+}$ thymi. EpCAM⁺ MHCII⁻ TECs (A, B) were analyzed for expression of MHC II (C, D) Ly51 (E, F), and CD80 (G, H). Percentages of each subset are on given on the FACS plot. Data is consistent with three separate sets of pooled experiments.

E17.5 *R26^{+/+}, Foxn1^{Cre/+}*

R26^{iTbx1/+}, Foxn1^{Cre/+}



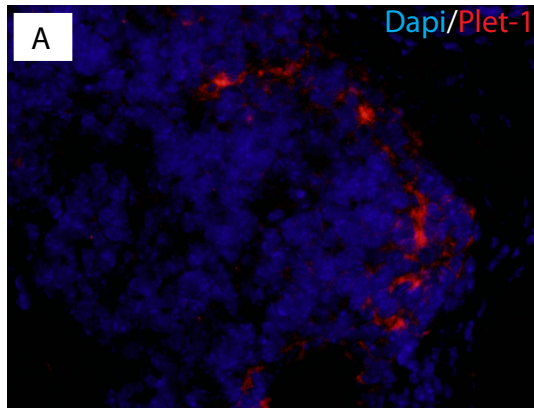
with only 31% comprising the total positive TEC population (Figure 6 D). These data are representative of three sets of pooled experiments. Expression of the cTEC specific marker Ly51 showed no obvious differences in expression between control and $R26^{iTbx1/+}$ thymi (Figure 6 E-F). CD80 is expressed on mature mTECs that express TRAs in the adult thymus. At E17.5 control TECs contain a small population of CD80 positive cells. In contrast, $R26^{iTbx1/+}$ TECs almost completely lacked any CD80 expression, suggesting a significant maturational defect (Figure 6 G-H). This data demonstrates that ectopic activation of *Tbx1* in *Foxn1*-expressing cells results in a block in TEC differentiation and a reduction in thymus cellularity.

R26^{iTbx1/+} are characterized by an accumulation of Plet-1 progenitor TECs

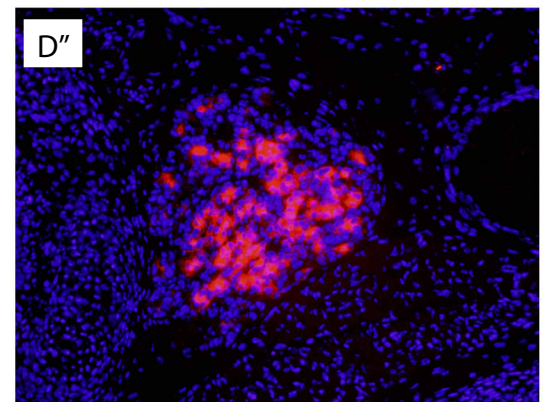
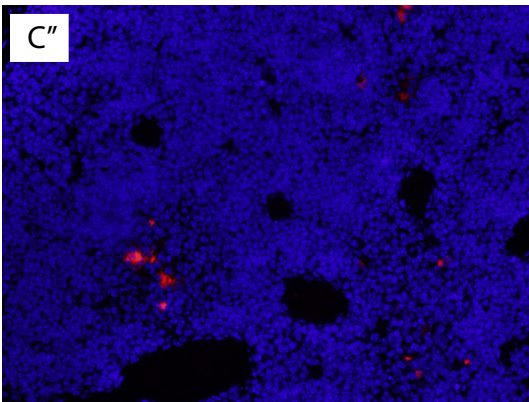
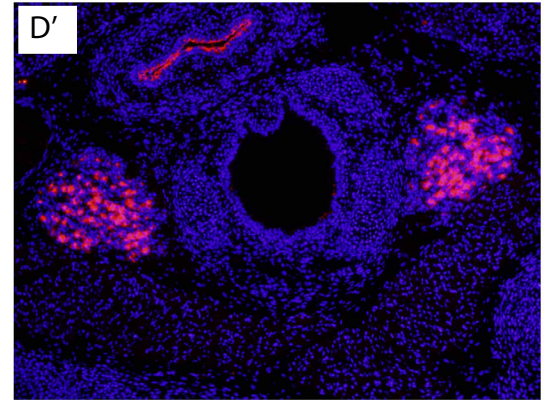
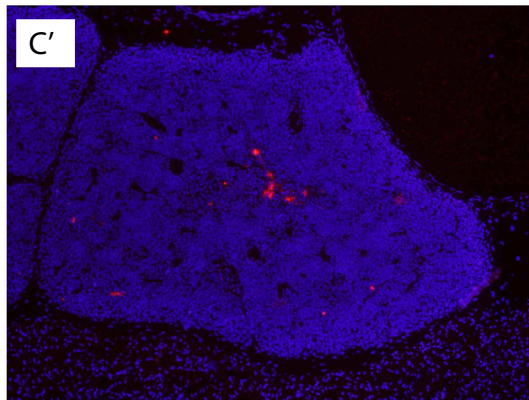
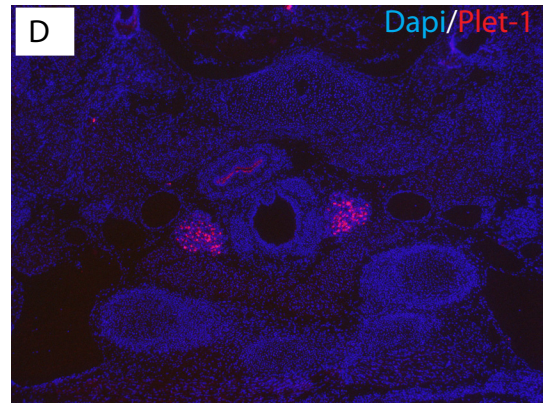
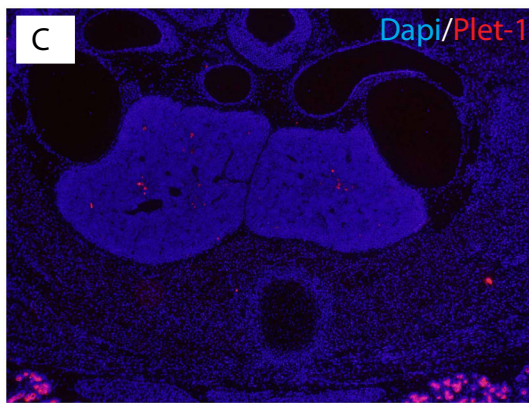
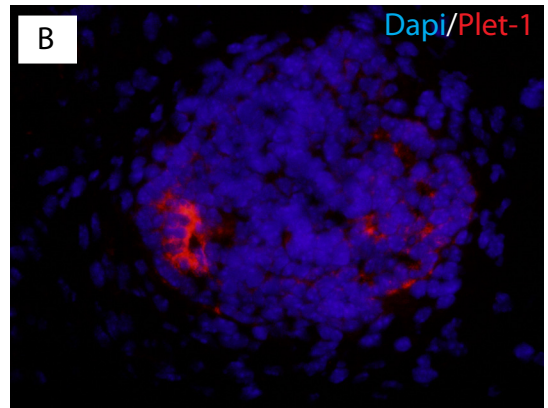
This block is further evidenced by the expression of Plet-1, a surface antigen expressed by a rare population of progenitor TECs. Plet-1 is initially expressed by a large percentage of TECs in early thymus organogenesis but its frequency decreases with developmental progression ((80) and unpublished result). Plet-1 positive TECs have also shown to be able to give rise to all epithelial cells within the thymus and also to support developing thymocytes when transplanted into a *Foxn1^{nu/nu}* host (18). Examination of E14.5 thymic lobes revealed a comparable pattern of expression between $R26^{iTbx1/+}$ and control thymi (Figure 7 A-B). In contrast, at E17.5 the percentage of Plet-1 positive cells within $R26^{iTbx1/+}$ thymi appeared dramatically increased (Figure 7 C-D”). $R26^{+/+}$ thymi contained only a few Plet-1 positive progenitors, mostly localized to the inner medullary regions, consistent with a previous report documenting normal patterns of expression at this

Figure 7. $R26^{iTbx1/+}$ thymi have an increased frequency of Plet-1+ cells at E17.5. (A-B) E14.5 Control and $R26^{iTbx1/+}$ sections stained for Dapi/Plet1 (200x) (n=3). (C-D'') E17.5 Control and $R26^{iTbx1/+}$ sections stained for Dapi and Plet-1 at (C-D) 40x, (C'-D') 10x and (C''-D'') (200x) (n=3 for E14.5 and 2 for E17.5).

R26^{+/+}, Foxn1^{Cre/+}



R26^{Tbx1/+}, Foxn1^{Cre/+}



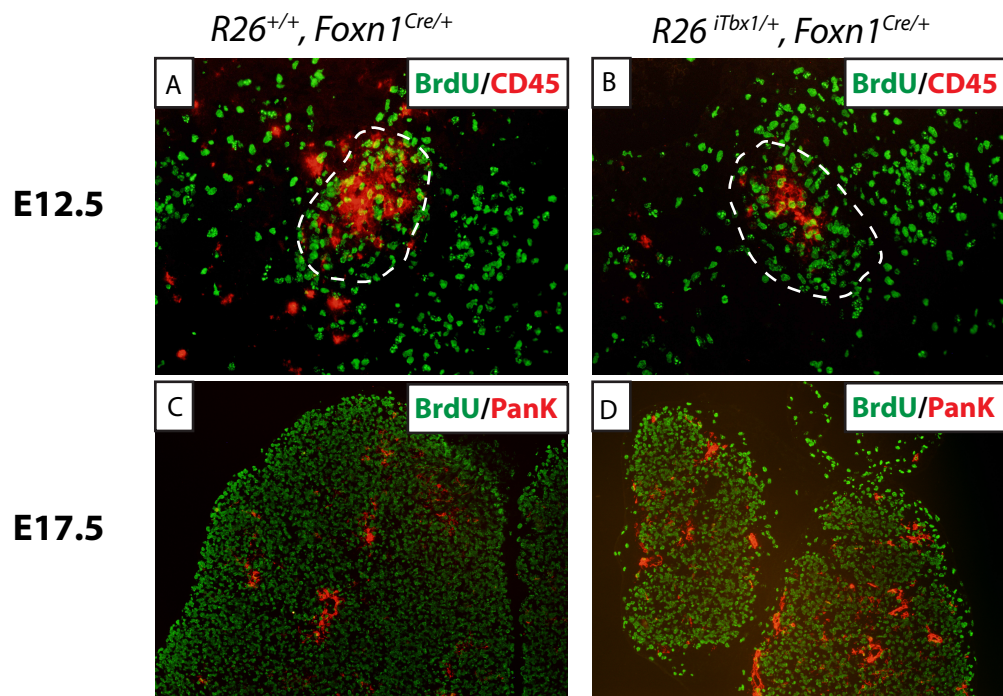
stage (unpublished data from the lab of Dr. Claire Blackburn) (Figure 7 C, C', C''). $R26^{iTbx1/+}$ thymi, on the other hand, showed an accumulation of Plet-1 positive cells throughout the fetal lobes (Figure 7 D, D', D''). This immature TEC phenotype was reminiscent of that found in athymic $Foxn1^{nu/nu}$ mice which are blocked at the earliest stages of TEC maturation and express Plet-1 in all thymic epithelial cells (18). This suggests an inability of $R26^{iTbx1/+}$ TECs to initiate and/ or complete a normal program of differentiation.

$R26^{iTbx1/+}$ E17.5 TECs proliferate at a frequency comparable to controls

Given the reduced cellularity and block in TEC differentiation in $R26^{iTbx1/+}$ thymi, we asked if these defects may result in or be attributable to aberrant proliferation. Immunohistochemistry and FACS analysis were utilized to address this question (Figure 8). Bromodeoxyuridine (BrdU) is a synthetic thymidine analog that is incorporated into the DNA of replicating cells, and therefore detects cells in S-phase. BrdU was injected into pregnant dams 90 minutes prior to sacrifice at E12.5 and E17.5. Thymic lobes were sectioned and stained for BrdU incorporation. No obvious defects in proliferation were noted in either E12.5 or E17.5 thymi stained (Figure 8 A-D).

FACS analysis was performed to quantify the percentage of proliferating cells for each genotype (Figure 8 F-K). Pregnant females were pulsed with BrdU and sacrificed after a 7-hour chase. Control and $R26^{iTbx1/+}$ thymi were identified by phenotype and pooled separately prior to for collagenase digestion to obtain single cell suspensions. We took a similar gating strategy as previously employed (refer to

Figure 8. Proliferation is not impaired in E17.5 $R26^{iTbx1/+}$ thymi. (A-D) BrdU and CD45 staining of E12.5 and E17.5 frozen thymic sections. Gating strategy for FACS analysis of pooled control and $R26^{iTbx1/+}$ thymi (E, F). TECs are $\text{EpCAM}^+\text{CD45}^-$ TECs; hematopoietic cells are $\text{EpCAM}^-\text{CD45}^+$ (J-K); non-TEC stromal cells are $\text{EpCAM}^-\text{CD45}^-$. The percentage of BrdU positive cells is shown in their respective gates. Data is consistent with 2 separate pooled experiments.



E17.5 BrdU FACS Analysis

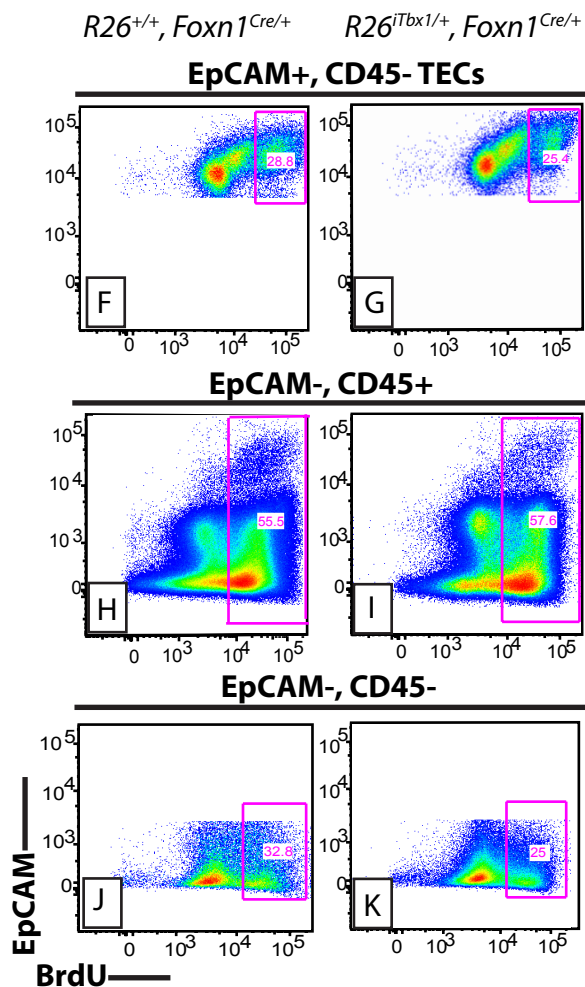
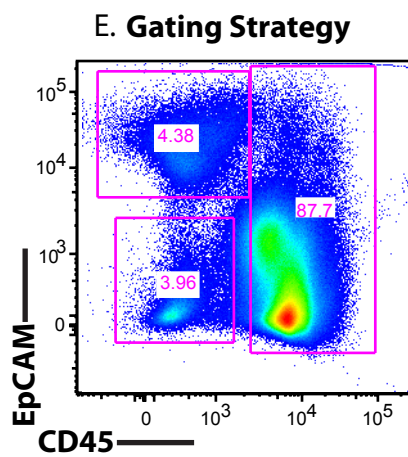


Figure 6) and gated on viable cells that were negative for CD45 and positive for EpCAM (Figure 8 E). We found no difference in the percentage of proliferating cells in $R26^{iTbx1/+}$ TECs as compared to the control TECs. This conclusion was confirmed using the proliferation specific marker Ki67, which labels dividing cells at all stages in the cell cycle (data not shown).

TEC-thymocyte interactions are essential for normal thymic development and are required mutually for maturation of both cell types. Differentiation blocks, for example a failure in MHCII expression and impaired medullary formation in the developing epithelium may therefore result in an impairment of thymocyte development and proliferation. A decrease in thymocyte proliferation could account for the hypoplastic thymus phenotype observed throughout ontogeny. However, gating on CD45⁺ hematopoietic cells (mainly thymocytes) showed no obvious difference in BrdU incorporation between $R26^{iTbx1/+}$ and control littermates (Figure 8 H-I). This was further confirmed using the same gating strategy on cells stained for Ki67 (data not shown). We also assessed proliferation of the group of non-epithelial stromal cells (e.g. fibroblasts, neural crest derived mesenchyme and endothelial cells) by gating on EpCAM⁻ CD45⁻ cells. Analysis of this cell population, showed a small decrease in the percentage of BrdU positive cells in $R26^{iTbx1/+}$ thymi relative to controls, although this difference is not appreciable (Figure 8 J-K)

Taken together these data suggest that proliferation of TECs, thymocytes and non-epithelial stromal cells is not significantly affected in $R26^{iTbx1/+}$ thymi compared to the control, thus the observed hypoplastic phenotype is not due to a reduced frequency of proliferating cells.

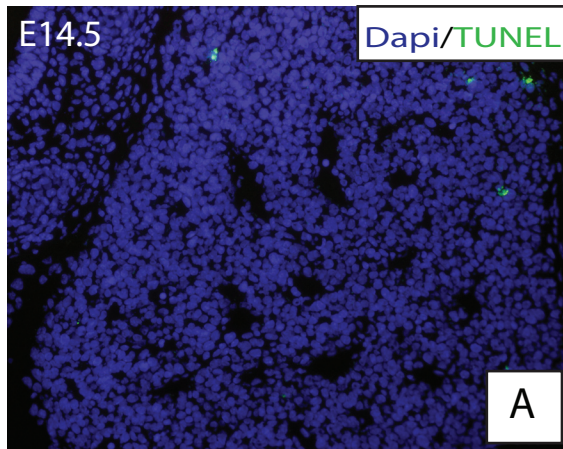
Fetal $R26^{iTbx1/+}$ thymi have an altered pattern of gene expression but not an increase in cell death

Considering the aberrant thymic morphology and significant decreases in overall cellularity observed in $R26^{iTbx1/+}$ fetal thymi, it is possible that changes in apoptosis contribute to this thymic phenotype. Terminal deoxynucleotidyl transferase mediated dUTP nick end labeling, or TUNEL staining, labels the free 3' ends of fragmented DNA that occur as a result of programmed cell death. It is therefore used as an effective read-out of apoptotic activity. We utilized this system to label cells undergoing programmed cell death in E14.5 and E17.5 control and $R26^{iTbx1/+}$ thymi (Figure 9). Examination of TUNEL positive cells at both ages revealed no obvious increase in apoptotic activity in $R26^{iTbx1/+}$ thymi compared to control littermates (Figure 9), suggesting changes in apoptosis do not account for the fetal thymic phenotypes observed. Therefore changes in cell number, thymic architecture and morphology are mediated by a mechanism independent of cell death during fetal development.

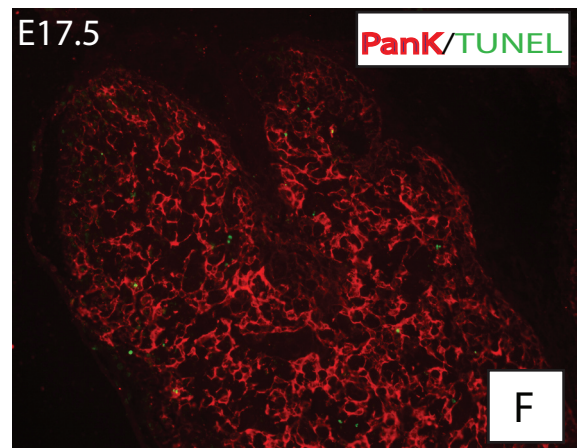
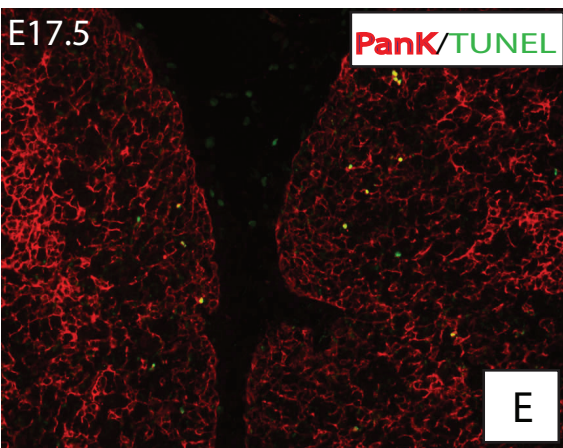
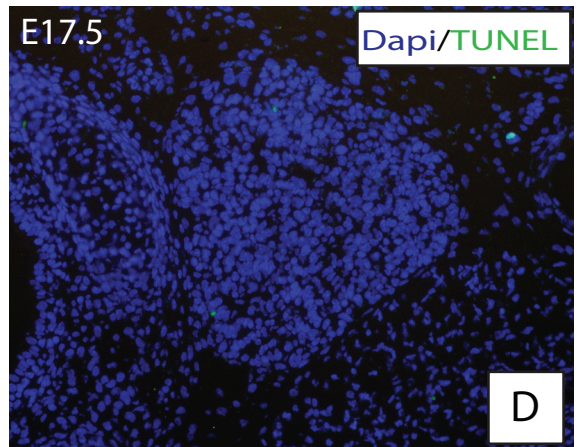
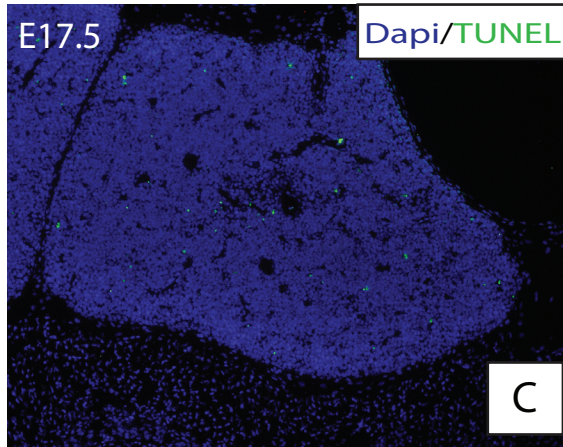
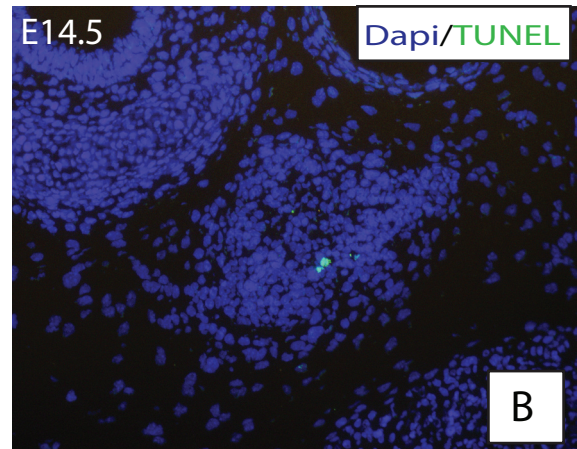
To examine transcriptional changes that result as a consequence of *Tbx1* activation in TECs we analyzed the expression of downstream candidate target genes such as *Gcm2*, *Hes1* and *Fgf8* as well as genes essential for normal thymic development such as *Foxn1* and *IL7* in sorted cells. cDNA was obtained from either E14.5 thymi as well as from thymocytes or TECs isolated by sorting pooled E17.5 thymi. The qRT-PCR analysis was performed by TaqMan gene expression arrays. The endogenous house keeping genes *GAPDH* or α -*tubulin* were used to normalize relative expression. For each $R26^{iTbx1/+}$ population analyzed the corresponding

Figure 9. $R26^{iTbx1/+}$ fetal thymic phenotypes do not result from an increase in apoptosis. (A-B) Frozen sections of E14.5 Dapi and TUNEL stained thymi in control and $R26^{iTbx1/+}$ mice (200X). (C-F) E17.5 thymi stained with Dapi and TUNEL (C-D) (100X) or pancytokeratin and TUNEL (E-F) 200X n= 2 pairs per age.

R26^{+/+}, Foxn1^{Cre/+}



R26^{iTbx1/+}, Foxn1^{Cre/+}



control population was used as a calibrator. As previously mentioned, *Tbx1* was expressed in *R26^{iTbx1/+}* thymi but not in control thymi (Figure 10, top and middle panels). At E17.5, CD45⁻, EpCAM⁺ TECs from pooled control thymi did not express *Tbx1*; however, TECs from *R26^{iTbx1/+}* littermates showed high levels of *Tbx1* expression. *Tbx1* was not expressed in EpCAM⁻, CD45⁺ hematopoietic cells or EpCAM⁻, CD45⁻ non-TEC stromal cells from control or *R26^{iTbx1/+}* mice (data not shown). The pattern of *Tbx1* gene expression coincides with expression of the GFP tag (Figure 2 B, bottom panel).

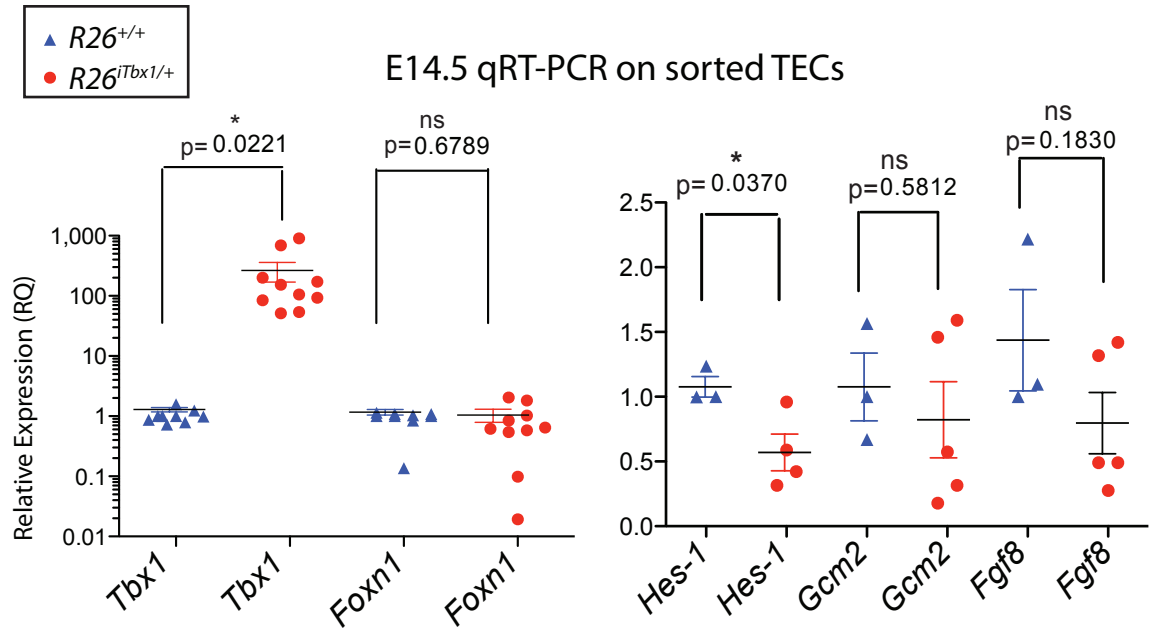
Given that *Foxn1* is required for development and homeostasis of TECs in the thymic microenvironment, we analyzed *Foxn1* expression to determine if a deficiency of *Foxn1* gene expression corresponds to impaired TEC development. At E14.5 we found no significant differences in *Foxn1* gene expression in *R26^{iTbx1/+}* thymi relative to controls (Figure 10 A). However, at E17.5 *Foxn1* levels were significantly reduced in *R26^{iTbx1/+}* TECs compared to controls (Figure 10 B). These data suggest that *Tbx1* expression is antagonistic for normal expression of *Foxn1* in fetal TECs.

Both *Gcm2* and the Notch-signaling component *Hes-1* are candidate *Tbx1* target genes. *Gcm2* mimics the pattern of expression of *Tbx1* at E10.5 in the 3rd PP and is required for proper parathyroid development. During organogenesis expression remains restricted to the dorsal-parathyroid fated domain and is excluded from the ventral-thymus fated domain. While *Gcm2* is required to establish the parathyroid-thymus fate boundary it is not expressed in the developing thymic epithelium and not associated with the normal TEC differentiation program. At

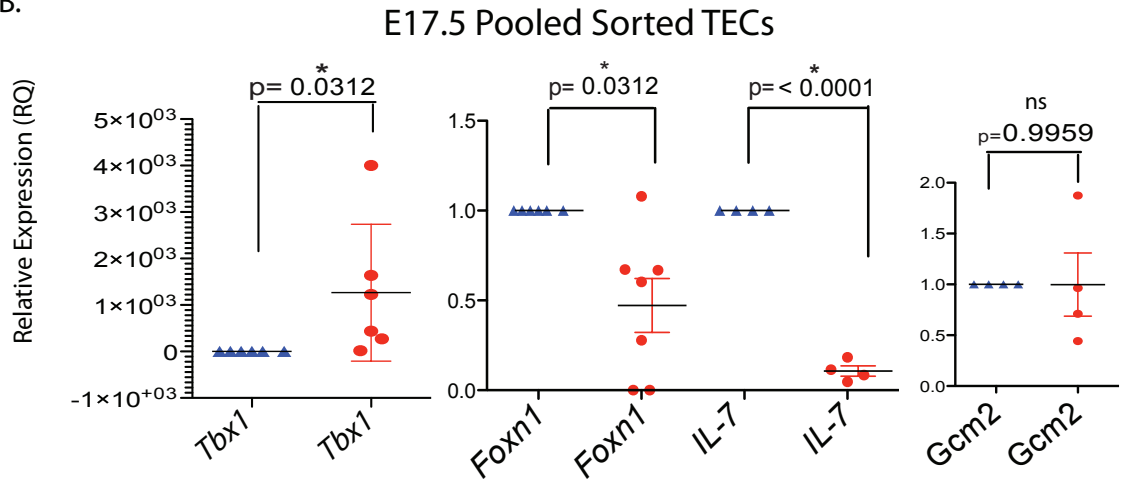
Figure 10. Expression of selected genes in $R26^{iThx1/+}$ fetal TECs.

qRT-PCR analysis of indicated gene expression patterns in (A) E14.5 individual thymi; and (B) E17.5 pooled sorted TECs, n = 3 pooled experiments (C) Preliminary qRT-PCR analysis of sorted E17.5 TECs. Standard t-test was performed to determine significance.

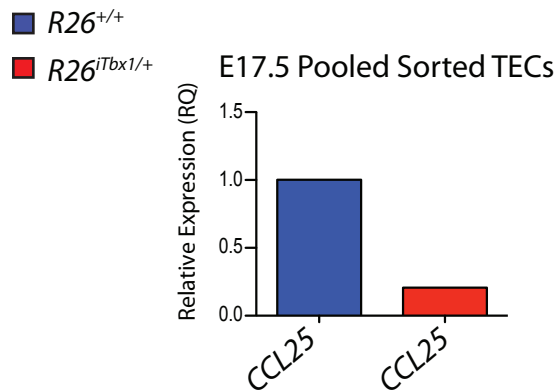
A.



B.



C.



E14.5 as well as E17.5, no significant difference in *Gcm2* expression was observed relative to controls (Figure 10).

Hes-1 is a component of the Notch signaling pathway and plays an essential role in development of the pharyngeal apparatus (81). *Tbx1* null mice have a reduction in Hes-1 and *Hes-1* null mice show a range of phenotypes reminiscent of the human DiGeorge syndrome (81). Examination of *Hes-1* in *R26^{iTbx1/+}* E14.5 thymi revealed a significant decrease in expression relative to controls with an average 50% reduction in expression (Figure 10 A). This is consistent with previous reports that both genes act in a linear fashion to exert their dynamic developmental effects.

Fgf8 is a downstream target gene of *Tbx1* that has been implicated in thymic development. In the secondary heart field *Tbx1* is required to respond to *Fgf8* signaling and maintain cardiac progenitor cells in an undifferentiated state. We analyzed relative expression of *Fgf8* to determine if ectopic *Tbx1* expression in TECs results in an altered expression pattern of this mitogen. At E14.5 we found no significant difference in expression between *R26^{iTbx1/+}* thymi and controls. This suggests that the agonistic role *Tbx1* plays in *Fgf8* expression is not evidenced at this time during fetal gestation.

IL-7 is a cytokine that is secreted by TECs and is required in a dose sensitive manner for survival and differentiation of thymocyte progenitors. In thymocytes it up-regulates the pro-survival gene *Bcl2*, allowing thymocytes to escape programmed cell death and continue to differentiate. IL-7R α chain, one of two chains that comprise the IL-7 receptor, can result in severe combined immunodeficiency syndrome (SCID) if deficient (reviewed in (11)). Mouse models which were treated

with an IL-7 neutralizing antibody or are deficient in *IL-7R α* are impaired in both B- and T-cell development (reviewed in (11)). Taken together IL-7 secretion by TECs is absolutely essential for the development of a functional immune system. The upstream factors which regulate expression of *IL-7* in TECs is not clear, but a thorough understanding of the mechanisms that control its expression has many therapeutic consequences, as it is currently being explored to increase T-cell output and antigen specific responses in certain immunocompromised individuals (reviewed in (11)).

Analysis of *IL-7* expression at E17.5 revealed a significant decrease in expression in *R26^{iTbx1/+}* TECs compared to TECs of control littermates (Figure 10 B). A decrease in *IL-7* expression may be attributable to an indirect or direct antagonism of this gene in TECs. Regardless, the decreased IL-7 expression in *R26^{iTbx1/+}* TECs coincides with defects found in early DN thymocyte subsets as will be discussed in a subsequent section (see later Figure 16).

CCL25 is a chemokine expressed by Foxn1-dependent TECs that attracts thymus seeding hematopoietic cells during early stages of thymus organogenesis (28). Athymic nude mice have a decrease in CCL25 expression and mice deficient in CCR9, the corresponding receptor for CCL25 fail to recruit early progenitors to the thymus and are characterized by an initial decrease in thymus cellularity (28). Preliminary data (one experiment) using E17.5 *R26^{iTbx1/+}* TECs suggests a decrease in CCL25 expression relative to controls (Figure 10 C). It is tempting to speculate that the hypoplastic phenotype observed in *R26^{iTbx1/+}* fetal mice results, at

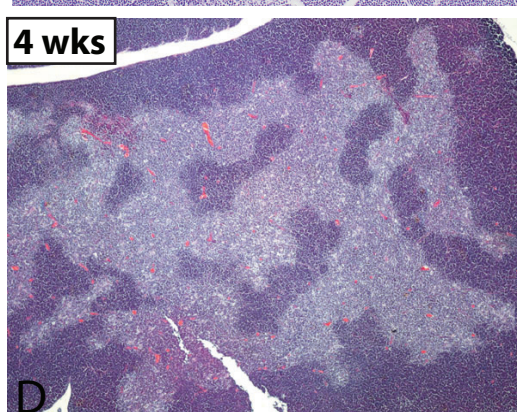
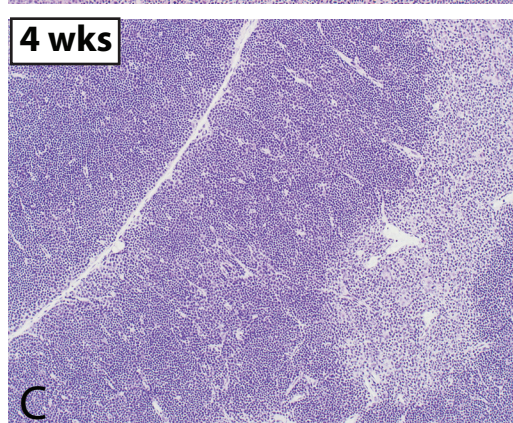
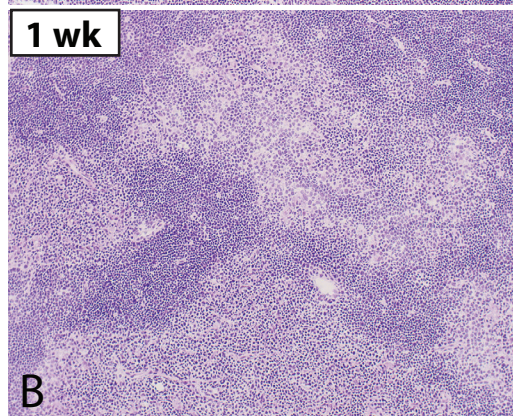
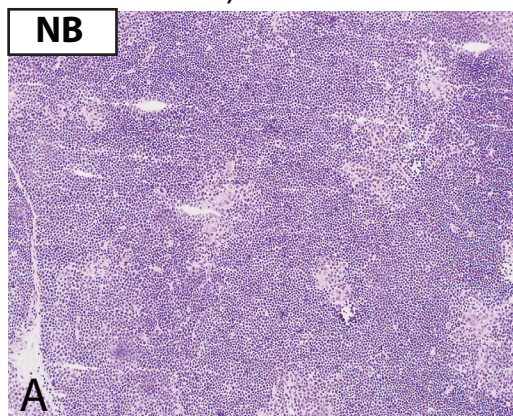
least in part, from a failure of thymus seeding progenitors to be guided by chemoattraction to the thymus rudiment.

Postnatal $R26^{i\text{Tbx}1/+}$ thymi are hypoplastic with aberrant thymic architecture

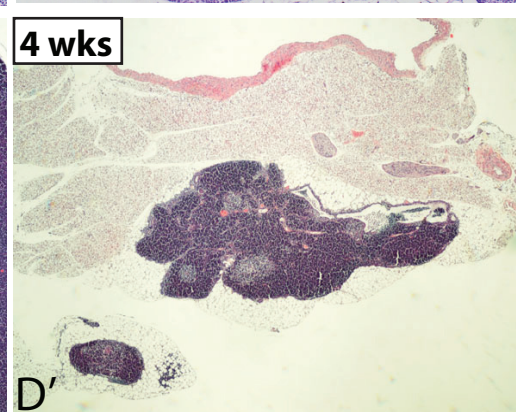
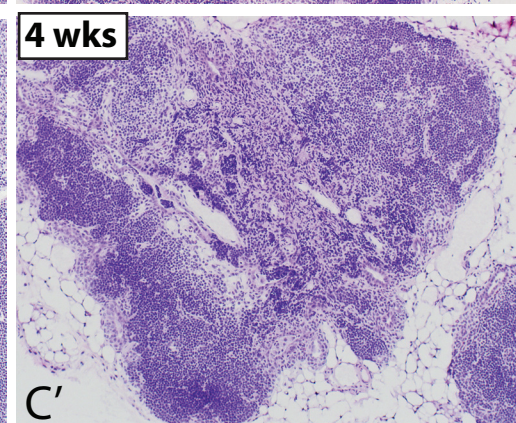
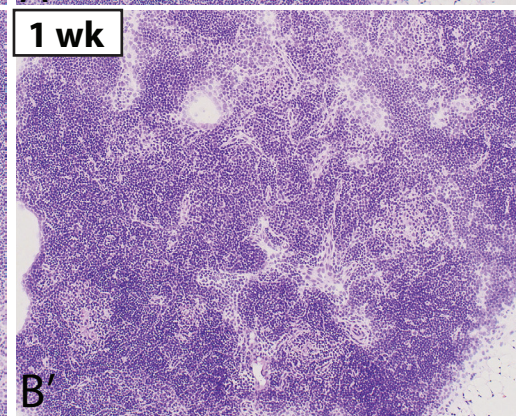
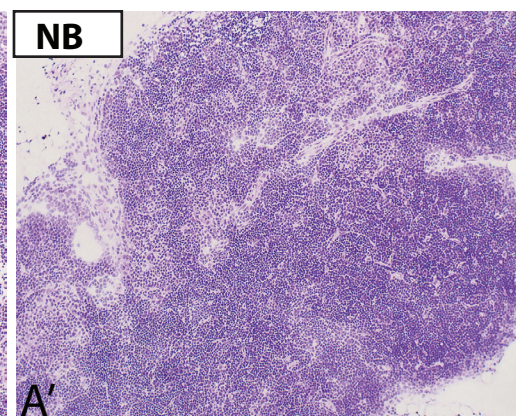
In order to determine if the thymic phenotype observed in fetal mice persisted in the adult we examined H&E sections at postnatal ages. Newborn (NB) control mice at 1-3 days of age, and mice at 1 week and 4 weeks of age had thymi with normal morphology in which cortical and medullary areas could clearly be delineated (Figure 11 A-D). In contrast, $R26^{i\text{Tbx}1/+}$ thymi at corresponding ages showed no clear demarcation of cortical and medullary boundaries (Figure 11 A'-D'). In addition, $R26^{i\text{Tbx}1/+}$ thymi had lobes that were progressively hypoplastic with age and contained regions that appeared acellular and highly lobulated. Thymi from these mice also contained areas of cells with darkly staining condensed nuclei, similar to cells undergoing apoptosis. Lighter staining areas dispersed throughout some lobes appeared stromal-like (Figure 11 A'-D') The phenotype observed in postnatal mice $R26^{i\text{Tbx}1/+}$ was more severe than that observed in fetal $R26^{i\text{Tbx}1/+}$ thymi (Figure 2), although the degree to which thymus cellularity and organization were impaired varied from animal to animal and even from lobe to lobe within the same animal. Taken together these data suggest that $R26^{i\text{Tbx}1/+}$ thymi do not rebound with age and instead continue to degenerate progressively.

Figure 11. Impaired architecture and organization of postnatal $R26^{Tbx1/+}$ thymi are progressive with age. Hematoxylin and eosin stained thymi of control and $R26^{Tbx1/+}$ thymi at NB (A, A'), 1wk (B, B'), and 4 wks of age (C-D'). A-C' are frozen stained sections at 100x. D and D' images are paraffin sections.

R26^{+/+}, Foxn1^{Cre/+}



R26^{iTbx1/+}, Foxn1^{Cre/+}



R26^{iTbx1/+} TECs are impaired in differentiation and organization

We analyzed markers of TEC differentiation and organization to assess postnatal TEC development and homeostasis. To evaluate the presence and localization of TEC subsets, the pattern of keratin expression and UEA-1 binding was determined by immunohistochemical analysis of frozen thymus sections from NB, 1 week, and 4 week mice (Figure 12). Control thymi had well-demarcated medullary regions containing previously described mTEC subsets. The major mTEC subset in the adult thymus co-expresses K5 and K14, but not K8 and does not bind UEA-1 (21). Another mTEC subset expresses K8 and binds UEA-1 but does not express K5 or K14. A minor TEC subset at the cortical-medullary junction co-expresses K5 and K8, but does not express K14 or bind UEA-1 (Figure 12 and Figure 13). *R26^{iTbx1/+}* thymi lacked a defined organizational architecture and instead contained areas that stained aberrantly. There were few well-organized medullary areas at any age and similar to the fetal *R26^{iTbx1/+}* fetal stages, some postnatal *R26^{iTbx1/+}* thymi appeared to be disintegrated. Note the small epithelial regions that are separated from the main lobes (Figure 13 B, E, K.) The thymus phenotype was consistently aberrant in the adult although the severity of disorganization varied from animal to animal and even between the thymus lobes within the same animal. While some thymic regions retained remnants of organized medullary regions, in most cases there was no distinct medullary organization and a paucity of mTECs (Figure 13 B-F, H-I, H'-I'). In particular, few UEA-1⁺ cells were present. Multiple cysts lined with K5⁺ epithelial cells were frequently observed (Figure 12 F-H, Figure 13 E-F).

Figure 12. *R26^{Tbx1/+}* postnatal thymi at newborn and 1 week of age have a block in TEC differentiation. (A, B) NB frozen sections of thymi stained with antibodies to detect K5 and K8 (200x), (C-D') K14, UEA-1 and Dapi (100x); (F-K) 1 week frozen thymic sections stained for K5 and K8 (40x), K14 and UEA-1 (100x). Note J and K were traced using Dapi staining (not shown).

R26^{+/+}, Foxn1^{Cre/+}

R26^{iTbx1/+}, Foxn1^{Cre/+}

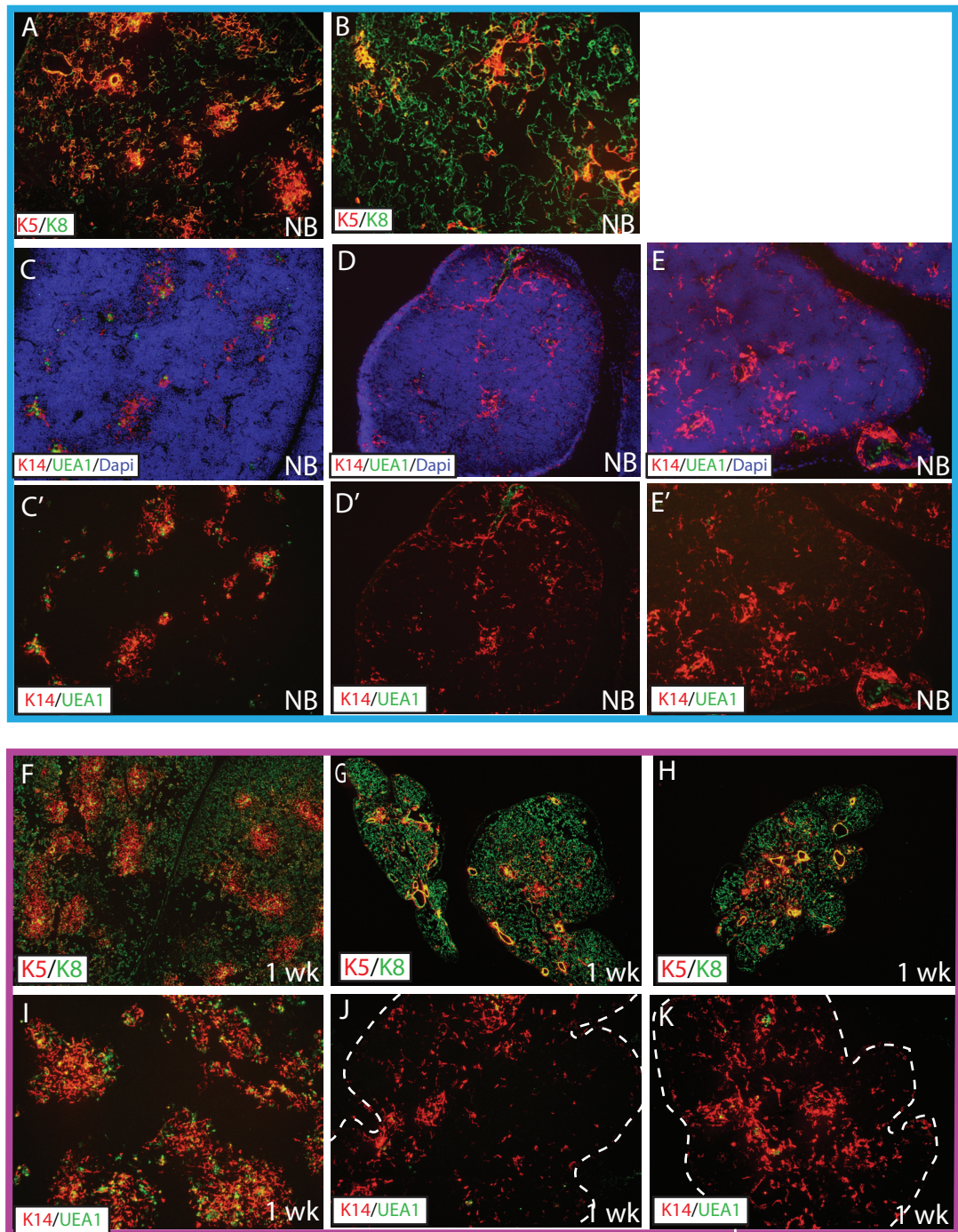
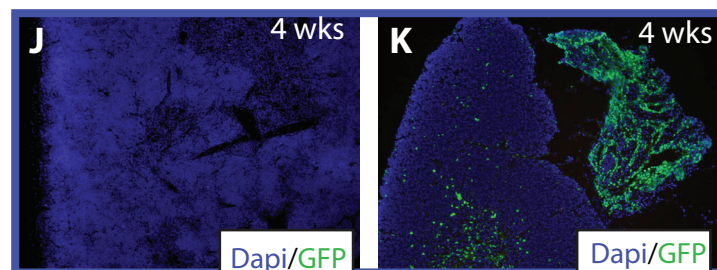
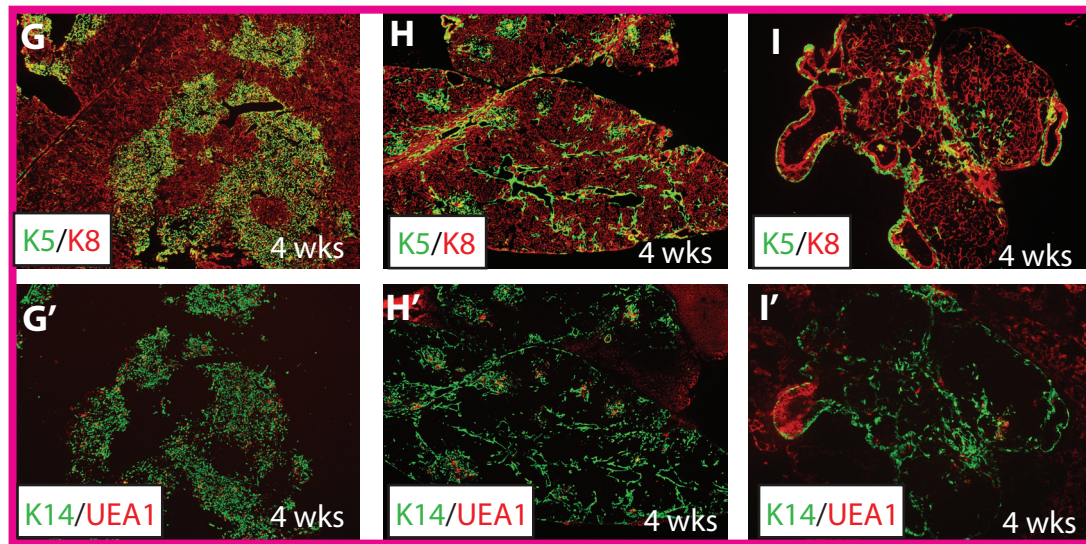
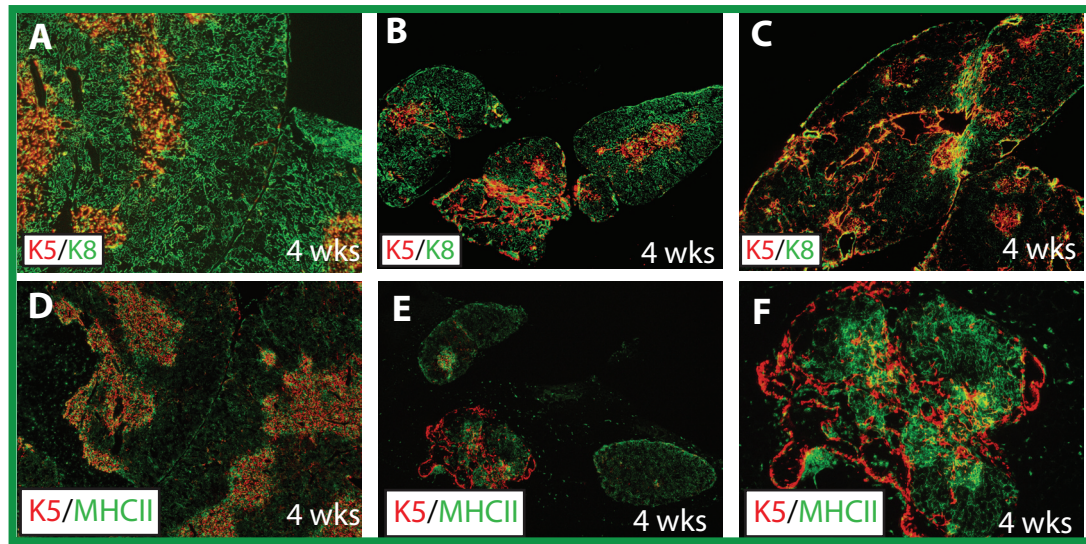


Figure 13. 4 wk $R26^{Tbx1/+}$ TECs sustain a block in differentiation. (A-C) 4 wk frozen thymi stained to detect K5 and K8 (40x), (D-F) K5 and MHC class II (40x). Serial sections of frozen 4wk thymi stained with (G-I') K5 and K8 or K14 and UEA-1 (40x). (J-K) Anti-GFP and Dapi stained frozen thymi (100x). n = at least 2 per genotype

R26^{+/+}, Foxn1^{Cre/+}

R26^{iTbx1/+}, Foxn1^{Cre/+}



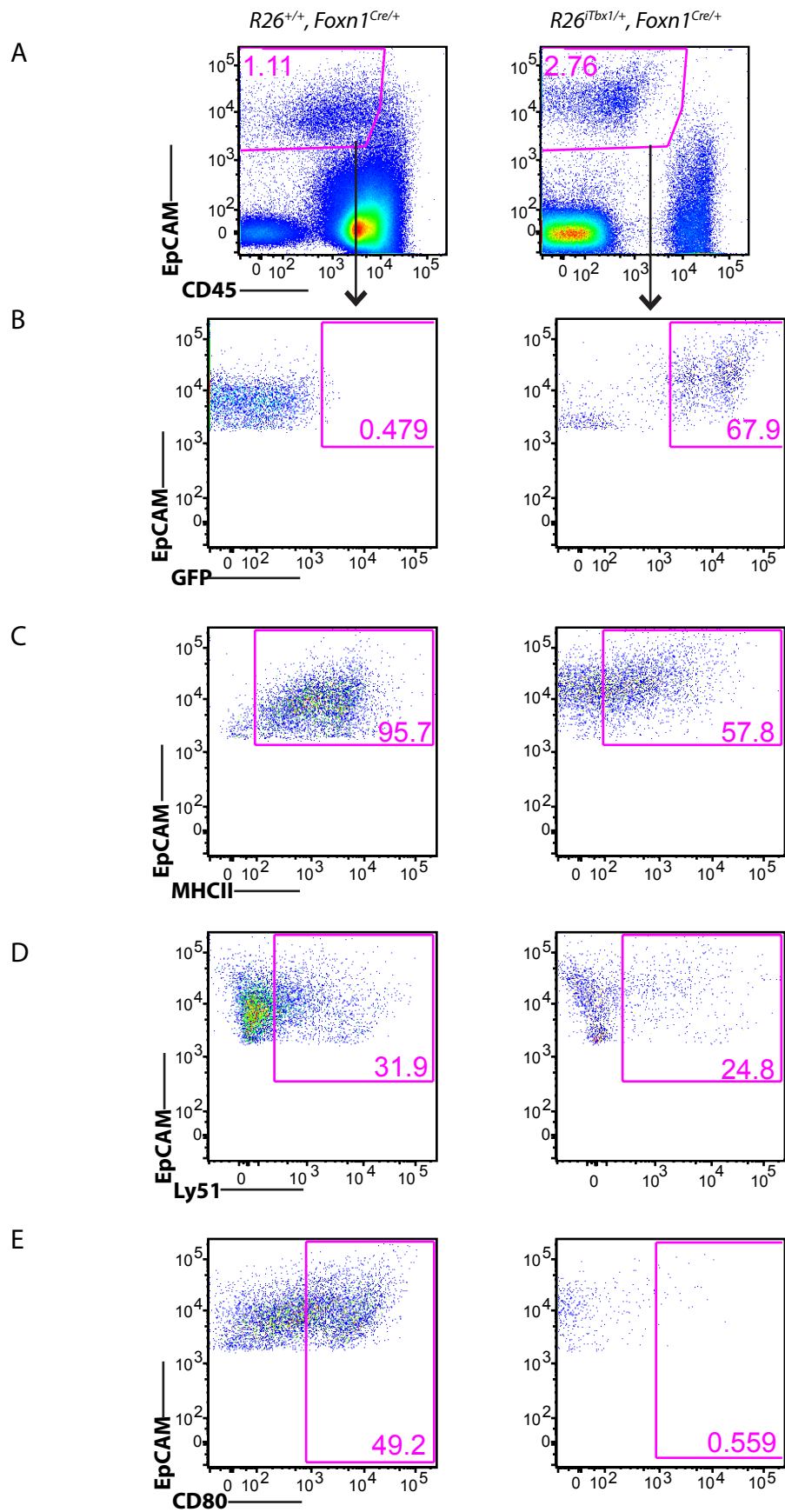
A positive correlation was found between the severity of the thymus phenotype and the extent of GFP expression. Figure 13 K shows GFP expressing cells throughout fragmented thymic tissue, whereas GFP⁺ cells are not as numerous in the relatively organized adjacent thymus lobe. GFP is a tag for the *iTbx1* allele. Taken together this data show that the *iTbx1* allele continues to be expressed in the adult thymus and as a result, defective organization, architecture and TEC maturation do not recover in the postnatal period.

We performed FACS analysis in order to further investigate the block in TEC differentiation observed by immunohistochemistry. TECs from 3-week old *R26^{iTbx1/+}* and control thymi were disaggregated as previously described. We used the same gating strategy previously employed for fetal TEC analysis and gated on EpCAM⁺, CD45⁻ TECs (Figure 14 A). Consistent with previous results, GFP was present in *R26^{iTbx1/+}* EpCAM⁺ CD45⁻ TECs but not in EpCAM⁻, CD45⁺ or EpCAM⁻, CD45⁻ populations (Figure 14 B). GFP was not observed in any population from control individuals. MHC class II and CD80 expression were reduced relative to controls (Figure 14 C, E). Similar to fetal *R26^{iTbx1/+}* TECs, Ly51 expression was comparable to controls. These data show that the block in TEC differentiation that is initiated during fetal development is sustained in adult *R26^{iTbx1/+}* thymi.

Plet-1⁺ progenitor cells are retained in adult *R26^{iTbx1/+}* thymi

Plet-1 is expressed at a high frequency on a large number of TEC progenitors during thymus organogenesis; however, this frequency declines with age

Figure 14. Postnatal TECs are impaired in differentiation in $R26^{iTbx1/+}$ thymi. FACS analysis of 3-week control and $R26^{iTbx1/+}$ thymi showing (A) EpCAM versus CD45. Gating on EPCAM⁺, CD45⁻ TECs analysis of (B) GFP, (C) MHCII, (D) Ly51, and (E) CD80 was performed on $R26^{iTbx1/+}$ thymi versus controls.

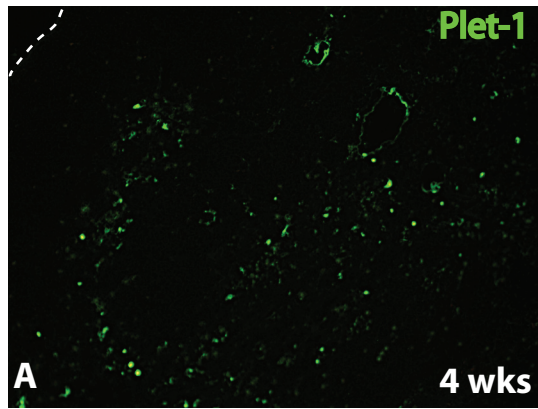


(unpublished results from Dr. Claire Blackburn's lab). During fetal development the relative number of Plet-1 positive cells does not change. Plet-1+ cells divide asymmetrically to self-renew and also give rise to more differentiated progenitors that replenish cortical and medullary subsets (unpublished results from Dr. Claire Blackburn's lab). We analyzed the frequency and localization of Plet-1+ TECs in adult $R26^{iTbx1/+}$ thymi to determine if the accumulation of progenitors observed in late fetal gestation persisted in the adult. Control thymi at 4wks of age contained scattered Plet-1 positive cells throughout the medulla (Figure 15 A, C). A few Plet-1 progenitors were also localized to outer cortical regions (Figure 15 C, D). In contrast, the hypoplastic, disorganized $R26^{iTbx1/+}$ thymi contained a dramatic increase in the frequency of Plet-1 positive cells that localized largely to the outer sub-capsular area but could also be found throughout the thymic lobes (Figure 15 B).

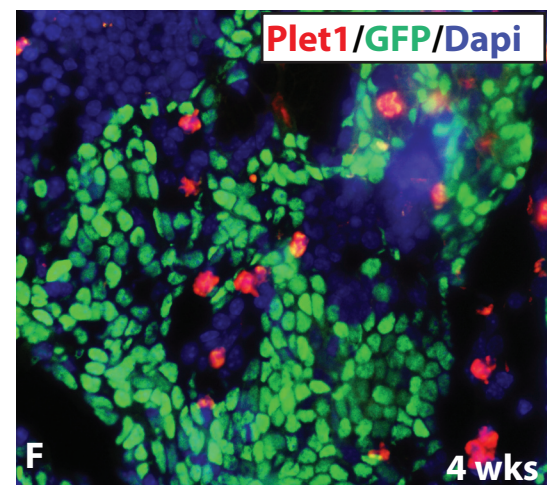
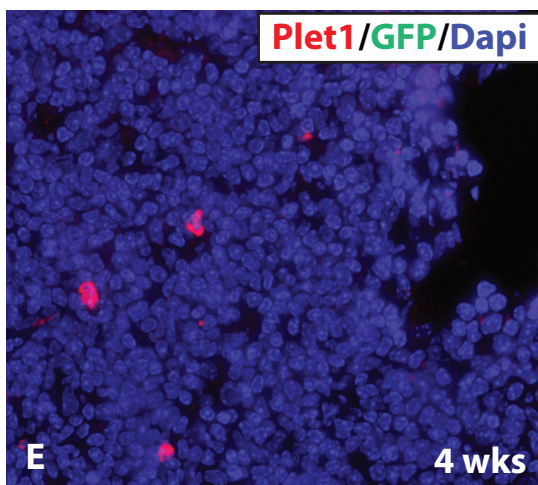
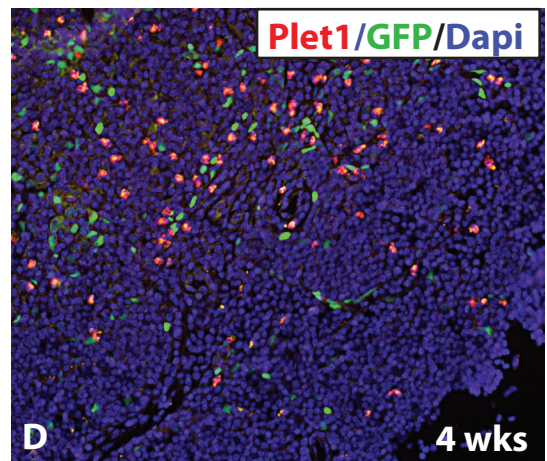
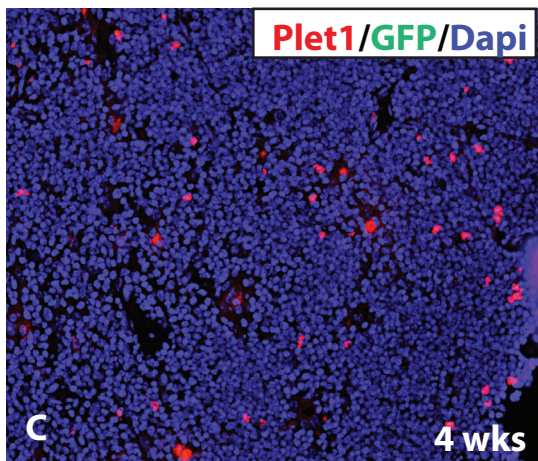
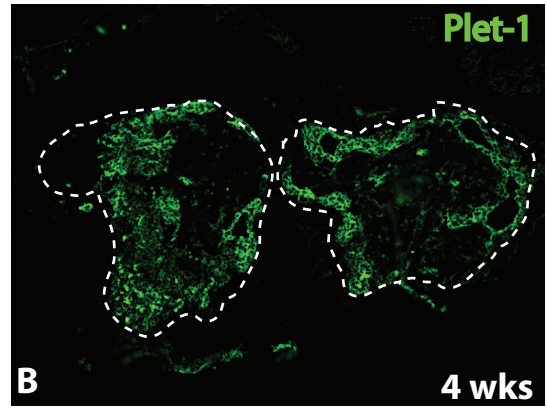
Surprisingly, many of the Plet-1 positive progenitor cells in $R26^{iTbx1/+}$ did not express detectable GFP. This could be due to 1) the levels of GFP are below the threshold of detection 2) silencing of the iTbx1 locus 3) generation from *Foxn1* negative cells that do not activate *Cre* in this model. In short, these data suggest that the accumulation of Plet-1 progenitors observed in fetal $R26^{iTbx1/+}$ thymi persists into adult stages and furthermore aberrantly localize to the cortical sub-capsular region.

Figure 15. Accumulation of Plet-1 progenitors is maintained in postnatal thymi. (A-B) Frozen Plet-1 stained sections from 4 wk thymi. Dashed line outlining fetal lobes was generated from tracing Dapi stained sections (not shown). (100x) (C-F) Plet-1, GFP and Dapi staining of 4wk frozen *R26^{iTbx1/+}* thymi (D, F) and controls (C, D) at (200x) middle panel or (400x) bottom panel, n = 2 individuals per genotype.

R26^{+/+}, Foxn1^{Cre/+}



R26^{iTbx1/+}, Foxn1^{Cre/+}



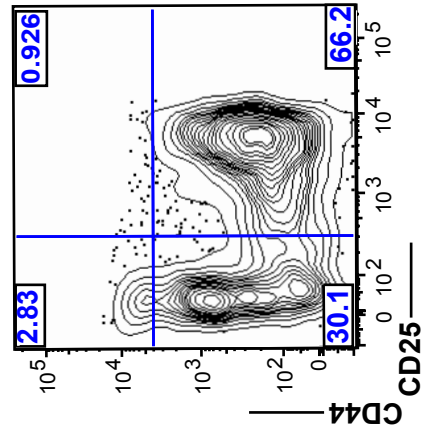
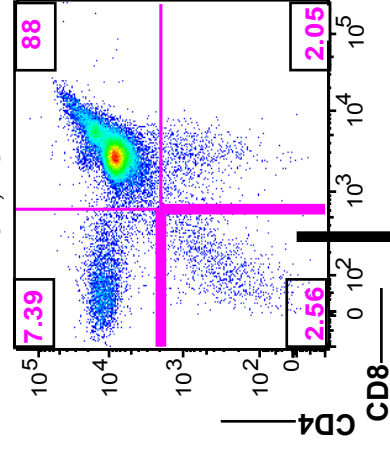
Thymocyte maturation is impaired in $R26^{i\text{Tbx}1/+}$ mice

Given that thymocyte-TEC crosstalk is essential for proper maturation of thymocytes, we analyzed thymocyte subsets in 3-week thymi defined by FACS analysis as a read-out of TEC functionality (Figure 16). CD4 and CD8 define the major thymocyte subsets, all which were present in $R26^{i\text{Tbx}1/+}$ thymi. However, two out of three $R26^{i\text{Tbx}1/+}$ thymi analyzed had a clear decrease in CD4 and CD8 SP thymocytes along with an increase in the percentage of DP thymocytes, relative to control thymi (top panel, second and fourth FACS plot) This suggests a partial block in the DP to SP stage of maturation. This block is likely a result of a decrease in MHCII by TECs, as MHCII expression by TECs is required for normal thymocyte maturation. A third individual, (top panel, third FACS plot) contained percentages that were more comparable to control thymi. This variability in thymocyte maturation may be attributable to the variations observed in TEC differentiation, as described earlier. Regardless, the total thymus cellularity observed is consistently reduced.

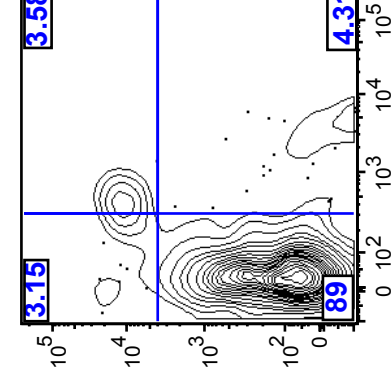
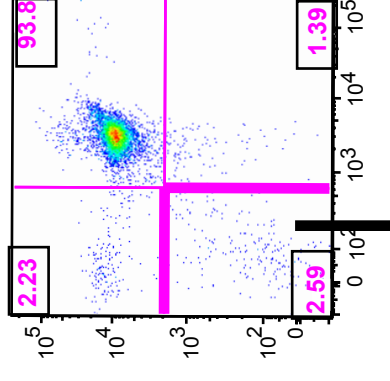
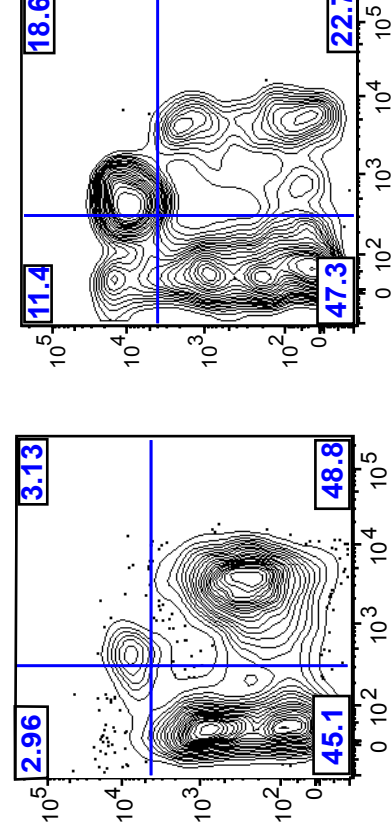
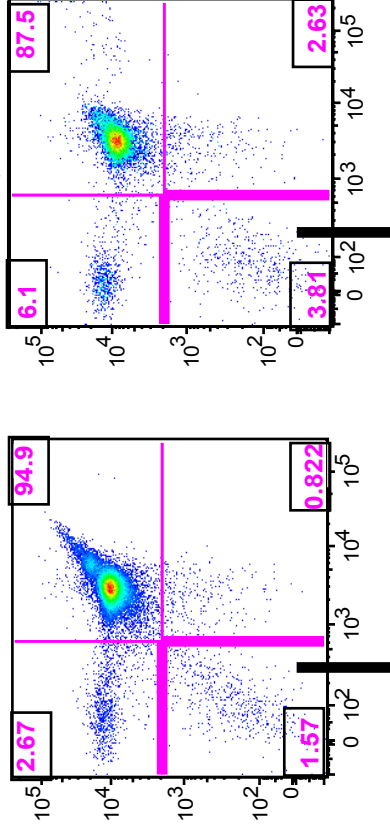
We also analyzed the distribution of thymocyte progenitor subsets in the DN population that are defined by expression of CD44 and CD25 (Figure 16, bottom panel) in order to determine if the reduction observed in overall cellularity could be explained by defects in early thymocyte maturation. All $R26^{i\text{Tbx}1/+}$ thymi had a DN1 to DN2 block as shown by the presence of a population expressing high levels of CD44 and intermediate levels of CD25 expression (Figure 16, bottom panel). This distinct population is not observed in control thymi. In addition, an increase in the percentage of DN4 thymocytes (CD25⁻, CD44⁻) and a decrease in DN3 thymocytes (CD25⁺, CD44⁻) was consistently observed in all three individuals relative to controls

Figure 16. Thymocyte maturation is impaired in postnatal R26^{iTbx1/+} thymi. CD4 versus CD8 FACS analysis of 3 wk thymi with percentages of each population indicated (top panel). DN thymocytes were further analyzed for CD44 and CD25 expression (bottom panel).

R26^{+/+}, Foxn1^{Cre/+}



R26^{ΔTbx1/+}, Foxn1^{Cre/+}



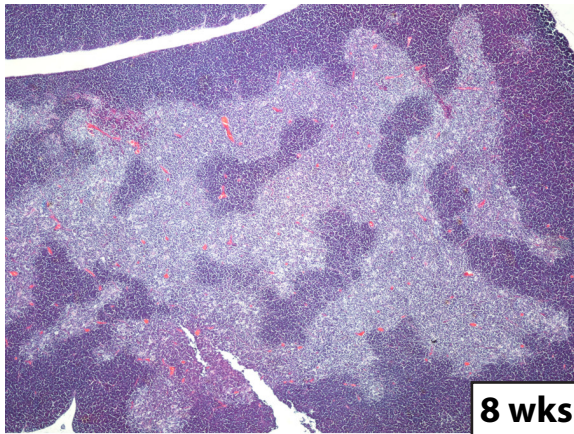
(Figure 16, bottom panel). Interestingly, very few DN3 thymocytes were present in one of the $R26^{iTbx1/+}$ thymi. This phenotype was similar to that reported by the Manley lab in $Foxn1^{\Delta/\Delta}$ mice (82). These mice lack the n-terminal region of *Foxn1* required specifically for TEC maturation. The observed defects in thymocyte maturation are likely to be a secondary consequence of the defects in TEC differentiation in $R26^{iTbx1/+}$ thymi.

Autoimmune manifestations arise in some $R26^{iTbx1/+}$ individuals

Given the observed blocks in thymocyte maturation and presumably defects in positive and negative selection, we considered whether the $R26^{iTbx1/+}$ adult mice developed autoimmunity. We suspected this may be the case since several of these mice had obvious eye defects. Eyes of several $R26^{iTbx1/+}$ mice had bulging eyes abnormally protruding from their skull. In addition, some of these mice also had their adjacent eye noticeably sunken into their eye socket. All of these effected mice were lethargic and moribund. Dr. Donna Kusewitz, DVM, Ph.D. necropsied and performed an in depth pathological evaluation on two $R26^{iTbx1/+}$ mice and littermate controls. In addition, to thymus hypoplasia both $R26^{iTbx1/+}$ mice had evidence of pathological abnormalities not observed in control littermates (Figure 17). Mild keratitis and marked fibroplasia was observed $R26^{iTbx1/+}$ corneas along with corneal conjunctivitis and inflammation of the intraorbital and extraorbital lacrimal glands and Meibomian glands of the eyelids (Figure 17 bottom panel, Figure 18). No obvious difference in goblet cell number was apparent. Furthermore, mites were

Figure 17. $R26^{iTbx1/+}$ 8 wk mice have hypoplastic thymi and lymphocytic infiltration in lacrimal glands of the eye. (Top and bottom panels) H&E stained sections of paraffin embedded thymi (top panel) and extraorbital lacrimal glands (bottom panel). Arrows indicate lymphoid infiltrates.

R26^{+/+}, Foxn1^{Cre/+}



R26^{iTbx1/+}, Foxn1^{Cre/+}

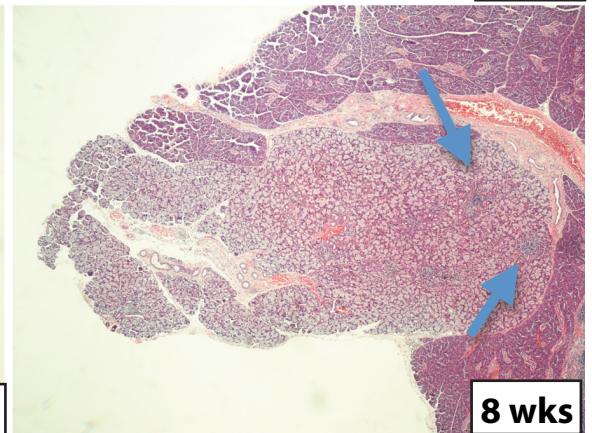
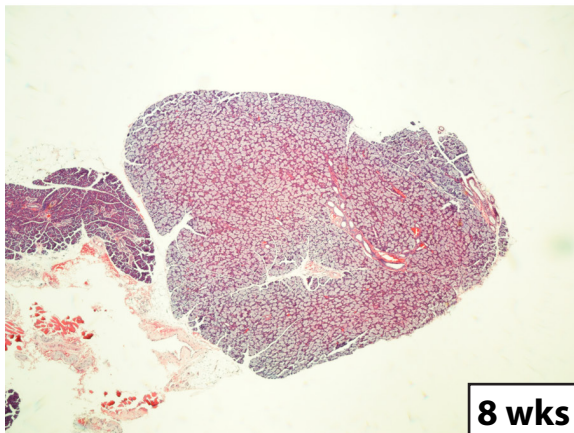
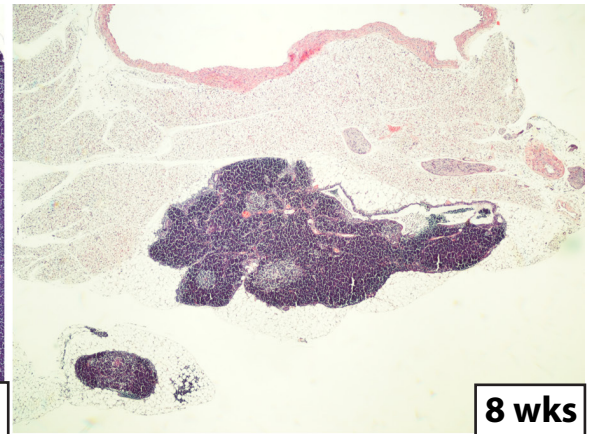
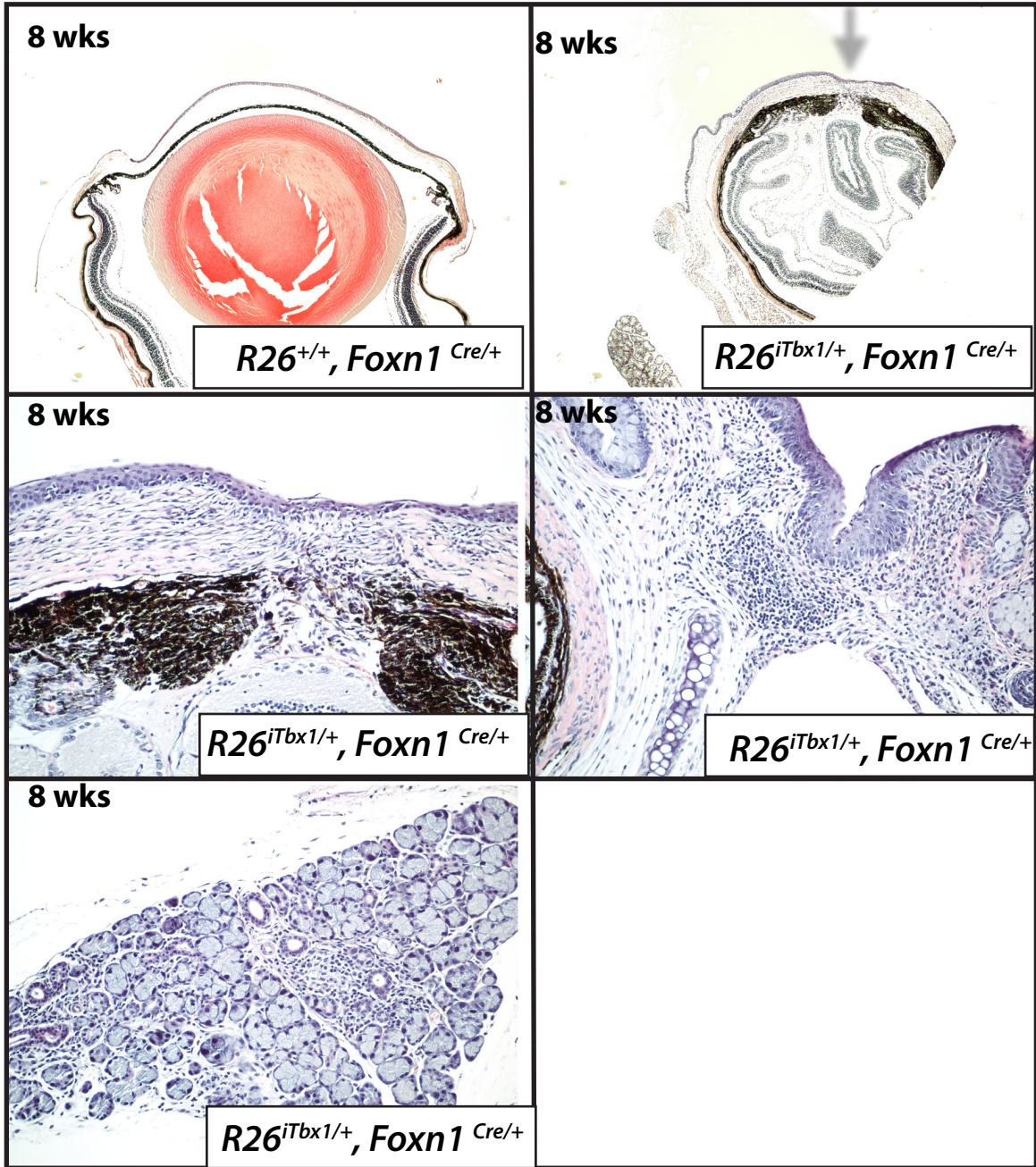


Figure 18. $R26^{iTbx1/+}$ eyes have inflammatory infiltrates not observed in controls. H&E stained corneal sections. $R26^{iTbx1/+}$ eyes show adhesion of cornea to iris (arrow). (Middle left) closer view of cornea iris adhesion in $R26^{iTbx1/+}$ mouse. (Middle right) lymphoid aggregates in conjunctiva of $R26^{iTbx1/+}$ mouse. (Lower left) intraorbital lacrimal gland in $R26^{iTbx1/+}$ mouse with lymphoid infiltrates.



found on the eyelids of $R26^{iTbx1/+}$ mice but not co-caged littermate controls, suggesting the possibility of an immune phenotype present in $R26^{iTbx1/+}$ mice that renders them more susceptible to parasitic infection. Other organs shown to develop lymphocytic infiltrates with autoimmunity such as the liver were only mildly affected, however this may be due to the age at which they were sacrificed. Older mice may have shown more severe autoimmune manifestations. However, mice with affected eyes were sacrificed at the noticeable onset of this phenotype and not allowed to age for ethical reasons.

Final reports obtained from the pathology core, concluded that the corneal, conjunctival and lacrimal gland lesions found were suggestive of an autoimmune phenotype, similar to that reported in *Aire*-deficient mice and mouse models for the immunodeficiency disorder *Sjogren* syndrome (83, 84). This suggests that sustained activation of *Tbx1* in TECs impairs the establishment of central tolerance.

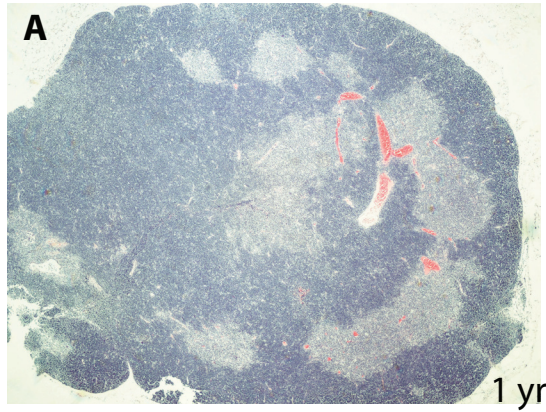
Necropsies performed on 1 yr $R26^{iTbx1/+}$ (n=2) and control littermates (n=2), did not reveal any corneal abnormalities in $R26^{iTbx1/+}$ mice relative to controls. No significant findings were observed in aged-mice of either genotype. However, thymi in both $R26^{iTbx1/+}$ individuals were severely hypoplastic, relative to controls. Although control thymi showed thymic degeneration consistent with age-related atrophy, $R26^{iTbx1/+}$ thymi were much smaller with an abnormal breakdown in normal thymic architecture. In addition, $R26^{iTbx1/+}$ thymi also contained cystic regions often lined with ciliated epithelium similar to the epithelial lining found in lung (Figure 19). This is consistent with cysts that form in the *nude* mouse (85). Previously investigators reported the presence of ciliated cysts in these *Foxn1* deficient mice (85). In

addition, later reports concluded that the presence of these cysts correlated inversely with regions occupied by thymocytes suggesting a different program of differentiation that is adopted by these TECs in the absence of thymocytes. Although this TEC population was blocked in maturation they were highly proliferative and likened to a progenitor-cell type, arising from the medullary epithelium. Furthermore, similar to cysts found in *R26^{iTbx1/+}* mice, these investigators also reported thymic epithelia that lined cysts to be positive for K5. This suggests that the cysts formed in *iTbx1* expressing mice may be phenotypically similar and may also consist of progenitor cells that fail to adopt the proper maturational program.

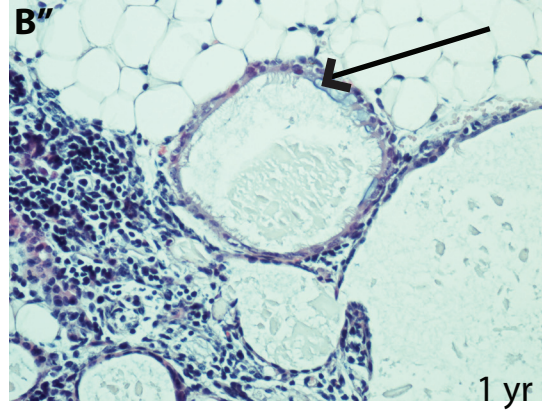
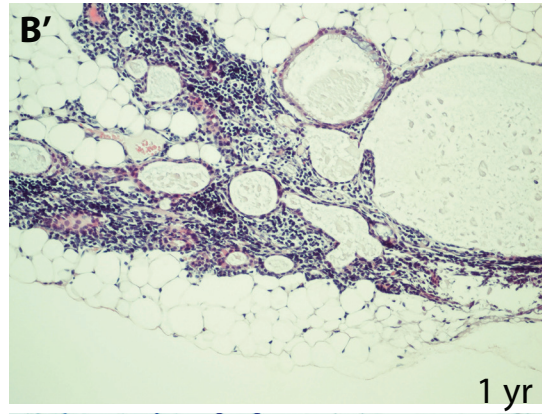
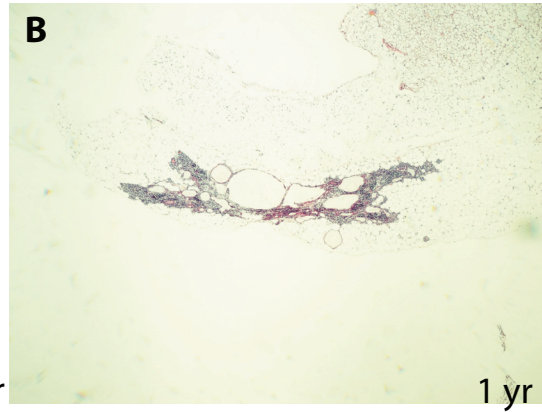
Together these data demonstrate that defects in TEC maturation and consequent aberrant thymocyte differentiation result in autoimmune pathology in adult *R26^{iTbx1/+}* mice.

Figure 19. Ciliated epithelial cysts are found in 1 yr $R26^{iTbx1/+}$ thymi. (A-B'') H&E stained sections of paraffin embedded 1 yr thymi. (A) control thymus, (B) $R26^{iTbx1/+}$ thymus, both taken at the same magnification. (B,B'') $R26^{iTbx1/+}$ thymi containing closer views of cysts within the thymus. The arrow indicates an area of respiratory epithelium characterized by cilia or secretory product lining a cyst.

R26^{+/+}, Foxn1^{Cre/+}



R26^{iTbx1/+}, Foxn1^{Cre/+}



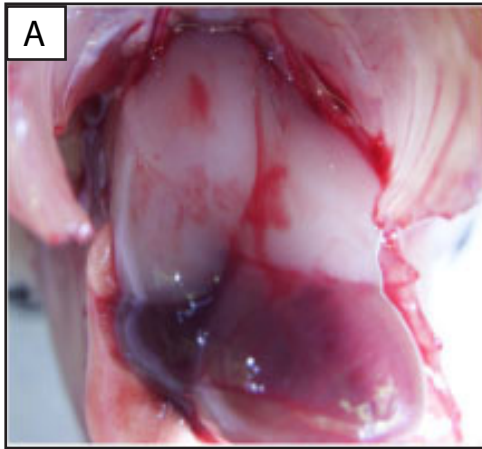
Chapter 2. Perithymic adipose tissue forms in the $R26^{iTbx1/+}$ postnatal thymus

Gross examination of adult $R26^{iTbx1/+}$ thymi *in situ* revealed an additional striking phenotype not observed in age-matched littermate controls. All postnatal mice examined, had hypoplastic thymic lobes that were embedded in adipose tissue (Figure 20). This thymic phenotype was not observed at any time in the developing embryo in controls or $R26^{iTbx1/+}$ thymi (Figure 21 A) indicating a dynamic accumulation or differentiation event occurring just subsequent to birth. Adipose tissue in $R26^{iTbx1/+}$ mice was confirmed using Oil-Red-O staining (Figure 21) and preliminarily with Ppar- γ staining (Figure 22 B). Oil-Red-O stains lipid accumulations while Ppar- γ is a transcription factor expressed by adipocytes and required for their development. The accumulation of adipose tissue was seen largely surrounding the exterior of the hypoplastic thymus lobes. However, in thymic sections Oil-Red-O and Ppar- γ positive cells were observed throughout the thymic lobes (Figure 21 B and Figure 22 B). Furthermore the amount of adipose tissue encasing thymic lobes appeared to correlate positively with age, as older $R26^{iTbx1/+}$ individuals contained thymi with the greatest extent of Oil-Red-O staining (Figure 21 B-D). The origin of the cells that generate the perithymic adipose tissue is not yet known. However, another thymic phenotype in $R26^{iTbx1/+}$ embryos may shed light on this phenomena.

During early stages of thymus organogenesis each thymus rudiment is surrounded by a NCC-derived capsule. The NCC-derived capsule provides growth factors such as Fgf-7 and Fgf-10, which are required for expansion of the developing epithelium. A well-demarcated NCC-derived capsule was detected

Figure 20. Gross examination $R26^{iTbx1/+}$ thymi *in situ* reveal perithymic adipose tissue. (A) Control mice show prominent thymic lobes localized anterior to the heart. (B, C)) Images taken at the same magnification of $R26^{iTbx1/+}$ thoracic cavities showing a hypoplastic thymus encased in adipose tissue. Note location is marked by a black box. (B' and C') Higher power images of the boxed areas in B and C showing perithymic adipose tissue.

R26^{+/+}, Foxn1^{Cre/+}



R26^{iTbx1/+}, Foxn1^{Cre/+}

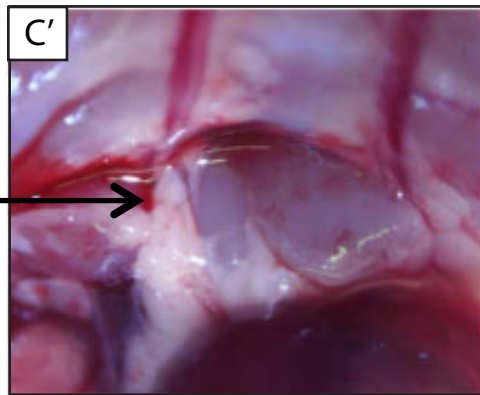
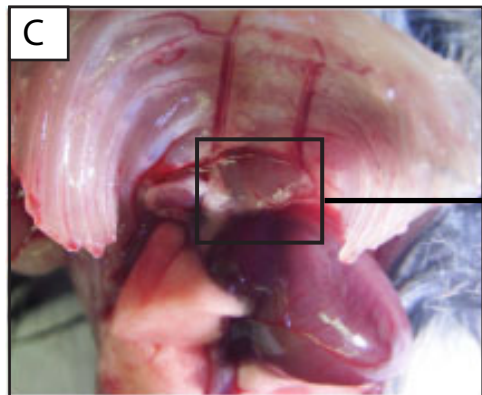
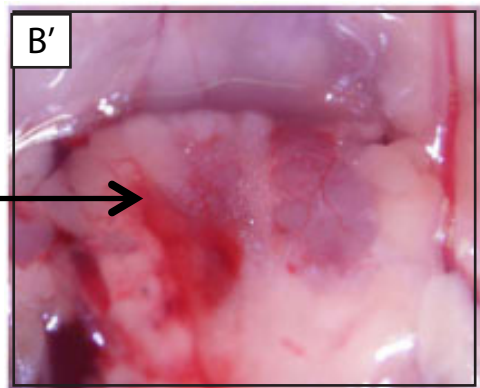
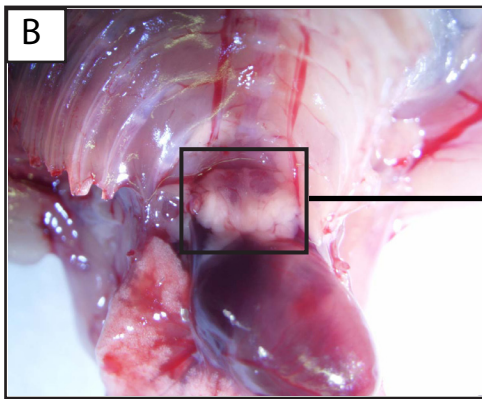
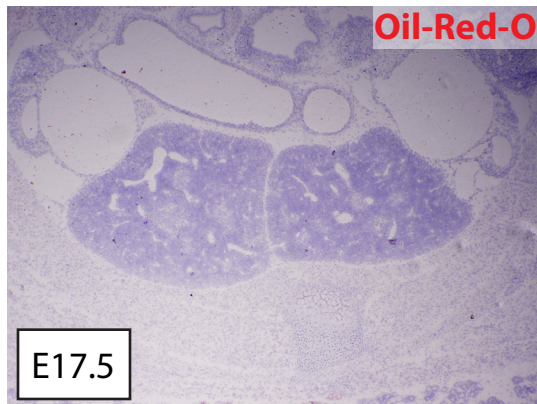


Figure 21. Adipocytes are not observed in fetal $R26^{iTbx1/+}$ thymi but accumulate progressively with postnatal age. Oil-Red-O staining of $R26^{iTbx1/+}$ thymi and controls at (A) E17.5, (B) NB (200x), (C (40x)) and D (200x)) 4 wks. Note that control thymi at E17.5 are taken at 40x, while E17.5 $R26^{iTbx1/+}$ thymi were captured at 100x for viewing purposes. n = at least two thymi per age per genotype.

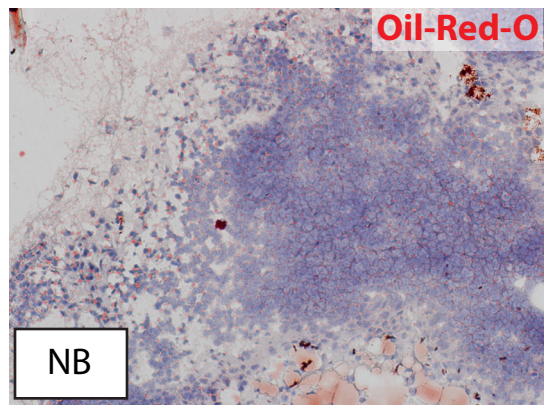
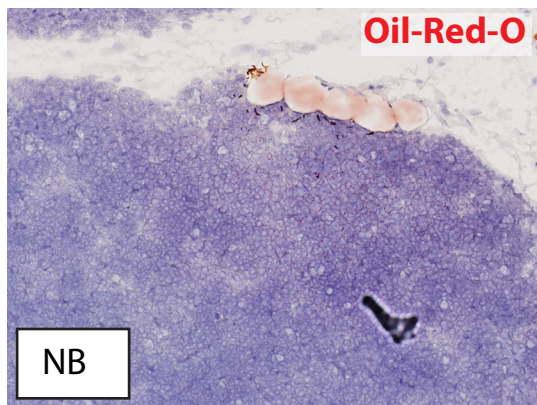
R26^{+/+}, Foxn1^{Cre/+}

R26^{iTbx1/+}, Foxn1^{Cre/+}

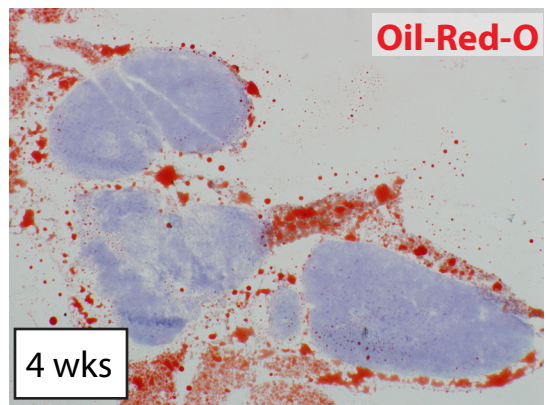
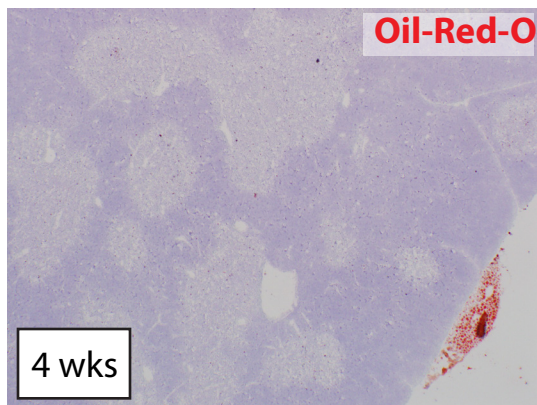
A



B



C



D

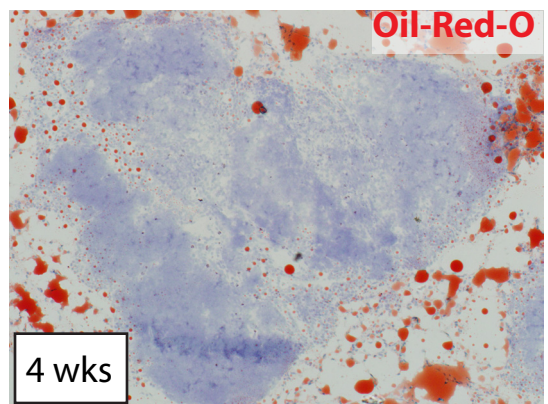
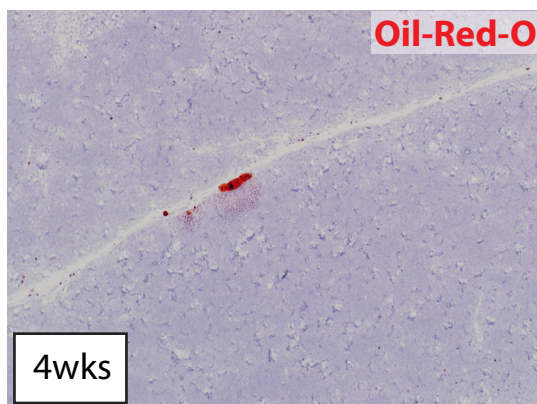
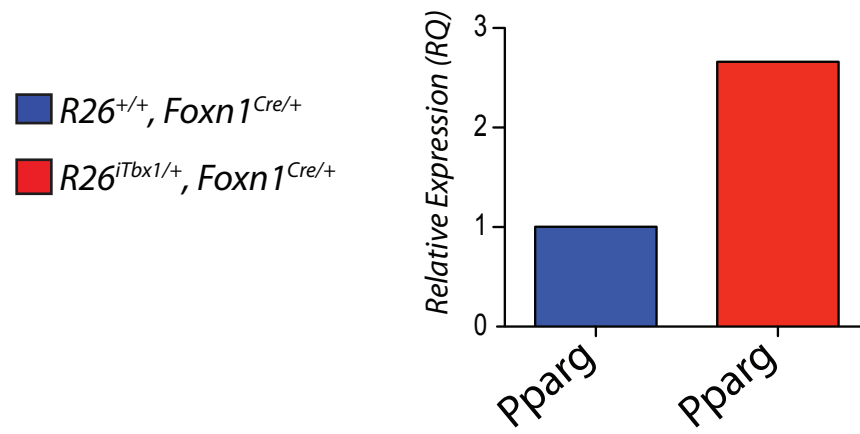
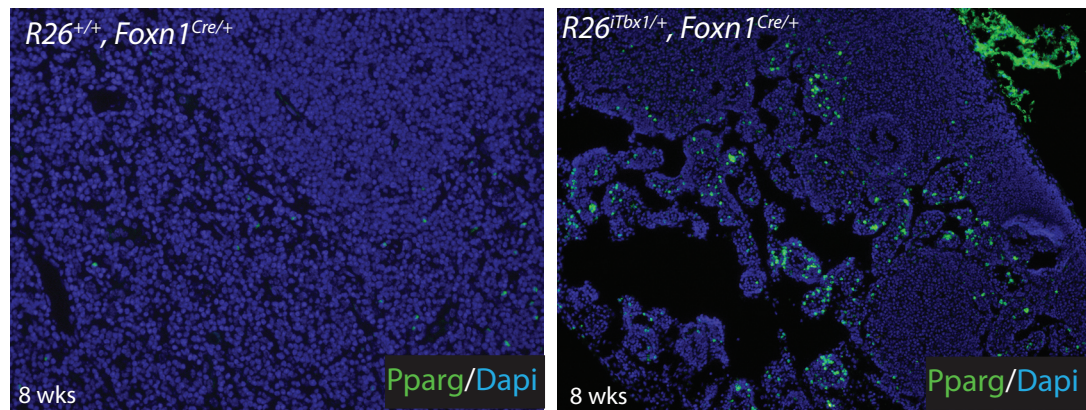


Figure 22. *Ppar-γ* is up-regulated in fetal stroma and prominent in *R26^{iTbx1/+}* postnatal thymi. (A) qRT-PCR of *Pparγ* on E17.5 control and *R26^{iTbx1/+}* pooled EpCAM⁺ CD45⁺ stromal cells. (B) *Pparγ* and Dapi staining of 8 week control and *R26^{iTbx1/+}* thymi. Both images captured at 200X.

A

E17.5 Pooled non-epithelial stroma

**B**

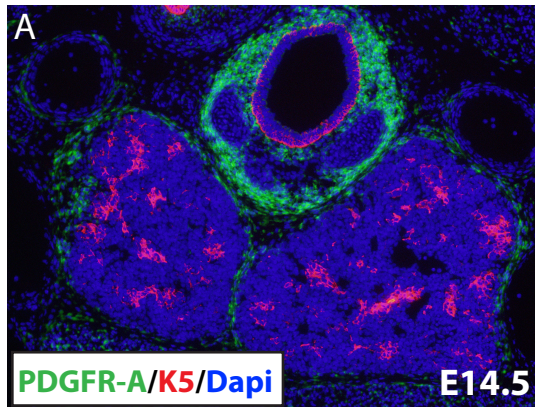
surrounding E14.5 control thymi by staining for PDGFR α , a marker of NCC-derived mesenchyme (Figure 23 A-B'). At E17.5 staining for PDGFR α revealed a NCC-derived capsule in controls. In addition, NCCs are present within the thymus epithelium at this stage (Figure 23 C-D). The immigration of NCCs into the thymic stroma is consistent with reports from other labs,(33), demonstrating that NCCs provide structural support for the developing thymic vasculature as they differentiate into pericytes. In striking contrast, we observed an expanded, thick PDGFR β capsule surrounding E14.5 and E17.5 in *R26^{iTbx1/+}* thymic lobes (Figure 23 B, B', D, See arrows). This capsule appeared to protrude into the thymus lobes creating a lobular appearance (Figure 22, B', D, see arrows). In addition, intense PDGFR β staining was observed in regions that appeared to be pinching off from the thymus lobe (Figure 23, D, see arrow). *R26^{iTbx1/+}* thymic NCC-derived capsules remained prominent even at late stages of gestation (Figure 23 D) and did not decrease in thickness with age as observed in E17.5 control thymi (Figure 23 C).

We analyzed postnatal thymi from 4 wk old mice for the persistence of NCC-derived mesenchyme and also for development of the thymic vasculature (Figure 24). Control thymi at 4 wks of age contained PDGFR β positive cells that lined

VE-Cadherin positive blood vessels (Figure 24 A, E). This is consistent with reported generation of pericytes from NC-derived cells (33). In striking contrast, *R26^{iTbx1/+}* thymi contained a dramatic increase in PDGFR β positive cells that were dispersed throughout the entire lobe. These cells did not always localize with the vasculature (Figure 24 B-D). Staining appeared prominent in areas that appeared to

Figure 23. Fetal $R26^{iTbx1/+}$ thymi are surrounded by a prominent NCC-derived capsule. (A-D') PDGFR α , K5 and Dapi staining of control and $R26^{iTbx1/+}$ thymic sections from E14.5 and E17.5 embryos. (A-B) Control and $R26^{iTbx1/+}$ E14.5 frozen sections (100x) or (A'-B') (200x). (C-D) E17.5 control and $R26^{iTbx1/+}$ frozen thymic sections stained for PDGFR α and K5 (100x). Arrows denote prominent capsule. n = at least 2 individuals per genotype.

R26^{+/+}, Foxn1^{Cre/+}



R26^{iTbx1/+}, Foxn1^{Cre/+}

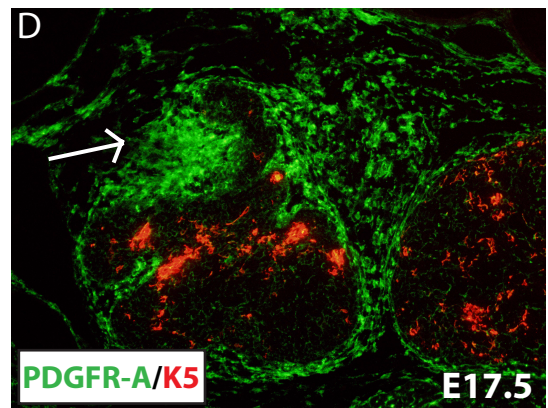
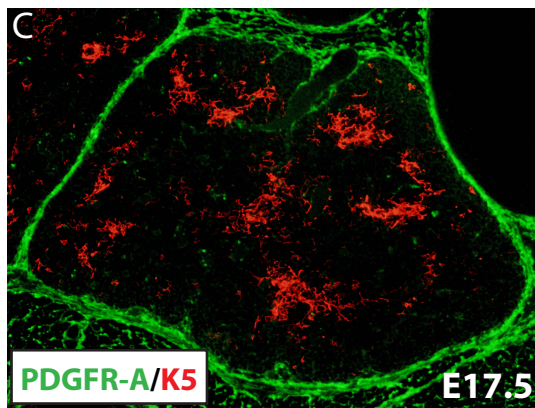
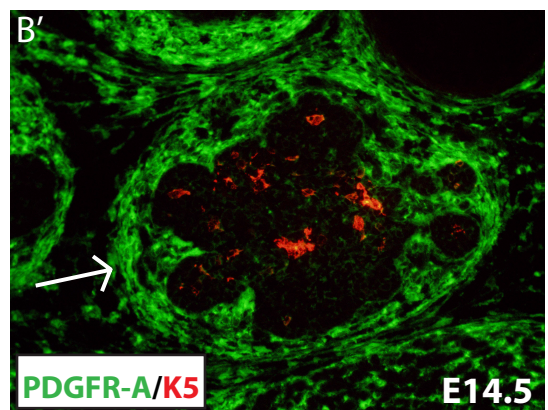
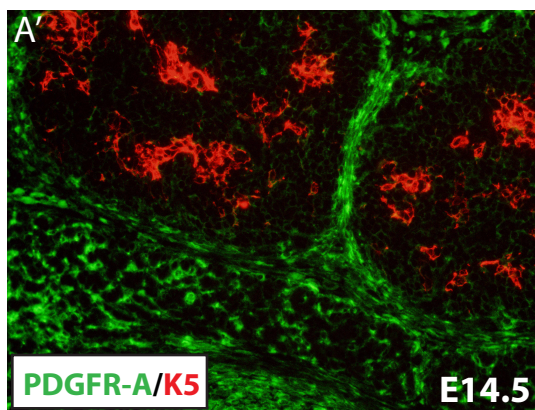
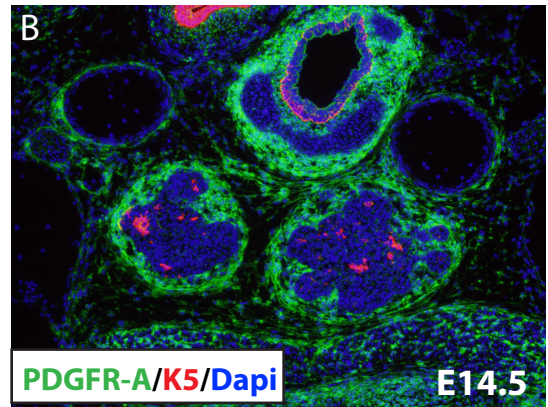
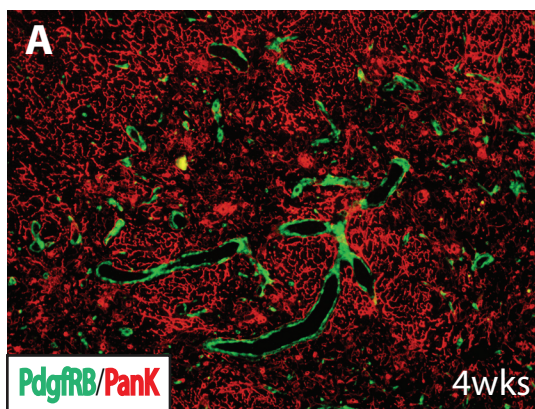
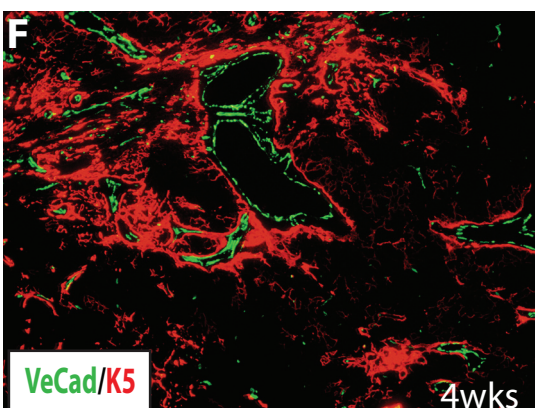
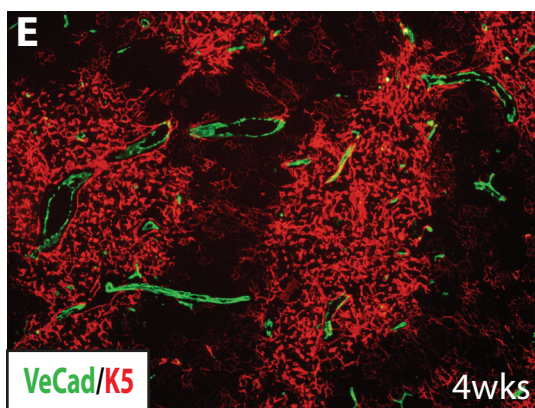
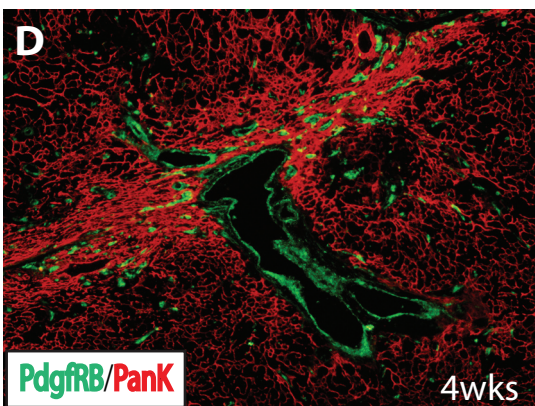
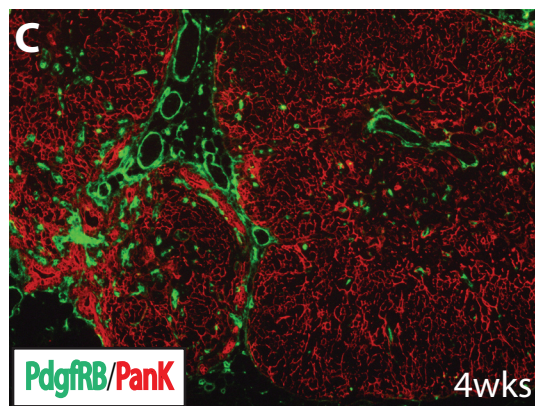
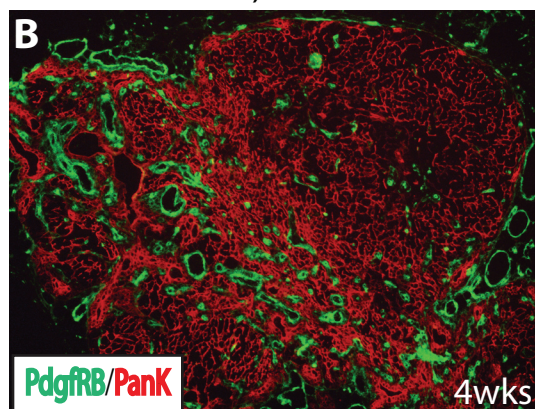


Figure 24. NCC-derived mesenchyme is aberrantly localized throughout postnatal $R26^{iTbx1/+}$ thymi. 4wk frozen thymi from control or $R26^{iTbx1/+}$ mice were stained with either PDGFR β and Pancytokeratin (A-D) or VE-Cadherin and K5 (E, F). All images captured at 100x. n = 2 individuals per genotype.

R26^{+/+}, Foxn1^{Cre/+}



R26^{iTbx1/+}, Foxn1^{Cre/+}



be budding off from the main lobe (Figure 24 C) and appeared almost invasive in nature.

It is tempting to speculate that postnatal adipose tissue arises from NCC-derived mesenchyme, given that this expanded capsule in fetal $R26^{iTbx1/+}$ thymi, precedes the appearance of postnatal adipose tissue. Lineage-tracing analyses are underway but are not yet completed. The finding of an obvious NCC phenotype in $R26^{iTbx1/+}$ thymi is particularly interestingly since the inducible *Tbx1* allele is not expressed in NCCs. This NCC phenotype is likely to be an indirect consequence attributable to an alteration in the essential crosstalk that occurs between TECs and NC-derived mesenchyme that is essential to orchestrate the developmental processes that result in thymus organogenesis.

Discussion

In conclusion, these studies support the hypothesis that forced activation of *Tbx1* in fetal TECs is not permissive for normal thymic development, and instead results in severe thymic hypoplasia, aberrant TEC differentiation and an overall decrease in thymus output. This is further evidenced by a loss of epithelial organization, defective thymocyte maturation, and abnormal NCC-derived mesenchymal invasion. In addition this progressive phenotype also coincided with an accumulation of postnatal adipose tissue, a feature often associated with degenerative thymi. The arrest of TEC differentiation was evidenced by aberrant expression of markers associated with differentiated TECs as well as by an

accumulation of Plet-1 positive progenitors in both fetal and adult thymi. *Foxn1*, a master regulator of TEC maturation and thymus homeostasis, was down-regulated in fetal TECs, suggesting that *Tbx1* expression negatively regulates this essential transcription factor. These defects did not arise secondary to defects in pouch formation or pouch patterning, as normal fate boundaries and pouch volume were comparable between *R26^{iTbx1/+}* and control mice. *R26^{iTbx1/+}* thymi consistently had an appreciable decrease in overall cellularity and hypoplastic thymi. Individuals that were most severely affected developed an autoimmune phenotype that manifested in corneal lesions and inflammatory infiltrations. Taken together, the data in this dissertation demonstrate that *Tbx1* expression must be down-regulated in the 3rd PP thymus-fated domain to permit *Foxn1* expression, TEC differentiation and normal thymus organogenesis and homeostasis.

Tbx1 plays many dynamic roles during development

Tbx1 plays many roles in different tissues during different times in development. Although the exact molecular mechanisms attributable to the thymic phenotypes observed in *R26^{iTbx1/+}* mice are still being elucidated we can glean clues to its actions by studying its functions in other tissues and organs, which utilize similar developmental pathways to achieve normal organogenesis. We can also analyze signaling pathways affected by *Tbx1* in other developmental systems. Often the developmental roles of these effector molecules are preserved from one structure to another and thus the resulting effects of these downstream targets may be recapitulated in thymus development.

Tbx1 is expressed in cardiac progenitor cells where it regulates their proliferation and differentiation (86). These progenitors give rise to the secondary heart field and contribute to formation of the outflow tract, atria and right ventricle (reviewed in (87)). In this cell population, proliferation is promoted by *Tbx1*, while differentiation is antagonized (86). Therefore loss of *Tbx1* expression is associated with premature differentiation of these progenitor cells, whereas ectopic expression of *Tbx1* suppresses differentiation (86). This suggests that *Tbx1* must be tightly regulated in order to balance the maintenance of a progenitor pool while still allowing for formation of more differentiated cell types. Previous studies have shown that *Tbx1* interacts with Fgf's to exert some of its downstream effects (68, 88).

Cardiac defects in *Tbx1* heterozygous mice could be partially rescued when *Fgf8* was ectopically expressed in *Tbx1* deficient cells, using a mouse model that knocked out *Tbx1* by knocking in *Fgf8* (89). This partial rescue was only observed when some expression of *Tbx1* was preserved indicating a requirement for *Tbx1* for an *Fgf8* response. This evidence implicates a role for *Tbx1* in cardiac morphogenesis and also reveals it acts in a linear pathway with *Fgf8* (63, 89, 90).

Consistent with a link between *Tbx1* and *Fgf8*, other investigators reported that a *Tbx1*-*Six1*/*Eya1*-*Fgf8* pathway is required for normal cardiovascular morphogenesis and craniofacial morphogenesis (63). *Six1* and *Eya1* regulate *Fgf8* in cardiac progenitors to sustain their survival and proliferation and thus regulate cardiovascular morphogenesis (63). This pathway is also employed in patterning the 3rd PP as discussed earlier (61). *Six1*^{-/-} mice did not have an altered expression pattern of *Tbx1* (61, 63). The penetrance of cardiovascular defects observed in

Tbx1^{+/-} mice increased almost 3-fold when crossed to mice deficient in *Eya1*, (*Tbx1*^{+/-}, *Eya1*^{+/-}). *Tbx1*^{+/-}, *Eya1*^{-/-} compound mutants displayed cardiovascular phenotypes that were 100% penetrant (63). An increase in penetrance was also observed when *Tbx1*^{+/-} mice were crossed to yield *Tbx1*^{+/-}, *Six1*^{+/-} compound mutants (63). These data suggest *Tbx1* lies upstream of *Six1* and *Eya1* in a common regulatory pathway that mediates Fgf8 signaling.

Tbx1 also regulates tooth morphogenesis. Tooth morphogenesis is an ideal system to study pathways involved in organogenesis, as many inductive interactions are required for tooth development. Crosstalk between NCC-derived mesenchyme and the oral epithelium is essential, similar to the requirement for crosstalk between these two tissues in thymus organogenesis. In short, formation of an epithelial bud occurs as the oral epithelium invades into underlying condensing mesenchyme. This results in formation of a tooth bud and eventually a “bell” stage tooth germ which later forms a tooth as cells within the late bud differentiate into ameloblasts that produce enamel and odontoblasts which produce dentin (reviewed in (91)). E16.5 *Tbx1*^{-/-} mice form smaller molars, lack cusps and have only a thin cell layer of pre-ameloblast (92). This phenotype is exacerbated at E18.5 as homozygous null mice form incisors that lack proliferating epithelial cells (92). *Tbx1* null mice were found to up-regulate the cyclin-dependent kinase inhibitor *p21*, which is normally down-regulated during cell division (92). This increase in *p21* expression was due to a lack of *Tbx1*-dependent PITX2 repression (92). PITX2 is a transcriptional activator of *p21* and is inhibited by binding of *Tbx1* to its C-terminal domain (92). Although we did not find a significant difference in proliferation

between *R26^{iTbx1/+}* and control thymi at E17.5, differences in proliferation may occur regulation occur at earlier or later developmental ages. For example *Tbx1* in TECs may maintain a slow-cycling progenitor population, such as Plet-1 positive TECs, by negatively regulating cell cycle inhibitors such as p21. Slight changes in proliferation at E17.5 may be beyond a detectable threshold but more apparent at later stages of maturation that have yet to be thoroughly analyzed in the context of cell division.

Bmp4 signaling is required for normal thymic development (93, 94). It has also been found to regulate development of cardiac progenitors (95) and mediate septation of the outflow tract. Recently, micro RNAs (miRNAs) were found in the 5' UTR of certain genes associated with cardiac development, including *Tbx1*. When activated by Bmps these miRNAs suppressed *Tbx1* and other genes such as *Isl1* known to be expressed in cardiac progenitors and promote myocardial differentiation (96). This evidence implies Bmp's indirectly negatively regulate *Tbx1*. In thymic development Bmp4 is expressed at E10.5 in the ventral-thymus fated domain in the 3rd PP and also in surrounding mesenchyme. Previous reports have shown that Bmp4 positively regulates thymus organogenesis by promoting *Foxn1* expression in TECs (93). Furthermore deletion of *Bmp4* in the endoderm and surrounding mesenchyme prior to *Foxn1*-expression resulted in morphological defects including failure of normal capsule formation and persistent of a thymic lumen (97). This suggests that inductive interactions between NCCs and thymic epithelial cells are required for proper organ formation. Given that *Tbx1* expression normally becomes restricted to the anterior dorsal parathyroid fated domain at E10.5, in a complimentary expression pattern to *Bmp4* and that these signaling

components are associated with opposing identities in the 3rd PP, it is possible that they may serve as mutually antagonistic regulators of cell fate in the 3rd PP. Forced expression of *Tbx1* in the ventral thymus fated domain may therefore negatively regulate expression of *Bmp4* in the endoderm resulting in abnormal thymic morphology and a decrease in *Foxn1* expression. It is also possible that ectopic activation of *Tbx1* in the ventral endoderm may result in aberrant signaling interactions between the epithelium and surrounding mesenchyme resulting in impaired formation of a NCC-derived capsule.

Coinciding with the notion that they may be acting in a regulatory loop, *Tbx1* has also shown to inhibit the Bmp signaling pathway by sequestering SMAD1 and thus preventing its interaction with SMAD4. Binding to the co-factor SMAD4 is required for nuclear translocation and transcriptional activation of downstream target genes. This binding has been shown to antagonize Bmp signaling and occurs independently of the DNA T-box binding domain.

Tbx1 has been shown to transcriptionally activate *Fgf10* in vitro (68). Several studies also reported in vivo findings that support this claim in the anterior heart field (88, 98). In pancreatic development mesenchymal-epithelial interactions are essential and in part mediated by signals from *Fgf10* expressed in the mesenchyme required for maintenance of epithelial progenitors (99). Furthermore, *Fgf10* signaling to the pancreatic epithelium acts during a specific developmental window and is concentration dependent. *Fgf10* null mice display a hypoplastic pancreas, however a clear understanding of its role in pancreagenesis was complicated by early embryonic lethality of mutant mice (100). To elucidate the role of *Fgf10*,

investigators drove expression ectopically in the pancreatic epithelium where it acted in an autocrine fashion and lead to an impairment of pancreatic epithelial differentiation (99). Analysis of markers that are used to identify early immature progenitors lead to the conclusion that this sustained expression arrested the epithelium in a progenitor state (99).

These examples are not inclusive of the roles played by *Tbx1* in development. Clearly there are many more, which will not be discussed in the scope of this thesis. While several transcriptional effects of *Tbx1* are mediated through its T-box binding domain, other effects are independent of this DNA-binding domain implying that *Tbx1* can regulate tissue morphogenesis by utilizing many diverse strategies that may be temporally or tissue-specific.

Blocks in TEC differentiation in $R26^{iTbx1/+}$ thymi coincide with a decrease in *Foxn1* expression

Thymic defects in $R26^{iTbx1/+}$ mice were observed as early as E12.5 since thymic rudiments already appeared hypoplastic compared to controls. This phenotype appeared progressive with age. Thymic lobes became highly lobulated and disorganized in fetal and adult $R26^{iTbx1/+}$ mice. These defects were not due to aberrant pouch formation as the pouch volume of $R26^{iTbx1/+}$ and $R26^{+/+}$ 3rd PPs were comparable. In addition, thymic defects were not attributable to alterations in patterning of the 3rd PP as *Foxn1* and *Gcm2* fated domains were not affected. Expression of GFP, a marker of *Tbx1* expression, was detected at E12.5 indicating successful *Cre*-mediated recombination and expression of *Tbx1*. However this does

not exclude the possibility that *Tbx1* may be expressed earlier within the 3rd PP, as expression of *Foxn1* has been shown to occur at E11.25. Regardless, conditional activation of the *iTbx1* allele using *Foxn1*^{Cre} does not appear to alter patterning of the 3rd PP with respect to either *Foxn1* or *Gcm2*.

Blocks in TEC differentiation and a breakdown in normal thymus morphology were evident as early as E14.5 in fetal development in *R26*^{*iTbx1/+*} thymi and sustained in the adult as evidenced by immunohistochemistry and FACS analysis. MHCII expression is expressed by E12.5 in the developing epithelium and is an early marker of TEC maturation and functionality. E17.5 *R26*^{*iTbx1/+*} TECs had a marked reduction in the expression of MHCII, implicating a block in one of the earliest stages of TEC maturation, required for the functional ability to present antigen to developing thymocytes. Further blocks of differentiation in *R26*^{*iTbx1/+*} thymi were evidenced by a decrease in the number of UEA⁺ cells, as well as by a decrease in the percentage of TECs that express the functional marker CD80. Furthermore, there was a variable and altered frequency of TEC subsets defined by expression of K5, K8 and K14 and these subsets were severely disorganized such that there were often no distinct cortical and medullary regions. This indicates that expression of *Tbx1* in TECs blocks their maturation and organization.

Blocks in TEC differentiation may be attributable in part to the reduction of *Foxn1* levels observed at E17.5 that occur as a result of ectopic sustained activation of *Tbx1* in TECs. *Foxn1* is essential for TEC differentiation and maintenance in a dose sensitive manner (47). The Manley lab generated *Foxn1*^{*lacZ*} mice by inserting an IRES-lacZ cassette into the 3'UTR of the *Foxn1* locus (49). Although fetal mice

express *lacZ* in a manner that recapitulates normal *Foxn1* expression, analysis of postnatal *Foxn1^{lacZ/lacZ}* thymi revealed a 50% reduction in *Foxn1* mRNA levels occurring as early as 1 wk after birth (47). The reduced gene dosage was attributable to hypermethylation of the *Foxn1* promoter region (47). *Foxn1^{lacZ/lacZ}* mice were crossed to *Foxn1^{nu/nu}* mice, to generate an allelic series for analysis of gene dosage effects (47). Down-regulation of *Foxn1* resulted in degeneration of the TEC compartment, thymic atrophy and a loss of specific TEC subsets. These defects directly correlated in severity with *Foxn1* levels (47). *Foxn1^{lacZ/lacZ}* and *Foxn1^{lacZ/nu}* thymi had a decrease in the overall percentage of MHCII^{hi} TECs and a loss of UEA1⁺ TECs compared to *Foxn1^{+/-lacZ}* thymi (47). MHCII^{hi} UEA1⁺ mTECs have been reported to express the highest levels of *Foxn1* mRNA and are therefore most sensitive to its reduction, with even slight changes in *Foxn1* transcription profoundly affecting this mTEC population (47). The phenotype in *Foxn1^{lacZ/lacZ}* mice is similar to that in *R26^{iTbx1/+}* thymi, supporting the premise that the reduction in *Foxn1* expression observed in *R26^{iTbx1/+}* TECs drives the aberrant TEC differentiation. It is interesting that *R26^{iTbx1/+}* thymi are able to retain expression of some cortical markers, notably Ly51 further coinciding with the notion that mTECs appear to be more severely affected and thus more sensitive to a reduction in *Foxn1* levels.

The idea that *Tbx1* may antagonize *Foxn1* directly has been investigated using Transcriptional Regulatory Elements Database (TRED) designed by the Micheal Zhang Laboratory at Cold Spring Harbor, which investigates regulatory elements upstream of transcriptional start sites for regions complimentary to known consensus binding sequences. Although a sequence capable of binding the T-box

binding domain was not found, this does not exclude the possibility that these two transcription factors directly interact. The *Foxn1* promoter region has yet to be thoroughly characterized, so a binding site for *Tbx1* may exist but has yet to be uncovered. It is also possible that *Tbx1* antagonizes *Foxn1* through a mechanism independent of its DNA binding site, as is the nature of its interaction with SMAD1 in craniofacial and cardiac development (described above). Lastly this inhibition may result indirectly, through interaction with other proteins that subsequently impinge upon *Foxn1*, as has been reported in the dental epithelium where *Tbx1* negatively regulates p21 by inhibiting its upstream activator *Pitx2*.

Sustained expression in $R26^{i\text{Tbx}1/+}$ TECs results in a progenitor arrest

The accumulation of Plet-1 positive TECs is suggestive of maturational arrest at an early TEC progenitor state. Interestingly at E17.5 but not E14.5 in $R26^{i\text{Tbx}1/+}$ thymi there was a dramatic retention of Plet-1 positive TECs. At E14.5, prior to this observed accumulation, *Foxn1* expression levels were comparable between control and $R26^{i\text{Tbx}1/+}$ thymi. While the frequency of Plet-1 positive TECs decreases with developmental age in control thymi, the frequency of Plet-1 progenitors increased in $R26^{i\text{Tbx}1/+}$ fetal thymi. Moreover, the accumulation of Plet-1+ progenitors was sustained in adult $R26^{i\text{Tbx}1/+}$ thymi. The onset of Plet-1 accumulation coincided with a decrease in *Foxn1* expression relative to controls. Co-staining for GFP and Plet-1 reveal that most Plet-1+ cells do not express *Tbx1* suggesting that they do not arise as a direct consequence of ectopic *Tbx1* activation. Indeed, *Foxn1* is not expressed until E11.25, after Plet-1 positive cells arise in the thymic epithelium. Furthermore,

Foxn1 is not required for the generation of Plet-1+ TEC precursors since *Foxn1*^{nu/nu} mice contain an immature thymic epithelial rudiment that is entirely Plet-1 positive (18).

It is thought that Plet-1 positive TECs replenish the epithelial microenvironment by asymmetric division, in which they self-renew and also give rise to another TEC that is directed to differentiate and adapt either a cortical or medullary fate (unpublished observation from the lab of Dr. Claire Blackburn). However the exact molecular mechanisms required for progenitor self-renewal and/or maintenance of an undifferentiated progenitor-like state is unknown. It has been observed that an age-related decline in the relative frequency of this population occurs with age as these progenitors fail to turn-over and self-renew (unpublished data from the Blackburn lab). Interestingly this age-progressive decline also correlates with a decrease in *Foxn1* expression, which is known to occur with age and also coincides with thymic involution and a gradual breakdown in the thymic microenvironment (47, 101). Considering these data I propose a model for the observed Plet-1 phenotype in *R26*^{iTbx1/+} thymi.

Given that Plet-1 positive cells accumulate in *Foxn1*^{nu/nu} mice and fail to differentiate it seems possible that *Foxn1* expression may be required in a non-cell autonomous fashion to drive asymmetric division of Plet-1 progenitors. In this model Plet-1 TECs divide into two daughter cells which both express low levels of Plet-1. This can be thought of as an intermediate state for each daughter cell, which is transient in nature. One progenitor TEC will up-regulate Plet-1 and serve to maintain the stem cell reserve that is required for thymic homeostasis, but the

second will receive *Foxn1*-dependent signals from neighboring TECs which will instruct it to down-regulate Plet-1 expression and further differentiate into a functional TEC. In the event that *Foxn1*-dependent signals are not seen by these Plet-1 positive TECs they can no longer asymmetrically divide. This would lead to a failure of normal TEC differentiation to occur. Consequently the thymic microenvironment can no longer be replenished. However, if this model holds true, *Foxn1*-independent signals must also play a role in establishment of this progenitor phenotype.

While an age-related decline in the turnover of Plet-1 positive TECs has been observed, this decline also coincides with an overall reduction in the percentage of Plet-1 positive TECs with age (unpublished data obtained from Blackburn lab), suggesting that this age related phenotype results from a failure of some instructive signal(s) to maintain the progenitor niche or progenitors themselves. While a decrease in *Foxn1* has been predicted to result in thymic involution it may not be required to sustain Plet-1 positive TECs, as *Foxn1*^{nu/nu} mice normally form an undifferentiated epithelial compartment consisting of Plet1+ cells that are sustained and arrested in a progenitor state. *Tbx1* plays many roles in development of various tissues, but is often associated with sustaining cells in an immature progenitor state and inhibits signaling pathways known to promote maturation (86, 92, 102).

Forced expression of Tbx1 in TECs negatively regulates Hes-1

We have evidence that *Tbx1* may be acting through the Notch-mediator *Hes1* in TECs to oppose differentiation and retain a pool of Plet-1 positive progenitors.

Notch signaling has been shown to have many roles in development that are context dependent. In hematopoietic stem cells (HSCs) it has been demonstrated to regulate proliferation, and self-renewal (reviewed in (103)). For example, activation of Notch signaling in cells within the HSC progenitor niche in bone marrow has been shown to be required for maintenance of the HSC pool. In thymic development, *Notch* activation is associated with T-lineage commitment and differentiation of early DN thymocytes (reviewed in (8)). In the intestine, and in neural development *Notch* has also been shown to play a role in fate determination (reviewed in (103)). In the developing mouse embryo, it has also been shown to be required for maintenance of muscle precursor cells (reviewed in (103)).

Recently *Hes1*, a major mediator of the Notch signaling pathway has been shown to be required in *Tbx1* positive cells for proper development of the pharyngeal arch arteries and thymus (81). In addition, *Hes1* is expressed in both cTEC and mTEC lineages (104). This suggests a requirement for bidirectional Notch signaling between developing thymocytes and TECs for normal maturation of both cell types. However, a cell-autonomous requirement for Notch signaling in TEC development has been difficult to ascertain given its promiscuous non-autonomous roles in numerous cell types within the thymus. For example, Notch signaling in T- and B-cells through its ligand DLL1 is implicated in normal TEC development. Therefore, the function of *Hes1* and/or the Notch signaling pathway in TECs in regards to their maturation has been largely unexplored.

The downstream Notch target gene *Hes1* has been shown to antagonize Notch signaling by binding to the Notch DNA-binding partner RBP-J κ (105). The decrease

in *Hes1* expression observed at E14.5 may contribute to an interruption of the normal pattern of asymmetric cell division of Plet-1 progenitors. It could also play a role normally in TECs to drive a program of differentiation. This leads to the establishment of a model whereby Notch signaling in TECs is normally initiated to sustain an early progenitor pool. This activation leads to transcription of its downstream effector molecule *Hes1*, which acts through a feed back loop to antagonize Notch signaling and promote the differentiation of a small subset of TEC progenitors in order to replenish the thymic microenvironment. However this feed-back loop in our *R26^{iTbx1/+}* mouse model is ultimately broken. *Tbx1* either directly or indirectly antagonizes *Hes1* expression in *R26^{iTbx1/+}* thymi leading to an increase in Notch signaling and thus an accumulation of Plet-1 positive progenitors that are unable to differentiate and adopt either a cortical or medullary fate. This may result in the resulting aberrant TEC phenotype observed. Of particular interest is the localization of the Plet-1 positive TECs themselves in *R26^{iTbx1/+}* thymi, as they appear to arise in clusters surrounding GFP positive TECs. This suggests the presence of cellular interactions occurring between both cell types. It is tempting to speculate that signals from *Tbx1*-expressing TECs, perhaps Notch, are permissive for the persistence of Plet-1 TECs.

CCL25 and IL-7 chemokines are reduced in *R26^{iTbx1/+}* TECs

Given the reduced *Foxn1* expression and the early block in TEC differentiation we analyzed expression of genes involved in thymocyte-TEC interactions that may be affected and contribute to the defects observed in *R26^{iTbx1/+}* thymi. CCL25 is

expressed by fetal TECs via *Foxn1*-independent and –dependent mechanisms (28). Although neither an increase in apoptosis or a decrease in proliferation was observed in fetal thymi to account for the dramatic decrease in total cellularity, a decrease in the TEC-expressed chemokine CCL25 was observed. This ligand is secreted by the developing primordium as well as by the more mature thymic epithelium later in gestation to attract thymus-seeding cells. CCL25 acts to support thymus colonization by binding to chemokine receptor CCR9 expressed on early hematopoietic progenitors (28). Mice deficient in CCR9 have a decrease in thymus cellularity that is attributable to defects in progenitor homing to the fetal thymus (28). This is also one of the developmental defects associated with TECs in *Foxn1*^{nu/nu} mice and results in their inability to attract hematopoietic progenitors. The decrease in CCL25 observed may occur as a secondary consequence attributable to a reduction in *Foxn1* or it may also be the result of other signaling aberrancies. In addition it may be that *Tbx1* directly antagonizes expression of CCL25. Regardless, this decrease in CCL25 expression could result in a decrease in the number of progenitors that initially colonize the fetal thymus and subsequently a decrease in cellularity.

Defective TEC differentiation is also evidenced by a decrease in *IL-7* at E17.5. This decrease consequently results in a failure of early thymic progenitors to be sustained in *R26*^{*iTbx1*/+} thymi, likely resulting in defects in early DN maturation observed. Defects in proliferation were not observed at this age, but may not be apparent, or are too subtle to detect. These subtle defects may later be compounded upon by a further collapse of the thymic microenvironment. In addition,

these defects may also precede or coincide with a failure of these early thymocytes to be sustained in epithelial niches that provide signals required for their development.

Thymocyte maturation in $R26^{iTbx1/+}$ thymi was reflective of a severely impaired thymic epithelium. These defects are directly attributable to the above described functional blocks in TEC differentiation, as crosstalk between the thymic epithelium and developing thymocytes is essential for T-cell maturation. All of the major subsets as defined by CD4 and CD8 were present in $R26^{iTbx1/+}$ thymi although some adult individuals contained diminished CD4⁺ and CD8⁺ populations consistent with a DP to SP block, while others contained subsets with percentages that were comparable to controls. This is likely attributable to variation in expression of MHC II within $R26^{iTbx1/+}$ thymus, with some individuals or lobes being more severely impaired. The overall cellularity was consistently drastically reduced in $R26^{iTbx1/+}$ thymi compared to controls. This is likely attributable to defects in the earliest stages of thymocyte maturation. In examining DN subsets characterized by expression of CD44 and CD25 we consistently found $R26^{iTbx1/+}$ thymi to contain an intermediate population that was CD25^{hi}CD44^{mid}, suggesting a partial DN1 to DN2 block. In addition we also observed aberrancies that correlated with the DN3 and DN4 stages of maturation. A decrease in DN3 was often found to occur in $R26^{iTbx1/+}$ thymi as well as a decrease in DN4. This thymocyte phenotype is reminiscent of that reported in $Foxn1^{lacz/lacz}$ mice by the Manley lab (47). This thymocyte phenotype is consistent with and likely attributable to the decrease in *Foxn1* observed in $R26^{iTbx1/+}$ thymi.

Development of a functional thymic epithelium is required for formation of a self-restricted, self-tolerant T-cell repertoire and therefore also essential in mediating central tolerance. Severe pathological lesions indicative of autoimmune manifestations were found by Dr. Donna Kusewit in $R26^{iTbx1/+}$ mice but not age-matched, littermate controls. In addition to severe thymus hypoplasia, fibroplasia of the cornea, mild keratitis, conjunctivitis and inflammation of both the intra- and extra- orbital lacrimal and Meibomian glands of the eyes were noted. These findings are consistent with autoimmune keratoconjunctivitis. This pathological lymphocytic infiltration is similar to lesions described in *Aire*-deficient mice (83) and other immunodeficient models, such as those mimicking Sjogren syndrome (84). This is further evidence of immune failure that is a consequence of a dysfunctional thymic epithelium.

Potential sources of postnatal adipose tissue

The perithymic adipose observed in postnatal $R26^{iTbx1/+}$ but not controls or in fetal thymi of either genotype is intriguing. Thymic adipose is a feature associated with involution and its accumulation is correlated with a loss of healthy thymic stromal tissue (reviewed in (106)). The molecular mechanisms responsible for this age-related involution are unknown, but a decrease in *Foxn1* has been found to contribute to this degeneration. While we do observe perithymic adipose that increases with postnatal age in $R26^{iTbx1/+}$ mice, we do not believe this model to mimic an accelerated form of thymic involution and thus is not a model for age-related thymic atrophy. The thymic epithelium in $R26^{iTbx1/+}$ mice fails to differentiate and

develop early on and thus a functional microenvironment is never achieved.

However, the cellular origin of perithymic adipose tissue is still unknown.

Given that this phenotype was apparent only after birth, we speculated that a possible rapid accumulation of adipocytes around the thymus during late stages of fetal gestation may occur, and result in the observed postnatal phenotype. However evidence for this theory was not found as Oil-Red-O staining in late fetal gestation was negative. This is also consistent with the thymic adipose tissue observed being morphologically similar to white adipose tissue, which is generated predominately after birth (107).

We therefore made three hypotheses as to cellular origins of surrounding perithymic adipose. Thymic adipose in *R26^{Tbx1/+}* mice arises from 1. An epithelial to mesenchymal cell transition (EMT) in which TECs adopt a mesenchymal fate, subsequent to their differentiation down an adipocyte lineage 2. A transition of NCCs into an adipocytes lineage or 3. Differentiation of non-NCC derived mesodermal mesenchyme into adipocytes.

First, we considered the possibility that the perithymic adipocyte accumulation could result from an epithelial-to-mesenchymal transition (EMT). This mechanism has been postulated to account for generation of thymic adipose tissue that results with involution (108). An increase in intrathymic adipose tissue correlates with an age-related decline of the orexigen ghrelin and its receptors in TECs (108). A deficiency in ghrelin-receptor signaling was also shown to facilitate an EMT transition in TECs as evidenced by an increase in the EMT associated marker

FSP-1, and lineage tracing analysis (108). These mesenchymal cells were found to up-regulate and express a number of pro-adipogenic markers such as PPAR γ -2 and CD36 and contribute to age-associated thymic adipose tissue. Furthermore, ghrelin supplementation in old mice was shown to partially reverse this age-associated phenotype (108). We therefore explored the possibility that the increase in thymic adiposity observed in postnatal $R26^{iTbx1/+}$ mice may be a result of an EMT transition and subsequent adoption of an adipocyte fate. However we did not find this to be the case. Thymic adipose in $R26^{iTbx1/+}$ mice was found to be GFP negative, demonstrating that this tissue was not epithelial in origin.

We next speculated that perithymic thymic adipose tissue arising in $R26^{iTbx1/+}$ thymi results from either a transition of NCCs or non-NCC derived mesenchyme, mesodermal mesenchyme, into an adipocyte fate. Mesodermal mesenchyme has been shown to give rise to adipose tissue (109). In addition, in vitro experiments using both cephalic and trunk NCCs from quail have shown that they can also differentiate into adipocytes when cultured under appropriate conditions that include retinoic acid (RA)(109). This suggests that these cells retain adipogenic potential. Furthermore, when $Sox10^{Cre}$, $R26^{YFP}$ mice were utilized to trace NCCs and their progeny it was found that a subset of adipocytes in the postnatal mouse arose from NCCs and not mesoderm (109). This led us to speculate that perithymic adipose arise from cells of either NCC or non-NCC derived mesenchymal origin.

It is interesting that the NCC-derived capsule surrounding $R26^{iTbx1/+}$ fetal thymi is increased in size relative to controls. The prominent NCC-derived capsule is maintained even at developmental stages where control NCC-derived capsules

decrease in prominence. In addition, NCC-derived mesenchymal were also in areas that appear to be budding off from the main lobe, suggesting that this phenotype may be invasive in nature. *Tbx1* expression has been shown to regulate NCC-migration in the pharyngeal arch arteries through regulation of the transcription factor *Gbx2* and aberrancies in this NCC migration pattern have also been observed in *Tbx1-null* mice suggesting a requirement for *Tbx1* in proper NCC migration (110). It is possible that ectopic *Tbx1* signaling from TECs lead to NCC migration pattern that promotes their accumulation in the *R26^{iTbx1/+}* perithymic capsule. Deficiencies or alterations in normal signaling pathways such as *Gbx2* from the thymic epithelium to adjacent mesenchyme could result in a NCC-phenotype.

Migration of NCCs into the thymic epithelium occurs normally in development at approximately E14.5 as they differentiate into pericytes, which play a supportive role in establishing and maintaining the thymic vasculature. Intrathymic NCC derivatives were observed in *R26^{iTbx1/+}* mice, however only some of these derivatives, which stained positive by PDGFR α , appeared to coincide with vascular regions as defined by VE-Cadherin staining. The functionality of these cells is not known and was not assessed. An accumulation in the subcapsular region clearly does not result from a failure of these NCCs to migrate into the epithelium, however an impairment in TEC differentiation may occur prior to entry into the thymic lobes.

Given that a prominent NCC-capsule is formed early in development and sustained in *R26^{iTbx1/+}* thymi and given the preliminary increase of *Ppar γ* observed in *R26^{iTbx1/+}* stroma, we propose that the thymic adipose tissue observed in postnatal *R26^{iTbx1/+}* thymi is of NCC origin. To test this assumption we are conducting lineage-

tracing analysis, using a NCC-specific *Wnt-1^{Flp}* mouse model. Since, activation of the *iTbx1* allele in *R26^{iTbx1/+}* mice utilizes the cre-lox system to achieve tissue-specific activation of *Tbx1* in TECs, we cannot use *Wnt-1^{Cre}* mice to indelibly label NCCs and their progeny, as this would result in *Tbx1* activation in NCCs. Therefore we obtained *Wnt-1^{Flp}* mice from Dr. Susan Dymecki, to take advantage of the FLP-FRT recombination system instead. These mice will be crossed to a dual reporter line, also obtained and generated in the Dymecki lab, in which both GFP and mCherry have been knocked into the *Rosa26 locus*, under the control of a CAG promoter, denoted *R26^{Frepe}*. In this model a FRT flanked stop cassette is upstream of an *mCherry* cassette, allowing for expression of the red mCherry protein upon *Flp*-mediated recombination.

We are currently crossing *Wnt-1^{Flp}*, *R26^{Frepe}* lines to *R26^{iTbx1/+}*, *Foxn1^{Cre/+}* lines to achieve a *Wnt-1^{Flp}*, *R26^{Frepe}*, *R26^{iTbx1}*, *Foxn1^{Cre}* expressing mouse. Given the elaborate nature of this cross, it has taken considerable time to generate the mice required for this experiment. Studies are currently underway to verify fidelity of expression of *Wnt1^{Flp}*, *R26^{Frepe}* reporter lines. Once confirmed, this line, *Wnt1^{Flp}*, *R26^{Frepe}* will be crossed to our *R26^{iTbx1}*, *Foxn1^{Cre}* model and allow for either the exclusion or confirmation of a NCC-origin for perithymic adipose tissue. NCCs and their progeny would express *mCherry*. Therefore, if the perithymic adipocytes are derived from NCCs they will express the mCherry reporter and be red in color. It is possible that thymic adipose tissue will not express mCherry when lineage tracing is performed, indicating that these cells are not NCC-derived. A non-NCC derived mesodermal mesenchymal origin will then be implied.

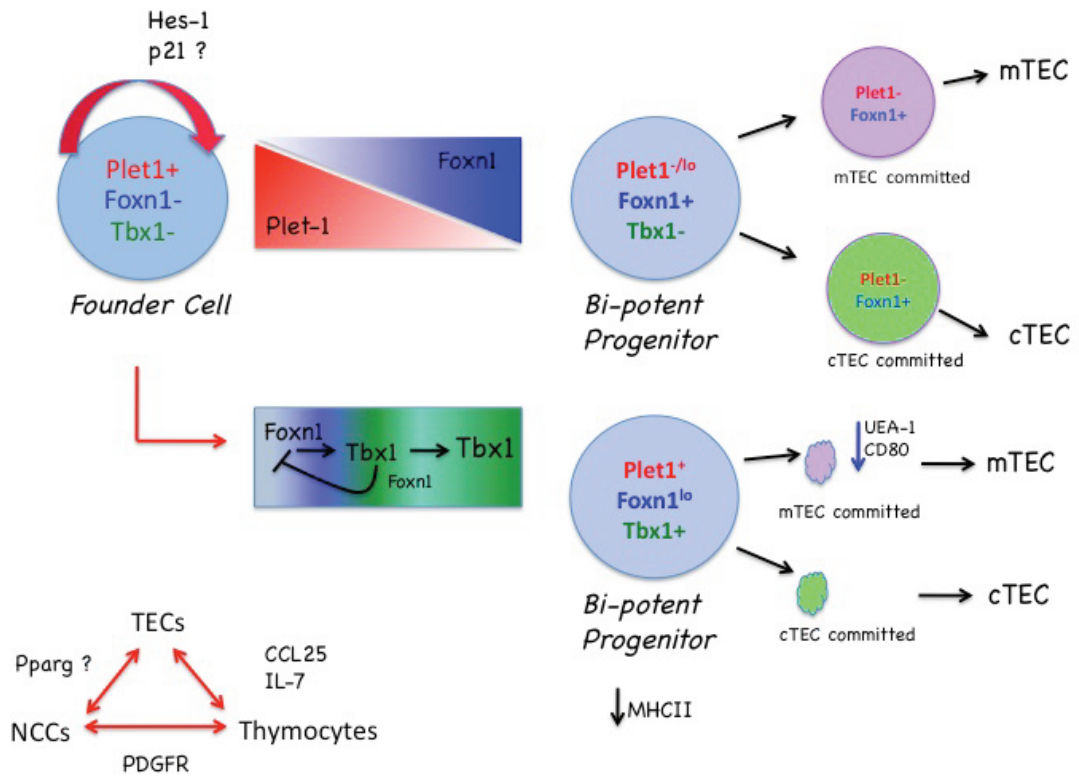
Conclusions

Taken together *Tbx1* expression in the ventral thymus-fated domain must be down-regulated for normal thymus organogenesis to occur and differentiation of the thymic epithelium to proceed. Reciprocal interactions between TECs, thymocytes and NCC-derived mesenchyme are mutually required for maturation of each cell type (Figure 25). Therefore, altered signaling events resulting in developmental blocks in one cell population have indirect but significant consequences for another.

This data suggest a model for thymus organogenesis in which a Plet-1 positive progenitor is established initially independent of *Foxn1* expression in the epithelium and gives rise to more differentiated cTEC and mTEC progenitors through asymmetric cell division (Figure 25). This differentiation coincides with a decrease in Plet-1 in normal thymi. However, in the *R26^{iTbx1/+}* thymus there is an accumulation of Plet-1 TECs. Maturation of precursors into functional TECs is blocked, as they fail to properly express MHCII and IL-7 required for thymocyte maturation and CCL25 required for attraction of early thymocyte seeding cells. Furthermore, the mTEC specific marker CD80 is markedly decreased suggesting an inability of *iTbx1* TECs to negatively select for and eliminate auto-reactive thymocytes. These defects are likely attributable to a decrease in *Foxn1* expression in TECs and consequently results in their inability to provide supportive signals required by developing thymocytes. Defective thymocyte development thus results indirectly as a consequence of aberrant TEC-thymocyte interactions that result from a failure in TEC maturation.

Although NCCs do not express the *iTbx1* allele, we hypothesize that the block in TEC differentiation leads to abnormal signaling from TECs to NCCs resulting in a NCC-phenotype, initially resulting in an expanded perithymic capsule and later to perithymic adipose tissue after birth. Furthermore, a failure of TEC-NCC crosstalk could indirectly lead to altered fate decisions in the NCC-derived mesenchyme. Taken together, data presented in this dissertation demonstrate that enforced *Tbx1*-expression negatively regulates TEC differentiation and *Foxn1* expression, which is required for TEC development and homeostasis. In addition, the block in TEC development prevents the crosstalk among epithelial, hematopoietic and NCCs that regulates development of each cell type. Therefore, *Tbx1* expression must be down-regulated in the ventral thymus-fated domain for mutual inductive interactions to be preserved and thymic development to proceed.

Figure 25. Model for TEC development in $R26^{iTbx1/+}$ mouse model. Development of a bipotent c/m-TEC progenitor occurs from a founder cell that is $Plet1^+$, $Tbx1^-$, $Foxn1^-$. This bipotent progenitor, $Plet1^{-/lo}$, $Tbx1^-$, $Foxn1^+$ gives rise to more differentially restricted TECs and eventually to mature c/m-TECs. In the $R26^{iTbx1/+}$ mouse model the majority of TECs are arrested at the Plet-1 positive stage and fail to further mature. These functional defects have indirect but significant affects on NCCs and thymocytes, which each mutually rely upon each other for inductive interactions for their development.



Bibliography

1. Singer, A., and R. Bosselut. 2004. CD4/CD8 coreceptors in thymocyte development, selection, and lineage commitment: analysis of the CD4/CD8 lineage decision. *Adv Immunol* 83:91-131.
2. Ciofani, M., and J. C. Zuniga-Pflucker. 2010. Determining gammadelta versus alphass T cell development. *Nat Rev Immunol* 10:657-663.
3. Romagnani, S. 2000. T-cell subsets (Th1 versus Th2). *Ann Allergy Asthma Immunol* 85:9-18; quiz 18, 21.
4. Umland, O., W. N. Mwangi, B. M. Anderson, J. C. Walker, and H. T. Petrie. 2007. The blood contains multiple distinct progenitor populations with clonogenic B and T lineage potential. *J Immunol* 178:4147-4152.
5. Takahama, Y. 2006. Journey through the thymus: stromal guides for T-cell development and selection. *Nat Rev Immunol* 6:127-135.
6. van Ewijk, W. 1991. T-cell differentiation is influenced by thymic microenvironments. *Annu Rev Immunol* 9:591-615.
7. Porritt, H. E., L. L. Rumfelt, S. Tabrizifard, T. M. Schmitt, J. C. Zuniga-Pflucker, and H. T. Petrie. 2004. Heterogeneity among DN1 prothymocytes reveals multiple progenitors with different capacities to generate T cell and non-T cell lineages. *Immunity* 20:735-745.
8. Laky, K., and B. J. Fowlkes. 2008. Notch signaling in CD4 and CD8 T cell development. *Curr Opin Immunol* 20:197-202.

9. Hernandez, J. B., R. H. Newton, and C. M. Walsh. 2010. Life and death in the thymus--cell death signaling during T cell development. *Curr Opin Cell Biol* 22:865-871.
10. Carpenter, A. C., and R. Bosselut. 2010. Decision checkpoints in the thymus. *Nat Immunol* 11:666-673.
11. Alpdogan, O., and M. R. van den Brink. 2005. IL-7 and IL-15: therapeutic cytokines for immunodeficiency. *Trends Immunol* 26:56-64.
12. El Kassar, N., P. J. Lucas, D. B. Klug, M. Zamisch, M. Merchant, C. V. Bare, B. Choudhury, S. O. Sharrow, E. Richie, C. L. Mackall, and R. E. Gress. 2004. A dose effect of IL-7 on thymocyte development. *Blood* 104:1419-1427.
13. von Freeden-Jeffry, U., N. Solvason, M. Howard, and R. Murray. 1997. The earliest T lineage-committed cells depend on IL-7 for Bcl-2 expression and normal cell cycle progression. *Immunity* 7:147-154.
14. Zamisch, M., B. Moore-Scott, D. M. Su, P. J. Lucas, N. Manley, and E. R. Richie. 2005. Ontogeny and regulation of IL-7-expressing thymic epithelial cells. *J Immunol* 174:60-67.
15. Anderson, M. S., and M. A. Su. 2011. Aire and T cell development. *Curr Opin Immunol* 23:198-206.
16. Alves, N. L., N. D. Huntington, J. J. Mention, O. Richard-Le Goff, and J. P. Di Santo. 2010. Cutting Edge: a thymocyte-thymic epithelial cell cross-talk dynamically regulates intrathymic IL-7 expression in vivo. *J Immunol* 184:5949-5953.

17. Manley, N. R., E. R. Richie, C. C. Blackburn, B. G. Condie, and J. Sage. 2011. Structure and function of the thymic microenvironment. *Front Biosci* 17:2461-2477.
18. Blackburn, C. C., C. L. Augustine, R. Li, R. P. Harvey, M. A. Malin, R. L. Boyd, J. F. Miller, and G. Morahan. 1996. The nu gene acts cell-autonomously and is required for differentiation of thymic epithelial progenitors. *Proc Natl Acad Sci U S A* 93:5742-5746.
19. Blackburn, C. C., and N. R. Manley. 2004. Developing a new paradigm for thymus organogenesis. *Nat Rev Immunol* 4:278-289.
20. Blackburn, C. C., N. R. Manley, D. B. Palmer, R. L. Boyd, G. Anderson, and M. A. Ritter. 2002. One for all and all for one: thymic epithelial stem cells and regeneration. *Trends Immunol* 23:391-395.
21. Klug, D. B., C. Carter, I. B. Gimenez-Conti, and E. R. Richie. 2002. Cutting edge: thymocyte-independent and thymocyte-dependent phases of epithelial patterning in the fetal thymus. *J Immunol* 169:2842-2845.
22. Shakib, S., G. E. Desanti, W. E. Jenkinson, S. M. Parnell, E. J. Jenkinson, and G. Anderson. 2009. Checkpoints in the development of thymic cortical epithelial cells. *J Immunol* 182:130-137.
23. Gill, J., M. Malin, G. A. Hollander, and R. Boyd. 2002. Generation of a complete thymic microenvironment by MTS24(+) thymic epithelial cells. *Nat Immunol* 3:635-642.

24. Shinohara, T., and T. Honjo. 1997. Studies in vitro on the mechanism of the epithelial/mesenchymal interaction in the early fetal thymus. *Eur J Immunol* 27:522-529.
25. Ripen, A. M., T. Nitta, S. Murata, K. Tanaka, and Y. Takahama. 2011. Ontogeny of thymic cortical epithelial cells expressing the thymoproteasome subunit beta5t. *Eur J Immunol* 41:1278-1287.
26. Nitta, T., I. Ohigashi, Y. Nakagawa, and Y. Takahama. 2011. Cytokine crosstalk for thymic medulla formation. *Curr Opin Immunol* 23:190-197.
27. Gabler, J., J. Arnold, and B. Kyewski. 2007. Promiscuous gene expression and the developmental dynamics of medullary thymic epithelial cells. *Eur J Immunol* 37:3363-3372.
28. Liu, C., F. Saito, Z. Liu, Y. Lei, S. Uehara, P. Love, M. Lipp, S. Kondo, N. Manley, and Y. Takahama. 2006. Coordination between CCR7- and CCR9-mediated chemokine signals in prevascular fetal thymus colonization. *Blood* 108:2531-2539.
29. Klug, D. B., C. Carter, E. Crouch, D. Roop, C. J. Conti, and E. R. Richie. 1998. Interdependence of cortical thymic epithelial cell differentiation and T-lineage commitment. *Proc Natl Acad Sci U S A* 95:11822-11827.
30. Owen, J. J., D. E. McLoughlin, R. K. Suniara, and E. J. Jenkinson. 2000. The role of mesenchyme in thymus development. *Curr Top Microbiol Immunol* 251:133-137.
31. Krispin, S., E. Nitzan, and C. Kalcheim. 2010. The dorsal neural tube: a dynamic setting for cell fate decisions. *Dev Neurobiol* 70:796-812.

32. Hutson, M. R., and M. L. Kirby. 2007. Model systems for the study of heart development and disease. Cardiac neural crest and conotruncal malformations. *Semin Cell Dev Biol* 18:101-110.
33. Foster, K., J. Sheridan, H. Veiga-Fernandes, K. Roderick, V. Pachnis, R. Adams, C. Blackburn, D. Kioussis, and M. Coles. 2008. Contribution of neural crest-derived cells in the embryonic and adult thymus. *J Immunol* 180:3183-3189.
34. Muller, S. M., C. C. Stolt, G. Terszowski, C. Blum, T. Amagai, N. Kessaris, P. Iannarelli, W. D. Richardson, M. Wegner, and H. R. Rodewald. 2008. Neural crest origin of perivascular mesenchyme in the adult thymus. *J Immunol* 180:5344-5351.
35. Auerbach, R. 1960. Morphogenetic interactions in the development of the mouse thymus gland. *Dev Biol* 2:271-284.
36. Bockman, D. E., and M. L. Kirby. 1984. Dependence of thymus development on derivatives of the neural crest. *Science* 223:498-500.
37. Jenkinson, W. E., E. J. Jenkinson, and G. Anderson. 2003. Differential requirement for mesenchyme in the proliferation and maturation of thymic epithelial progenitors. *J Exp Med* 198:325-332.
38. Dooley, J., M. Erickson, W. J. Larochelle, G. O. Gillard, and A. G. Farr. 2007. FGFR2IIIb signaling regulates thymic epithelial differentiation. *Dev Dyn* 236:3459-3471.

39. Itoi, M., and T. Amagai. 1998. Inductive role of fibroblastic cell lines in development of the mouse thymus anlage in organ culture. *Cell Immunol* 183:32-41.
40. Suniara, R. K., E. J. Jenkinson, and J. J. Owen. 2000. An essential role for thymic mesenchyme in early T cell development. *J Exp Med* 191:1051-1056.
41. Griffith, A. V., K. Cardenas, C. Carter, J. Gordon, A. Iberg, K. Engleka, J. A. Epstein, N. R. Manley, and E. R. Richie. 2009. Increased thymus- and decreased parathyroid-fated organ domains in *Spotch* mutant embryos. *Dev Biol* 327:216-227.
42. Manley, N. R. 2000. Thymus organogenesis and molecular mechanisms of thymic epithelial cell differentiation. *Semin Immunol* 12:421-428.
43. Gordon, J., A. R. Bennett, C. C. Blackburn, and N. R. Manley. 2001. *Gcm2* and *Foxn1* mark early parathyroid- and thymus-specific domains in the developing third pharyngeal pouch. *Mech Dev* 103:141-143.
44. Gordon, J., V. A. Wilson, N. F. Blair, J. Sheridan, A. Farley, L. Wilson, N. R. Manley, and C. C. Blackburn. 2004. Functional evidence for a single endodermal origin for the thymic epithelium. *Nat Immunol* 5:546-553.
45. Grevellec, A., and A. S. Tucker. 2010. The pharyngeal pouches and clefts: Development, evolution, structure and derivatives. *Semin Cell Dev Biol* 21:325-332.
46. Manley, N. R., and C. C. Blackburn. 2003. A developmental look at thymus organogenesis: where do the non-hematopoietic cells in the thymus come from? *Curr Opin Immunol* 15:225-232.

47. Chen, L., S. Xiao, and N. R. Manley. 2009. Foxn1 is required to maintain the postnatal thymic microenvironment in a dosage-sensitive manner. *Blood* 113:567-574.
48. Liu, Z., S. Yu, and N. R. Manley. 2007. Gcm2 is required for the differentiation and survival of parathyroid precursor cells in the parathyroid/thymus primordia. *Dev Biol* 305:333-346.
49. Gordon, J., S. Xiao, B. Hughes, 3rd, D. M. Su, S. P. Navarre, B. G. Condie, and N. R. Manley. 2007. Specific expression of lacZ and cre recombinase in fetal thymic epithelial cells by multiplex gene targeting at the Foxn1 locus. *BMC Dev Biol* 7:69.
50. Jenkinson, W. E., A. Bacon, A. J. White, G. Anderson, and E. J. Jenkinson. 2008. An epithelial progenitor pool regulates thymus growth. *J Immunol* 181:6101-6108.
51. Moore-Scott, B. A., and N. R. Manley. 2005. Differential expression of Sonic hedgehog along the anterior-posterior axis regulates patterning of pharyngeal pouch endoderm and pharyngeal endoderm-derived organs. *Dev Biol* 278:323-335.
52. Scimone, M. L., I. Aifantis, I. Apostolou, H. von Boehmer, and U. H. von Andrian. 2006. A multistep adhesion cascade for lymphoid progenitor cell homing to the thymus. *Proc Natl Acad Sci U S A* 103:7006-7011.
53. Foster, K. E., J. Gordon, K. Cardenas, H. Veiga-Fernandes, T. Makinen, E. Grigorieva, D. G. Wilkinson, C. C. Blackburn, E. Richie, N. R. Manley, R. H. Adams, D. Kioussis, and M. C. Coles. 2010. EphB-ephrin-B2 interactions are

- required for thymus migration during organogenesis. *Proc Natl Acad Sci U S A* 107:13414-13419.
54. Rodewald, H. R. 2008. Thymus organogenesis. *Annu Rev Immunol* 26:355-388.
 55. Muller, S. M., G. Terszowski, C. Blum, C. Haller, V. Anquez, S. Kuschert, P. Carmeliet, H. G. Augustin, and H. R. Rodewald. 2005. Gene targeting of VEGF-A in thymus epithelium disrupts thymus blood vessel architecture. *Proc Natl Acad Sci U S A* 102:10587-10592.
 56. Manley, N. R., and M. R. Capecchi. 1995. The role of Hoxa-3 in mouse thymus and thyroid development. *Development* 121:1989-2003.
 57. Manley, N. R., and M. R. Capecchi. 1998. Hox group 3 paralogs regulate the development and migration of the thymus, thyroid, and parathyroid glands. *Dev Biol* 195:1-15.
 58. Manley, N. R., and B. G. Condie. 2010. Transcriptional regulation of thymus organogenesis and thymic epithelial cell differentiation. *Prog Mol Biol Transl Sci* 92:103-120.
 59. Su, D., S. Ellis, A. Napier, K. Lee, and N. R. Manley. 2001. Hoxa3 and pax1 regulate epithelial cell death and proliferation during thymus and parathyroid organogenesis. *Dev Biol* 236:316-329.
 60. Su, D. M., and N. R. Manley. 2000. Hoxa3 and pax1 transcription factors regulate the ability of fetal thymic epithelial cells to promote thymocyte development. *J Immunol* 164:5753-5760.

61. Zou, D., D. Silvius, J. Davenport, R. Grifone, P. Maire, and P. X. Xu. 2006. Patterning of the third pharyngeal pouch into thymus/parathyroid by Six and Eya1. *Dev Biol* 293:499-512.
62. Xu, P. X., W. Zheng, C. Laclef, P. Maire, R. L. Maas, H. Peters, and X. Xu. 2002. Eya1 is required for the morphogenesis of mammalian thymus, parathyroid and thyroid. *Development* 129:3033-3044.
63. Guo, C., Y. Sun, B. Zhou, R. M. Adam, X. Li, W. T. Pu, B. E. Morrow, and A. Moon. 2011. A Tbx1-Six1/Eya1-Fgf8 genetic pathway controls mammalian cardiovascular and craniofacial morphogenesis. *J Clin Invest* 121:1585-1595.
64. Garg, V., C. Yamagishi, T. Hu, I. S. Kathiriy, H. Yamagishi, and D. Srivastava. 2001. Tbx1, a DiGeorge syndrome candidate gene, is regulated by sonic hedgehog during pharyngeal arch development. *Dev Biol* 235:62-73.
65. Yamagishi, H., J. Maeda, T. Hu, J. McAnally, S. J. Conway, T. Kume, E. N. Meyers, C. Yamagishi, and D. Srivastava. 2003. Tbx1 is regulated by tissue-specific forkhead proteins through a common Sonic hedgehog-responsive enhancer. *Genes Dev* 17:269-281.
66. Baldini, A. 2005. Dissecting contiguous gene defects: TBX1. *Curr Opin Genet Dev* 15:279-284.
67. Scambler, P. J. 2010. 22q11 deletion syndrome: a role for TBX1 in pharyngeal and cardiovascular development. *Pediatr Cardiol* 31:378-390.
68. Aggarwal, V. S., J. Liao, A. Bondarev, T. Schimmang, M. Lewandoski, J. Locker, A. Shanske, M. Campione, and B. E. Morrow. 2006. Dissection of

- Tbx1 and Fgf interactions in mouse models of 22q11DS suggests functional redundancy. *Hum Mol Genet* 15:3219-3228.
69. Liao, J., V. S. Aggarwal, S. Nowotschin, A. Bondarev, S. Lipner, and B. E. Morrow. 2008. Identification of downstream genetic pathways of Tbx1 in the second heart field. *Dev Biol* 316:524-537.
 70. Zhang, L., T. Zhong, Y. Wang, Q. Jiang, H. Song, and Y. Gui. 2006. TBX1, a DiGeorge syndrome candidate gene, is inhibited by retinoic acid. *Int J Dev Biol* 50:55-61.
 71. Stennard, F. A., and R. P. Harvey. 2005. T-box transcription factors and their roles in regulatory hierarchies in the developing heart. *Development* 132:4897-4910.
 72. Jerome, L. A., and V. E. Papaioannou. 2001. DiGeorge syndrome phenotype in mice mutant for the T-box gene, Tbx1. *Nat Genet* 27:286-291.
 73. Vitelli, F., M. Morishima, I. Taddei, E. A. Lindsay, and A. Baldini. 2002. Tbx1 mutation causes multiple cardiovascular defects and disrupts neural crest and cranial nerve migratory pathways. *Hum Mol Genet* 11:915-922.
 74. Arnold, J. S., U. Werling, E. M. Braunstein, J. Liao, S. Nowotschin, W. Edelmann, J. M. Hebert, and B. E. Morrow. 2006. Inactivation of Tbx1 in the pharyngeal endoderm results in 22q11DS malformations. *Development* 133:977-987.
 75. Hebert, J. M., and S. K. McConnell. 2000. Targeting of cre to the Foxg1 (BF-1) locus mediates loxP recombination in the telencephalon and other developing head structures. *Dev Biol* 222:296-306.

76. Moraes, F., A. Novoa, L. A. Jerome-Majewska, V. E. Papaioannou, and M. Mallo. 2005. Tbx1 is required for proper neural crest migration and to stabilize spatial patterns during middle and inner ear development. *Mech Dev* 122:199-212.
77. Zhang, Z., T. Huynh, and A. Baldini. 2006. Mesodermal expression of Tbx1 is necessary and sufficient for pharyngeal arch and cardiac outflow tract development. *Development* 133:3587-3595.
78. Xu, H., F. Cerrato, and A. Baldini. 2005. Timed mutation and cell-fate mapping reveal reiterated roles of Tbx1 during embryogenesis, and a crucial function during segmentation of the pharyngeal system via regulation of endoderm expansion. *Development* 132:4387-4395.
79. Gray, D. H., A. L. Fletcher, M. Hammett, N. Seach, T. Ueno, L. F. Young, J. Barbuto, R. L. Boyd, and A. P. Chidgey. 2008. Unbiased analysis, enrichment and purification of thymic stromal cells. *J Immunol Methods* 329:56-66.
80. Depreter, M. G., N. F. Blair, T. L. Gaskell, C. S. Nowell, K. Davern, A. Pagliocca, F. H. Stenhouse, A. M. Farley, A. Fraser, J. Vrana, K. Robertson, G. Morahan, S. R. Tomlinson, and C. C. Blackburn. 2008. Identification of Plet-1 as a specific marker of early thymic epithelial progenitor cells. *Proc Natl Acad Sci U S A* 105:961-966.
81. van Bueren, K. L., I. Papangelis, F. Rochais, K. Pearce, C. Roberts, A. Calmont, D. Szumska, R. G. Kelly, S. Bhattacharya, and P. J. Scambler. 2010. Hes1 expression is reduced in Tbx1 null cells and is required for the

- development of structures affected in 22q11 deletion syndrome. *Dev Biol* 340:369-380.
82. Xiao, S., and N. R. Manley. 2010. Impaired thymic selection and abnormal antigen-specific T cell responses in *Foxn1*(Delta/Delta) mutant mice. *PLoS One* 5:e15396.
83. Yeh, S., C. S. de Paiva, C. S. Hwang, K. Trinca, A. Lingappan, J. K. Rafati, W. J. Farley, D. Q. Li, and S. C. Pflugfelder. 2009. Spontaneous T cell mediated keratoconjunctivitis in *Aire*-deficient mice. *Br J Ophthalmol* 93:1260-1264.
84. Chiorini, J. A., D. Cihakova, C. E. Ouellette, and P. Caturegli. 2009. Sjogren syndrome: advances in the pathogenesis from animal models. *J Autoimmun* 33:190-196.
85. Van Vliet, E., E. J. Jenkinson, R. Kingston, J. J. Owen, and W. Van Ewijk. 1985. Stromal cell types in the developing thymus of the normal and nude mouse embryo. *Eur J Immunol* 15:675-681.
86. Chen, L., F. G. Fulcoli, S. Tang, and A. Baldini. 2009. *Tbx1* regulates proliferation and differentiation of multipotent heart progenitors. *Circ Res* 105:842-851.
87. Greulich, F., C. Rudat, and A. Kispert. 2011. Mechanisms of T-box gene function in the developing heart. *Cardiovasc Res* 91:212-222.
88. Hu, T., H. Yamagishi, J. Maeda, J. McAnally, C. Yamagishi, and D. Srivastava. 2004. *Tbx1* regulates fibroblast growth factors in the anterior

- heart field through a reinforcing autoregulatory loop involving forkhead transcription factors. *Development* 131:5491-5502.
89. Vitelli, F., Z. Zhang, T. Huynh, A. Sobotka, A. Mupo, and A. Baldini. 2006. Fgf8 expression in the Tbx1 domain causes skeletal abnormalities and modifies the aortic arch but not the outflow tract phenotype of Tbx1 mutants. *Dev Biol* 295:559-570.
 90. Lania, G., Z. Zhang, T. Huynh, C. Caprio, A. M. Moon, F. Vitelli, and A. Baldini. 2009. Early thyroid development requires a Tbx1-Fgf8 pathway. *Dev Biol* 328:109-117.
 91. Tucker, A., and P. Sharpe. 2004. The cutting-edge of mammalian development; how the embryo makes teeth. *Nat Rev Genet* 5:499-508.
 92. Cao, H., S. Florez, M. Amen, T. Huynh, Z. Skobe, A. Baldini, and B. A. Amendt. 2010. Tbx1 regulates progenitor cell proliferation in the dental epithelium by modulating Pitx2 activation of p21. *Dev Biol* 347:289-300.
 93. Bleul, C. C., and T. Boehm. 2005. BMP signaling is required for normal thymus development. *J Immunol* 175:5213-5221.
 94. Patel, S. R., J. Gordon, F. Mahbub, C. C. Blackburn, and N. R. Manley. 2006. Bmp4 and Noggin expression during early thymus and parathyroid organogenesis. *Gene Expr Patterns* 6:794-799.
 95. Liu, W., J. Selever, D. Wang, M. F. Lu, K. A. Moses, R. J. Schwartz, and J. F. Martin. 2004. Bmp4 signaling is required for outflow-tract septation and branchial-arch artery remodeling. *Proc Natl Acad Sci U S A* 101:4489-4494.

96. Wang, J., S. B. Greene, M. Bonilla-Claudio, Y. Tao, J. Zhang, Y. Bai, Z. Huang, B. L. Black, F. Wang, and J. F. Martin. 2010. Bmp signaling regulates myocardial differentiation from cardiac progenitors through a MicroRNA-mediated mechanism. *Dev Cell* 19:903-912.
97. Gordon, J., S. R. Patel, Y. Mishina, and N. R. Manley. 2010. Evidence for an early role for BMP4 signaling in thymus and parathyroid morphogenesis. *Dev Biol* 339:141-154.
98. Vitelli, F., I. Taddei, M. Morishima, E. N. Meyers, E. A. Lindsay, and A. Baldini. 2002. A genetic link between Tbx1 and fibroblast growth factor signaling. *Development* 129:4605-4611.
99. Norgaard, G. A., J. N. Jensen, and J. Jensen. 2003. FGF10 signaling maintains the pancreatic progenitor cell state revealing a novel role of Notch in organ development. *Dev Biol* 264:323-338.
100. Bhushan, A., N. Itoh, S. Kato, J. P. Thiery, P. Czernichow, S. Bellusci, and R. Scharfmann. 2001. Fgf10 is essential for maintaining the proliferative capacity of epithelial progenitor cells during early pancreatic organogenesis. *Development* 128:5109-5117.
101. Su, D. M., S. Navarre, W. J. Oh, B. G. Condie, and N. R. Manley. 2003. A domain of Foxn1 required for crosstalk-dependent thymic epithelial cell differentiation. *Nat Immunol* 4:1128-1135.
102. Fulcoli, F. G., T. Huynh, P. J. Scambler, and A. Baldini. 2009. Tbx1 regulates the BMP-Smad1 pathway in a transcription independent manner. *PLoS One* 4:e6049.

103. Liu, J., C. Sato, M. Cerletti, and A. Wagers. 2010. Notch signaling in the regulation of stem cell self-renewal and differentiation. *Curr Top Dev Biol* 92:367-409.
104. Masuda, K., W. T. Germeraad, R. Satoh, M. Itoi, T. Ikawa, N. Minato, Y. Katsura, W. van Ewijk, and H. Kawamoto. 2009. Notch activation in thymic epithelial cells induces development of thymic microenvironments. *Mol Immunol* 46:1756-1767.
105. King, I. N., I. S. Kathiriya, M. Murakami, M. Nakagawa, K. A. Gardner, D. Srivastava, and O. Nakagawa. 2006. Hrt and Hes negatively regulate Notch signaling through interactions with RBP-Jkappa. *Biochem Biophys Res Commun* 345:446-452.
106. Gill, J., M. Malin, J. Sutherland, D. Gray, G. Hollander, and R. Boyd. 2003. Thymic generation and regeneration. *Immunol Rev* 195:28-50.
107. Olson, L. E., and P. Soriano. 2011. PDGFRbeta Signaling Regulates Mural Cell Plasticity and Inhibits Fat Development. *Dev Cell* 20:815-826.
108. Youm, Y. H., H. Yang, Y. Sun, R. G. Smith, N. R. Manley, B. Vandanmagsar, and V. D. Dixit. 2009. Deficient ghrelin receptor-mediated signaling compromises thymic stromal cell microenvironment by accelerating thymic adiposity. *J Biol Chem* 284:7068-7077.
109. Billon, N., P. Iannarelli, M. C. Monteiro, C. Glavieux-Pardanaud, W. D. Richardson, N. Kessar, C. Dani, and E. Dupin. 2007. The generation of adipocytes by the neural crest. *Development* 134:2283-2292.

110. Calmont, A., S. Ivins, K. L. Van Bueren, I. Papangeli, V. Kyriakopoulou, W. D. Andrews, J. F. Martin, A. M. Moon, E. A. Illingworth, M. A. Basson, and P. J. Scambler. 2009. Tbx1 controls cardiac neural crest cell migration during arch artery development by regulating Gbx2 expression in the pharyngeal ectoderm. *Development* 136:3173-3183.

Kim T. Cardenas
501A Paige, TX, 78659
Phone: 210-849-1042
kcardenas@mdanderson.org

Current Position

Graduate Research Assistant and Ph.D. Candidate, The University of Texas at Houston Health Science Center, M.D. Anderson Cancer Research Center Science Park, Supervisor: Dr. Ellen Richie

Current GPA- 4.0

Education

B.S. Biology, Chemistry Minor, Summa Cum Laude, University of Texas at San Antonio, 2004

Research Skills

- Western and Southern Blot Analysis
- Stable transfection and gene expression analysis in cell culture lines.
- Maintenance and breeding of experimental mouse lines
- PCR and RT-PCR and DNA cloning
- DNA, RNA and protein isolation from cells and tissue
- *In situ* hybridization on mouse embryonic tissue
- Immunohistochemistry
- Fluorescence-activated cell sorting of thymic epithelial cells and lymphoid subsets
- Histological processing and sectioning of both frozen and paraffin embedded tissue

Publications

Paola Rojas, Fernando Benavides, Jorge Blando, Carlos Perez, **Kim Cardenas**, Ellen Richie, Erik S. Knudsen, David G. Johnson, Adrain Senderowicz, Marcelo L. Rodriguez-Puebla, Claudio Conti. Enhanced skin carcinogenesis and lack of thymus hyperplasia in transgenic mice expressing human cyclin D1b (CCND1b). **Mol Carcinog.** 2008 Oct;48(6):508-16.

Ann Griffin, **Kim Cardenas**, Carla Carter, Julie Gordon, Aimee Iberg, Kurt Engleka, Jonathan Epstein, Nancy R. Maley, Ellen Richie. Increased thymus- and decreased parathyroid-fated Organ domains in Splotch mutant embryos. **Dev Biol**. 2009.Mar 1; 327(1):216-27.

John F. Repass, Micheline N. Laurent, Carla Carter, Boris Reizis. Mark Bedford, **Kim Cardenas**, Priyanka Narang, Mark Coles, Ellen Richie. IL7-hCD25 and IL7-Cre BAC Transgenic Mouse Lines: New Tools for Analysis of IL-7 Expressing Cells. **Genesis**. 2009. Apr; 47(4):281-7.

Katie Foster, Julie Gordon, **Kim Cardenas**, Henrique Veiga-Fernandes, Taija Makinen, Elena Grigorieva, David Wilkinson, Ellen Richie, Clare Blackburn, Nancy Manley, Ralf Adams, Dimitris Kioussis, Mark Coles. EphB-ephrin-B2 interactions are required for thymus migration during organogenesis. **PNAS**. 2010. July 27; 107(30):13414-9.

Teaching Experience

- Summer Undergraduate Research Program (SURP) student mentor, (May-Aug. 2008)
- Graduate Student Tutor (Oct. 2008- Current)
- COEP lecturer and mentor for local students, (Mar. 2010- Current)

Oral presentations

2009, May. American Association of Immunology Annual Meeting (AAI). *Tbx1* antagonizes thymus fate.

2010, March. ThymOz VI- An International Workshop on T Lymphocytes. Enforced *Tbx1* expression in fetal thymus impairs TEC differentiation.

2010, October. Cold Spring Harbor Laboratory- Meeting of Mouse Genetics and Development. Enforced *Tbx1* expression in fetal thymus is incompatible with TEC differentiation.

Awards

The Federation of American Societies for Experimental Biology/Minority Access to Research Careers Program/ AAI Travel Award-2009

Molecular Carcinogenesis Program Travel Award for attendance to the AAI
Advanced Course in Immunology-2009

1st Place Poster Presentation, Science Park Research Division Department
of Molecular Carcinogenesis Graduate Student Retreat-2010

References

Ellen Richie, Ph.D.
Professor, Department of Carcinogenesis
The University of Texas M.D. Anderson Cancer Center
1801 Park Road 1C, Unit 116
P.O. Box 389
Smithville, Texas, 78957
Tel: (512)-237- 9435
Email: erichie@mdanderson.org

Nancy R. Manley, Ph.D.
Associate Professor
Chair of Interdepartmental Developmental Biology
Genetics Department
S270B Coverdell Center
University of Georgia
Athens, Georgia, 30602
Tel: (706)-542-5861
Fax: (706)-583-0590
Email: nmanley@uga.edu

Mark Bedford, Ph.D.
Professor, Department of Carcinogenesis
The University of Texas M.D. Anderson Cancer Center
1801 Park Road 1C, Unit 116
P.O. Box 389
Smithville, Texas, 78957
Tel: (512)-237-9539
Email: mtbedford@mdanderson.org